Advances in structural robustness of reinforced concrete moment resisting frames

Elena Miceli
* * * * * *

Supervisors
Prof. Paolo Castaldo, Supervisor
Prof. Giuseppe Carlo Marano, Co-Supervisor

Politecnico di Torino
15th July 2024

I hereby declare that, the contents and organisation of this dissertation constitute my own original work and does not compromise in any way the rights of third parties, including those relating to the security of personal data.

……………………………....

Elena Miceli

Turin, 15th July 2024

Summary

In the past decades, structural robustness has become an important issue all over the world due to the occurrence of catastrophic events causing progressive collapses. A typical example is the terrorist attack of the 9/11, where two 110-story skyscrapers collapsed, damaging or destroying nearby buildings.

Nowadays, structures and infrastructures are designed to withstand to normal actions, determined as function of their probabilities of occurrence with respect to a certain period of life. On the other hand, accidental actions are LPHC events (i.e., low-probability high-consequence), meaning that those events are unlike to occur but determine high consequences in terms of human and economic losses. When a LPHC event takes place, the structures which are able to avoid a collapse that is progressive and/or disproportionate with respect to the initial damage are defined robust.

Several guidelines and literature studies have focused on improving the robustness of multi-story buildings. Most of them recognized the need for tying structural elements by arranging a continuous reinforcement over the supports. Others suggest placing a symmetrical longitudinal reinforcement between the upper and the lower chord close to the support. In addition, a crucial role to enhance structural robustness of a frame is played by the membrane and horizontal actions made by the slab and the orthogonal (out-of-plane) structural system. Furthermore, the actual code rules do not provide any evaluation of a progressive collapse risk assessment as well as the associated safety levels (i.e., reliability index) for buildings but only recommended values are suggested.

The goal of this thesis is to enhance the robustness of reinforced concrete buildings located in seismic area by improving the design of the plane frames and including the three-dimensional effects. In addition, a strain-based approach is proposed to study the safety level associated with these improvements at the

ultimate limit state in case of a progressive collapse scenario implying the removal of a supporting column.

To reach these goals, the first step is to study and justify both existing and new proposals to enhance structural robustness. Then, deterministic non-linear displacement-controlled pushdown analyses are performed on many frames analyzing different column-loss scenarios. In detail, the two-dimensional frames are defined by modifying the longitudinal reinforcement arrangement and also including the effects of the orthogonal (out-of-plane) framed system. The output of the non-linear analysis are studied in order to investigate the bearing capacity of the structural configurations as well as the catenary effects activation. These outputs are essential to deterministically identify the combination of longitudinal reinforcement arrangement able to enhance the structural behavior in case of progressive collapse.

Then, from the output of the deterministic analysis, three different configurations have been selected and probabilistically investigated in order to validate the design proposals by computing the safety level associated with a central supporting column loss. More in detail, one configuration is the one designed according to seismic codes, while the other two are identified as the better solutions within the deterministic analysis. These two frames adopt a combination of the following criteria: continuous reinforcement along the beams over the supports, adoption of the same reinforcement amount in all the floors and symmetric in cross-sections in order to exploit a global Vierendeel behavior and presence of two levels of side face rebars. This full-probabilistic analysis has allowed the definition of the safety level in terms of reliability associated with the three different frames.

In addition, this thesis investigates the possibility of applying the superposition principle on the response of the two orthogonal frames to define the global 3D structural behavior under a common supporting column removal. Specifically, many column-loss scenarios are investigated on the same three structural configurations studied within the reliability analysis. By means of deterministic analyses, the thesis has demonstrated the validity of the superposition of the plane non-linear capacity curves of the two orthogonal frames involved in the failure scenario to define the global capacity curve.

Results have demonstrated that the adoption of a continuous longitudinal reinforcement over the supports up to 1/3 of the beam length and the presence of side face rebars are crucial in anticipating the catenary effect and guaranteeing an adequate safety level (i.e., larger than 1). This combination of longitudinal reinforcement is a trade off between principles of robustness, sustainability, seismic design and safety.

Contents

List of Tables

List of Figures

Preface

The present PhD dissertation aims at exploring possible design enhancements for the robustness of new reinforced concrete (RC) ordinary buildings designed in seismic area, against a supporting column removal scenario. At present, actual code rules lack in providing indications on the safety levels that a RC building should guarantee against a column removal scenario, but mainly prescriptive rules are recommended.

Chapter 1 is about a deep overview of the basic concepts behind structural robustness. At first, an examination is given about the historical context that has driven the development of structural robustness principles, together with fundamental definitions related to progressive and disproportionate collapse found in existing literature. Next, the concept of the risks associated with progressive collapse is defined, emphasizing the ongoing need for research in this field. The chapter also discusses strategies outlined in current guidelines and building codes aimed at mitigating the risks of progressive collapse. An analysis of key indicators used to quantify and measure structural robustness is presented. Finally, the chapter focuses on the structural response of cast-in-situ reinforced concrete (RC) structures when subjected to abnormal scenarios such as column removal.

Chapter 2 discusses the fundamental concepts for the formulation of structural reliability analysis. It starts with an introduction to probabilistic analysis, outlining the basics of this analytical approach. Then, an overview of the primary uncertainties that impact structural engineering problems is provided, distinguishing between aleatory and epistemic ones. Furthermore, the chapter delves into the definition of the Limit State Function and assesses the performance requirements that must be ensured for new structures. Lastly, it explores various reliability methods, including level III, level II, level I, and level 0 methods, discussing their characteristics and applications.

Chapter 3 describes the case study involving the application and discussion of robustness design improvements. It begins with an overview of the seismic design procedure for two multistorey reinforced concrete buildings, one composed by only seismic resistant frames as much regular as possible and the second one constituted

by both seismic resistant and secondary frames with different dimensions of beams and columns. Following that, it explains the finite element modelling assumptions used to conduct all the non-linear analyses performed within this dissertation. The modelling assumptions are based on the validation against an experimental test of a beam-column subassembly extracted from a building designed in seismic area. In addition, the method adopted to model the contribution of the orthogonal two-dimensional framed system, by means of equivalent springs, is explained. These equivalent springs are placed in the beam-column nodes of each frame under study and are calibrated both with a linear and non-linear approach.

Chapter 4 illustrates and justifies many design modifications on the longitudinal reinforcement arrangement, implemented to enhance the structural robustness of the RC buildings. Then, a detailed deterministic parametric analysis is carried out to evaluate the effectiveness of various design suggestions in enhancing structural robustness. These modifications are applied to the longitudinal reinforcement of the beams and are: *support continuity*, *continuity*, *symmetry in cross-section* of longitudinal reinforcement, enhancement of Vierendeel behavior by placing both *global* and *partial equal* reinforcement among the floors and the influence of *side face reinforcement bars*. In addition, the 3D effects exerted by the orthogonal (out-of-plane) framed system on the two-dimensional frames is studied by considering the influence of equivalent translational elastic springs placed in each beam-column node. To compare these enhancements, non-linear finite element (NLFE) pushdown analyses are developed, applying a monotonically increasing vertical displacement at the point of column removal and registering the corresponding reaction. Two distinct failure scenarios are considered during the analyses. The findings indicate significant improvements in structural robustness for the proposed solutions, particularly concerning the efficacy of *side face reinforcement bars* in enhancing both flexural and catenary behavior.

Chapter 5 is about the probabilistic assessment of the robustness of three different configurations selected as the most relevant frames according to the results of the deterministic analyses given in the previous chapter. One frame is designed according to actual code rules and other two are obtained by applying the robustness improvements proposed in the previous chapter. In all the three frames the contribution of the orthogonal framed system is accounted for by means of equivalent elastic springs placed on beam-column nodes. The reliability assessment is conducted using a strain-based 5-step procedure employing a full probabilistic approach (i.e., considering aleatory properties of both materials and loads), generating for each of the basic variables 100 realizations. Subsequently, displacement-controlled pushdown NLFE analyses are performed on the 300 sampled models to determine energy-based dynamic amplification factors. Then, probabilistic static-equivalent NLFE analyses are executed for the 300 realizations, simulating a central supporting column removal and appropriately amplifying the gravity loads on the central spans. The strains of both confined concrete and reinforcement at various points are monitored and probabilistically modelled.

Ultimately, convolution integrals between aleatory strains and corresponding aleatory ultimate thresholds are computed to derive failure probabilities concerning the ultimate limit state. The results provide insights into the reliability levels of structural elements within the three configurations, highlighting important safety advantages when adopting robustness improvements. In this way, the proposed solutions, demonstrated effective, sustainable and safe, are studied in the next chapter in order to deterministically evaluate the 3D global response.

Chapter 6 aims at assessing the robustness of the 3D structure analyzing the deterministic response of the two frames directly involved in the failure scenario in the orthogonal directions. In detail, the building is composed by both seismic resistant frames and secondary frames and the three structural configurations already analyzed from a reliability point of view are investigated. For each of the three design configurations, four different failure scenarios are considered, involving the removal of specific supporting columns. In addition, the contribution of the frame, located along the orthogonal (out-of-plane) direction, is considered by means of non-linear translation springs. The results demonstrate the importance of calibrating the non-linear constitutive laws of the springs, especially, for large vertical displacements and for frames having wide beams due to their large contribution in terms of ductility. By comparing the results of the superimposed capacity curve of the frames in the two orthogonal directions and the one obtained from a 3D analysis, the validation of the superposition principle is obtained. This confirms the possibility of designing a 3D structure in terms of robustness without the need of developing a full 3D analysis but focusing on the design of planar frames. Finally, the energetic equivalence approach is applied on the achieved global capacity curves to highlight the benefits of the robustness design improvements.

The achievements of the research activity during the PhD brought to the following scientific publications:

Journal papers

- **E. Miceli**, D. Gino, P. Castaldo (2024): Approaches to estimate global safety factors for reliability assessment of RC structures using non-linear numerical analyses – *Engineering Structures* 118248
- **E. Miceli**, S. Ferrara, P. Castaldo (2024): *Confinement effects within the seismic design of reinforced concrete frames: a reliability assessment and comparison – Engineering Structures*
- G. Bertagnoli, M. Ferrara, **E. Miceli**, P. Castaldo, L. Giordano (2024): Safety assessment of an existing bridge deck subject to different damage scenarios through the global safety format ECOV – *Engineering Structures*, 306, 117859 (DOI: 10.1016/j.engstruct.2024.117859)
- M. Ferrara, D. Gino, **E. Miceli**, L. Giordano, M. Malavisi, G. Bertagnoli (2024): Safety assessment of existing prestressed reinforced concrete bridge decks through different approaches - *Structural concrete : journal of the fib* (DOI: 10.1002/suco.202301049)
- D. Gino, **E. Miceli,** P. Castaldo, A. Recupero, G. Mancini (2024): Strain-based method for assessment of global resistance safety factors for NLNAs of reinforced concrete structures - *Engineering Structures*, 304, 117625 (DOI: 10.1016/j.engstruct.2024.117625)
- **E. Miceli**, P. Castaldo (2024): Robustness Improvements for 2D Reinforced Concrete Moment Resisting Frames: Parametric Study by Means of NLFE Analyses, *Structural concrete : journal of the fib*, 25(1), 9–31 (DOI: 10.1002/suco.202300443)
- P. Castaldo, **E. Miceli** (2023): Optimal single concave sliding device properties for isolated multi-span continuous deck bridges depending on the ground motion characteristics, Soil Dynamics and Earthquake Engineering, 173, 108128 (DOI: 10.1016/j.soildyn.2023.108128)
- D. Gino, **E. Miceli**, L. Giordano, G. C. Marano, P. Castaldo (2023): Influence of Masonry Infills on Seismic Performance of an Existing RC Building Retrofitted by Means of FPS Devices, Applied Science, 13, 3509 (DOI: 10.3390/app13063509)
- P. Castaldo, **E. Miceli** (2023): Evaluation of the Failure Probability of a 2D RC Frame Subjected to Column Loss, Journal of Modern Mechanical Engineering and Technology, 10, 1–10. (DOI: 10.31875/2409-9848.2023.10.01
- P. Castaldo, G. Amendola, L. Giordano, **E. Miceli** (2022): Seismic reliability assessment of isolated multi-span continuous deck bridges, Ingegneria Sismica - International Journal of Earthquake Engineering, Anno XXXIX – Num. 3

Conference papers

- P. Castaldo, D. Gino, G. Amendola, **E. Miceli** (2020): *Model uncertainties in NLFEAs of RC systems under cyclic loads*, EURODYN 2020 Proceedings of the XI International Conference on Structural Dynamics, Athens, Greece
- P. Castaldo, G. Amendola, D. Gino, **E. Miceli** (2020): *Seismic performance of bridges isolated with DCFP devices*, EURODYN 2020 XI International Conference on Structural Dynamics, Athens, Greece
- P. Castaldo, G. Amendola, L. Giordano, D. Gino, **E. Miceli** (2021): *Seismic reliability of bridges isolated with FPS*, COMPDYN 2021 8th International Conference on Computational Methods in Structural Dynamics and Earthquake Engineering, Athens, Greece
- **E. Miceli**, G. C. Marano (2021): *Determination of epistemic uncertainties in non-linear finite-element analyses of slender reinforced concrete elements,* 2nd *fib* Italy YMG Symposium on Concrete and Concrete Structures, Rome, Italy
- **E. Miceli** (2022): *Influence of near fault records on the optimal performance of isolated continuous bridges*, 5th International Symposium New Metropolitan Perspectives, Reggio Calabria, Italy
- P. Castaldo, **E. Miceli**, D. Gino (2022): *Safety assessment in reliability terms of bridges equipped with isolator devices*, 3rd European Conference on Earthquake Engineering & Seismology, Bucharest, Romania
- **E. Miceli**, G. Amendola (2022): *Optimal response of isolated bridges subjected to near fault seismic inputs*, 3rd European Conference on Earthquake Engineering & Seismology, Bucharest, Romania
- **E. Miceli**, G. Amendola, C. Anerdi, D. Gino, L. Giordano (2022): *Non-linear analyses of slender RC members: on the assessment of global factors for safety verification,* Proc. of the 14th *fib* International PhD Symposium in Civil Engineering, Rome, Italy
- **E. Miceli**, P. Castaldo (2022): *Robustness analysis of reinforced concrete structures: design issues,* Proc. of the 14th *fib* International PhD Symposium in Civil Engineering, Rome, Italy
- **E. Miceli** (2022): *Seismic Response of Viaducts and Bridges Isolated with FPS*, WMCAUS 7th World Multidisciplinary Civil Engineering – Architecture – Urban Planning Symposium, Prague, Czech Republic
- **E. Miceli**, L. Giordano (2022): *Influence of the Pier-abutment-deck interaction on the Seismic Response of Bridges Equipped with FPS*, XIX ANIDIS Congress, Seismic Engineering in Italy, Turin, Italy
- D. Gino, **E. Miceli**, P. Castaldo (2022): *Seismic reliability analysis of isolated deck bridges using friction pendulum devices,* XIX ANIDIS Congress, Seismic Engineering in Italy, Turin, Italy
- P. Castaldo, G. Amendola, L. Giordano, **E. Miceli**, D. Gino (2022): *Seismic Performance Of Bridges Isolated By DCFP Devices: A*

Parametric Analysis, XXVIII CONGRESSO C.T.A., Francavilla a Mare, Italy.

- P. Castaldo, D. Gino, L. Giordano, G. Amendola, **E. Miceli** (2022): *Seismic Reliability Of Bridges Equipped With FPS*, XXVIII CONGRESSO C.T.A., Francavilla a Mare, Italy

- P. Castaldo, **E. Miceli**, D. Gino, G. Amendola, L. Giordano (2022): *Seismic Performance Of Bridges Equipped With FPS*, XXVIII CONGRESSO C.T.A., Francavilla a Mare, Italy

- P. Castaldo, **E. Miceli**, D. Gino (2022): *Robustness of reinforced concrete frames in seismic zone: preliminary results*, ICC Concrete in the Ecological Transition, Napoli, Italy

- Castaldo P., D. Gino, G. Amendola, **E. Miceli**, M. Mori, M. Mariscotti, B. Magrì, L. Giordano, G. Mancini (2022): *Experimental evaluation of the structural response of a reinforced concrete bridge beam: preliminary results*, ITALIAN CONCRETE DAYS Giornate AICAP 2022 - Congresso CTE "IL CALCESTRUZZO NELLA TRANSIZIONE ECOLOGICA", Napoli, Italy

- D. Gino, P. Castaldo, **E. Miceli** (2022): *Comparison of different approaches to derive global safety factors for non-linear analyses of slender RC members*, ITALIAN CONCRETE DAYS Giornate AICAP 2022 - Congresso CTE "IL CALCESTRUZZO NELLA TRANSIZIONE ECOLOGICA", Napoli, Italy

- **E. Miceli**, D. Gino, A. Ricioppo, G. Amendola , L. Giordano and P. Castaldo (2023): *Optimal properties of single concave friction pendulum bearings for the isolation of bridges subjected to far field records*, 9th International Conference on Computational Methods in Structural Dynamics and Earthquake Engineering, Athens (COMPDYN), Athens, Greece

- D. Gino, **E. Miceli**, A. Ricioppo, G. Amendola, L. Giordano, P. Castaldo (2023): *Evaluation of the effect of masonry infills on response of RC buildings equipped with FPS devices: a case study*, 9th International Conference on Computational Methods in Structural Dynamics and Earthquake Engineering (COMPDYN), Athens, Greece

- P. Darò, D. La Mazza, E. Tetta, G. Lastrico, I. Alovisi, **E. Miceli**, D. Gino, G. Amendola, L. Giordano, P. Castaldo, G. Mancini, M. Mariscotti, M. Garozzo, M. Deiana, B. Magrì (2023): *Full-scale experimental testing on a reinforced bridge RC beam: structural response and SHM results*, *fib* Symposium 2023 - Building for the future: Durable, Sustainable, Resilient, Istanbul, Turkey

Technical book

- Valutazione della sicurezza di strutture e infrastrutture in cemento armato: l'esperienza del viadotto Mollere, Casa Editrice la fiaccola srl, 2022

Chapter 1

Structural robustness

1.1 Introduction

Structural robustness against an accidental action is an intrinsic property of a structure related to its ability to avoid a collapse that is disproportionate with respect to the original damage causing the collapse. In general, accidental actions are low-probability high-consequences (LPHC) events, indicating their very low occurrence probability but extreme consequences in terms of both human and economic losses. Those actions are in general not included in the design or, if considered, with a lower intensity than what is related to a very low occurrence probability.

Nowadays many standards and guidelines provide different tools, mainly prescriptive, to include these concepts in the design and sizing criteria. However, it is not easy to transfer the concept of structural robustness into design criteria due to the difficulties in accounting for all the possible extreme events in the design as well as to the issue of introducing excessive rigidity in the structural system. Furthermore, an important topic is to find a balance between robustness criteria and sustainability principles since the tendency of a robust-based design is to stiffen the structure as much as possible as well as to rely on the redundancy of the structural elements.

This chapter is organized as follows: at first an overview of the historical reasons behind structural robustness is given, accompanied by the basic definitions present in literature regarding progressive and disproportionate collapse. Then, risk assessment for progressive collapse is deepened by defining the level of safety that is nowadays accepted and the need for further studies on this topic. Strategies for progressive collapse as present in the actual guidelines and codes are then explained followed by an overview on the main indices that are used to measure structural robustness. Finally, a focus on the structural behavior of cast-in-situ reinforced concrete (RC) structures in case of abnormal scenario is given, by defining membrane and catenary effects as well as the behavior of subassemblies under progressive collapse.

1.2 History and principles of structural robustness

1.2.1 History overview

The progressive collapse of structures became an important issue after the collapse of the Ronan Point Building in London, occurred on May 16th 1968. The 22-story prefabricated pre-cast concrete structure collapsed because of a gas explosion in the kitchen of a flat located at the eighteenth floor, forcing the blowing out of the concrete panels at the corner. Then, since those panels were bearing elements, all the stories above the eighteenth collapsed. After that, due to the heavy weight of the above stories, all the remaining floors on the south-east corner failed in a sort of chain reaction or, in other words, progressive collapse. A significant imagine of this failure is shown in Figure 1.1.

Figure 1.1 Ronan Point Building collapse, May 16th 1968, London (UK).

For sure this was not the first case of a progressive collapse occurred in the past history, but this event is worldwide recognized as the starting point of the debate on structural robustness sparked by engineers and stakeholders. In fact, the pre-Ronan Point collapses were mainly attributed to construction errors. On the other hand, both the fatalities that the Ronan point failure caused (i.e., 4 deaths and 17 injuries), and the public fears, stoked by media reports, brought to an official parliamentary inquiry commissioned by the government. The inquiry (Griffith et al., 1968) concluded that the reason for the collapse of the 1968 event was not due to a shortcoming in the design knowledge or any defect in the construction process. For this reason, the first disproportionate collapse regulations in the history were issued via Circulars of the Ministry of Housing and Local Government of the UK (i.e., MHLG, 1968) and then in the Building Regulations (HMSO, 1972). At first, the British requirements regarded mainly a prescriptive detailing method for the design and assessment of key elements (especially walls) against internal gas explosion. Lately, the assessment was extended to other types of hazards but still

focused on precast buildings, since it was believed that reinforced concrete (RC) frames were unlikely to be subjected to progressive collapse.

It was only after two other collapses that the rest of the world started debating about including progressive collapse in guidelines and standards: the bombing on the A.P. Murrah Federal Building (Oklahoma, 1995) and the aircraft impact on the structures of the World Trade Center (New York, 2001).

Figure 1.2 Alfred P. Murrah Federal Building, April 19th 1995, Oklahoma City (USA).

Figure 1.3 World Trade Center collapse, September 11th 2001, New York City (USA).

The A.P. Murrah Federal Building was an ordinary cast-in-situ RC structure of nine floors and a plan size of 67 m x 30 m. The explosion was estimated to correspond to a detonation of 1800 kg of TNT at the north side of the building, causing the collapse of a side intermediate column and, consequently, the two adjacent ones. Due to the loss of these three supporting columns, one third of the building collapsed, causing 169 deaths and 800 injuries (Figure 1.2).

As for the well known 9/11 event, two planes were hijacked against the twin towers (Figure 1.3), leading to the collapse of them, bringing destruction of the remaining five structures in the World Trade Center complex and destroying many

of the nearby buildings. This event caused the death of around 3000 people and 4000 were injured.

These two disasters pointed out the inadequacies in the past regulations since they were based on the occurrence of a single hazard and discarded the potential loss of a single member. In addition, it was clear the need to modify the concepts behind tolerable or acceptable risk within the design decisions. Starting from those years, many regulations (ASCE, 1998; ASCE, 2005; ASCE, 2017; GSA, 2003; GSA, 2013; GSA, 2016; CEN, 2006; IBC, 2009, UFC, 2009) were updated including disproportionate collapse requirements. More details on the state of the art of actual design guidelines on progressive collapse are given in the following sections.

1.2.2 Definitions and classifications

Many are the definitions proposed by papers, books and building codes about progressive or disproportionate collapse (Table 1.1) and robustness (

Table 1.2) as extensively collected by Adam et al. (2018).

A key concept is the difference between *progressive* and *disproportionate* collapse. Progressive collapse is related to a damage that involves one or more structural components and progressively extends to other components influencing the entire or a large part of the structural system. This type of collapse is also defined *chain collapse* or *domino effect* (Starossek, 2007). Disproportionate collapse is based on the identification of the size of the collapse which should be disproportionate compared to the initial event. Thus, the former can be qualitatively described and refers to a specific mode of collapse, the second needs quantifications in order to be defined and refers to the extension of the area affected by the event. In addition, a progressive collapse does not imply any disproportion as well as a disproportionate collapse does not need to be characterized by a failure propagation. On the other hand, structural robustness represents the ability of a structure to prevent a collapse, either disproportionate or progressive, under abnormal loading. Structural robustness depends not only on the characteristics of the structural system in terms of ductility, redundancy and strength but also on the type of abnormal event.

An abnormal load can be of natural or anthropic origins, for which three categories can be recognized:

- Category 1: hazards resulting from natural phenomena. This category include: seismic induced phenomena (earthquakes and tsunamis), natural gravitative phenomena (debris slides, debris flows, rockfalls, snow avalanches, volcanic eruptions), foundation settlements (subsidence and water-table level variation), hydraulic phenomena (flooding) and meteorological phenomena (storms, tornadoes and ice formations).
- Category 2: hazards caused intentionally by humans. In those cases, the actions can be brought back to the following loads: fire, free-field

explosion, confined explosion, impacts of vehicles, boats or aircraft. Finally, this category include vandalism and terrorism whose action is more difficult to be evaluated.

- Category 3: hazards caused by conceptual errors in the design and/or execution of the facility. Examples are: wrong structural modelling or choice of foundation type or types of joint and connections, incorrect size of structural detailing, incorrect evaluation of degradation phenomena or incorrect use of material.

While events falling in Category 1 can be treated from a statistical point of view based on the past records, hazards coming from Category 2, especially in case of vandalisms or terrorist attacks, are difficult to be modelled in terms of occurrence probabilities. For these reasons, for actions in Category 2 it is better to refer to the strategic role of the construction compared to the possible victims involved in a terrorist attack and to the type of construction (i.e., hospitals, government facilities, monuments, churches, …). Finally, actions in Category 3 can not be evaluated from a statistical point of view but there exist measures to mitigate those risks through quality control checks and verifications.

Table 1.1 Summary of the definitions for *progressive* and *disproportionate* collapse.

Reference	Definition
Allen and Schriever (1972)	Progressive collapse […] can be defined as the phenomenon in which local failure is followed by collapse of adjoining members which in turn is followed by further collapse and so on, so that widespread collapse occurs as a result of local failure.
GSA (2003)	Progressive collapse is a situation where local failure of a primary structural component leads to the collapse of adjoining members which, in turn, leads to additional collapse. Hence, the total damage is disproportionate to the original cause.
ASCE (2005)	Progressive collapse is defined as the spread of an initial local failure from element to element resulting, eventually, in the collapse of an entire structure or a disproportionately large part of it.
Ellingwood (2006)	A progressive collapse initiates as a result of local structural damage and develops, in a chain reaction mechanism, into a failure that is disproportionate to the initiating local damage.
NISTIR (2007)	Progressive collapse - The spread of local damage, from an initiating event, from element to element resulting, eventually, in the collapse of an entire structure or a disproportionately large part of it; also known as disproportionate collapse.
Starossek and Haberland (2010)	Disproportionate collapse. A collapse that is characterized by a pronounced disproportion between a relatively minor event and the ensuing collapse of a major part or the whole of a structure. Progressive collapse. A collapse that commences with the failure of one or a few structural components and then progresses over successively affected other components.
Agarwal and England (2008)	Disproportionate collapse results from small damage or a minor action leading to the collapse of a relatively large part of the structure. […] Progressive collapse is the spread of damage through a chain reaction, for example through neighboring members or storey by storey. […] Often progressive collapse is disproportionate but the converse may not be true.
Parisi and Augenti (2012)	Progressive collapse […] is a chain reaction mechanism resulting in a pronounced disproportion in size between a relatively minor triggering event and resulting collapse, that is, between the initial amount of directly damaged elements and the final amount of failed elements.

Table 1.2 Summary of the definitions for structural robustness.

Reference	Definition
Bontempi et al. (2007)	The robustness of a structure, intended as its ability not to suffer disproportionate damages as a result of limited initial failure, is an intrinsic requirement, inherent to the structural system organization.
GSA (2003)	Robustness – Ability of a structure or structural components to resist damage without premature and/or brittle failure due to events like explosions, impacts, fire or consequences of human error, due to its vigorous strength and toughness.
Biondini et al. (2008)	Structural robustness can be viewed as the ability of the system to suffer an amount of damage not disproportionate with respect to the causes of the damage itself.
JCSS (2008)	The robustness of a system is defined as the ratio between the direct risks and the total risks (total risks is equal to the sum of direct and indirect risks), for a specified time frame and considering all relevant exposure events and all relevant damage states for the constituents of the system.
Vrouwenvelder (2008)	The notion of robustness is that a structure should not be too sensitive to local damage, whatever the source of damage.
fib (2012)	Robustness is a specific aspect of structural safety that refers to the ability of a system subject to accidental or exceptional loadings (such as fire, explosions, impact or consequences of human errors) to sustain local damage to some structural components without experiencing a disproportionate degree of overall distress or collapse.
Brett and Lu (2013)	[…] ability of a structure in withstanding an abnormal event involving a localized failure with limited levels of consequences, or simply structural damages.
CEN (2006)	Robustness: The ability of a structure to withstand events like fire, explosions, impact or the consequences of human error, without being damaged to an extent disproportionate to the original cause.

1.3 Assessment of progressive collapse risk

In the context of structural robustness, it is important to identify the tolerable risk to which a structure can be subjected under abnormal conditions, knowing that nullifying the risk is impossible, especially in case of LPHC events. Currently the majority of the codes and guidelines are mainly qualitative and based on deterministic approaches, however the use of a probabilistic approach is strongly advised and still needs to be covered from the international scientific community.

1.3.1 Risk evaluation

From a general point of view, risk (R) is obtained from the combination of three quantities: the Hazard (H), Vulnerability (V) and Exposure (E).

Hazard is the probability that an action or event or state, that can potentially cause harm, occurs in a given area and time interval. Vulnerability is the probability of a structural system to suffer consequences due to the occurrence of one or more events. Exposure is the measure of losses when a harmful event occurs, in terms of human losses, economic and cultural value.

Consequences can be divided into human safety (i.e., fatalities or injuries), business (loss of income or customers), economic (damage to the building or the surrounding properties), environmental (reversible or irreversible damage) and socio-political (increase of public fears, loss of reputation, loss of political support). In Eurocode EN 1991-1-7, structures are qualitatively categorized as function of

their consequence of failure and divided into Consequence Classes (CCs) as follows:

- *Consequence class 1 – limited consequences*:
  "single occupancy houses not exceeding 4 storeys / agricultural buildings / buildings into which people rarely go, provided no part of the building is closer to another building, or area where people do go, than a distance of 1½ times the building height"

- *Consequence class 2 – medium consequences – 2a (lower risk group)*:
  "5 storey single occupancy houses / hotels not exceeding 4 storeys / flats, apartments and other residential buildings not exceeding 4 storeys / offices not exceeding 4 storeys / industrial buildings not exceeding 3 storeys / retailing premises not exceeding 3 storeys of less than 1000 m^2 floor area in each storey / single storey educational buildings / all buildings not exceeding two storeys to which the public are admitted and which contain floor areas not exceeding 2000 m^2 at each storey";

- *Consequence class 2 – medium consequences – 2b (upper risk group)*:
  "hotels, flats, apartments and other residential buildings greater than 4 storeys but not exceeding 15 storeys / educational buildings greater than single storey but not exceeding 15 storeys / retailing premises greater than 3 storeys but not exceeding 15 storeys / hospitals not exceeding 3 storeys / offices greater than 4 storeys but not exceeding 15 storeys / all buildings to which the public are admitted and which contain floor areas exceeding 2000 m^2 but not exceeding 5000 m^2 at each storey / car parking not exceeding 6 storeys";

- *Consequence class 3 – high consequences*:
  "all buildings defined above as Class 2 Lower and Upper Consequences Class that exceed the limits on area and number of storeys / all buildings to which members of the public are admitted in significant numbers / stadia accommodating more than 5000 spectators / buildings containing hazardous substances and/or processes".

While for CC1 structures no specific considerations are necessary, for CC2 it is recommended a prescriptive design and detailing rules as well as simplified analyses with equivalent static loads are suggested. More details on the prescriptive design approach are given in the following section. Regarding CC3 structures, a systematic risk analysis should be considered, involving the use of dynamic analyses and non-linear models.

The perception of risk strongly depends on the actors involved in the risk-assessment such as analysts, individuals, governments and decision-makers. In general, individuals have a tendency to perceive the risk related to the event focusing on its magnitude rather than on its consequences. For instance, people

perceive an airplane crash riskier than road accidents, even if from a statistical point of view road accident imply a larger hazard than an airplane crash, being more frequent. Thus, the level of acceptable risk is strongly subjective and requires many quantitative and qualitative considerations.

Progressive collapse risk assessment in case of buildings has to be related to the risk of structural collapse. In general, the level of risk associated to structural collapse is identified as *de minimis* risk (Pate-Cornell, 1994), which represents the probability below which the society does not require regulatory action. This value is assumed to be 10^{-7}/year. A more detailed evaluation on the risk of progressive collapse is given in the following subsection.

1.3.2 Probabilistic risk analysis (PRA)

Probabilistic risk analysis can be adopted to quantify the risk associated with an extreme event. Robustness is related to the consequences of a local damage caused by an abnormal load. In this case the risk can be computed as follows:

$$P[C] = P[C \mid LD] \cdot P[LD \mid H] \cdot P[H] \qquad (1.1)$$

where:

- *P[H]* is the occurrence probability of the abnormal event *H*, assumed equal to the mean annual occurrence rate λ_H;
- *P[LD|H]* is the probability of local damage *LD* given the occurrence of the event *H*;
- *P[C|LD]* is the probability of structural collapse *C* given the state of local damage *LD*;
- *P[C]* is the annual probability of structural collapse *C*.

In order to mitigate the risk associated with a disproportionate or progressive collapse, three different measures are possible:

- *hazard mitigation* which is based on the reduction of the probability of occurrence of accidental events. This can be dealt by isolating the structure from exposure to such events, reducing the value of *P[H]*;
- *local vulnerability mitigation*, based on the reduction of the direct consequence of an accidental event, i.e., *P[LD|H]*, reducing the possibility of a disproportionate or progressive collapse because the local damage does not occur. This is done by acting on the local behavior of structural elements by strengthening or protecting them;
- *global vulnerability mitigation*, based on the reduction of the consequence of a local damage, i.e., *P[C|LD]* which reduces the possibility of a disproportionate or progressive collapse. This is done by acting on the global behavior of the structure by means of robustness measures.

While the first two mitigation strategies are related to the prevention of the collapse activation, the second is based on the prevention of the damage propagation, and, thus, it is strictly related to the concept of robustness. Furthermore, the reduction of *P[LD|H]* can be uneconomic and difficult to be realized because it is required to consider all the possible hazardous events and consequent local damages. For this reason, if no measures are considered to mitigate the local damage in case of an accidental condition (i.e., if *P[LD|H]* is equal to unity), the probability of collapse given in Eq. (1.1) becomes:

$$P[C] \approx P[\mathrm{C} \,|\, \mathrm{LD}] \cdot \lambda_H \qquad (1.2)$$

By assuming that the probability of extreme events is in the order of 10^{-6}/year to 10^{-5}/year (Burnett, 1975; Ellingwood and Leyendecker, 1978), knowing that an acceptable risk level for global collapse is equal to the *de minimis* (i.e., 10^{-7}/year) and substituting those values in Eq. (1.2), the target for *P[C|LD]* is in the order of 10^{-2}/year to 10^{-1}/year. This value of conditional collapse probability corresponds to a target reliability level β_t of 1.5. This target reliability is the recommended value given in CNR Guidelines (CNR, 2018). As a conclusion, it should be underlined that the target reliability level β_t is conditional to the local damage definition. Thus, the worst situation in terms of location of local damages should be selected depending on the configuration of both the structural and no-structural elements in the building.

More details on structural reliability are given in Chapter 2.

1.4 Design methods against progressive collapse in International Codes

1.4.1 Overview of design strategies

Design approaches to treat accidental scenario can be classified according to ASCE/SEI 7-05 (2005) as function of:

- type of approach: prescriptive or performance-based design;
- method used for the design of the structural system: direct or indirect design;
- definition of the risk scenario: threat-specific or threat-independent design.

Prescriptive or performance-based design method

A schematic representation of the approach to increase robustness based on the typology of design (i.e., prescriptive or performance-based) is given in Figure 1.4 as studied by Haberland and Starossek (2009).

Prescriptive approach is also defined code-based design due to the fact that it is based on prescriptive tools incorporated in building codes and guidelines. This approach provides minimum requirements that the structure should maintain (e.g.,

minimum strength of materials, minimum stiffness of members, minimum quantity of reinforcement detailing). Since those prescriptions are based on experience with similar building structures, it is not possible to apply this approach to buildings having irregular or uncommon configurations. In case of a prescriptive approach, you can assume to always adopt an indirect design method, since you do not need to directly define the objectives and the verifications, as illustrated in Figure 1.4.

On the other hand, performance-based design explicitly accounts for the performance of the structure under the accidental condition and, thus, requires the identification of the hazard scenarios. The structural engineer does not need to apply any prescribed approach and thus has more flexibility if compared to the previous case but needs to meet the required performance. A performance-based approach can be either direct or indirect and the hazard scenario can be both threat-specific or threat-independent.
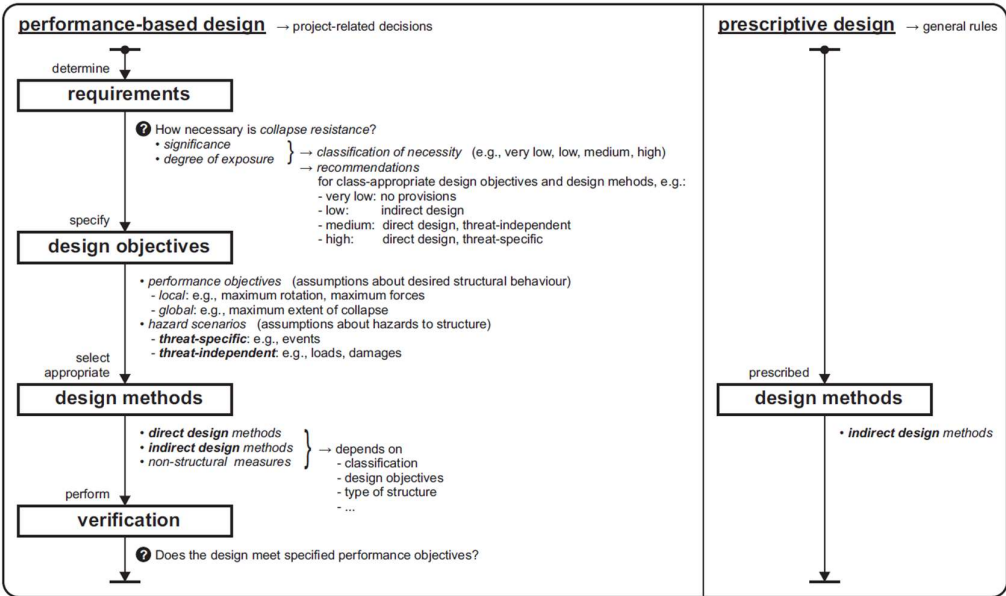
Figure 1.4 Framework for prescriptive and performance-based design method (Haberland and Starossek, 2009).

Direct or indirect design method

Those type of approaches are the most common in guidelines and standards for the prevention of progressive collapse. The difference is that indirect approaches impose limitations on the choice of the structural system and are mainly prescriptive, while direct ones explicitly evaluate the resistance of the structure.

Indirect design methods are mainly prescriptive and enhance robustness by guaranteeing the redundancy of the system (i.e., increasing the level of connection between the components of the system, increasing the membrane capacity of beams and slabs, increase the redistribution of stresses along the members).

In particular, this method aims at imposing minimum levels of strength, ductility and continuity. From a practical point of view, this method reckons on (Figure 1.5):

- tie elements (peripheral and internal ties in the two main directions of the floor, horizontal ties between columns or walls, vertical ties);
- redundancy (provide a secondary load path by means of transfer girder systems or upper-level trusses).

Ties are in general the most common among indirect design methods and are mainly applied to structures with low risk of progressive collapse. The tying in codes (i.e., EN1991-1-7; ASCE/SEI 7-16; IBC09; UFC 4-023-03) are achieved by providing a minimum tying force requirement.
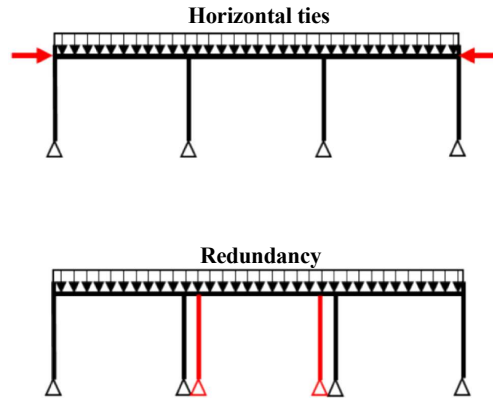
Figure 1.5 Schematic representation of *indirect design methods* (Voulpiotis et al., 2022).

The direct design method is performed by the explicit evaluation of the resistance capacity of the structure against disproportionate collapse.
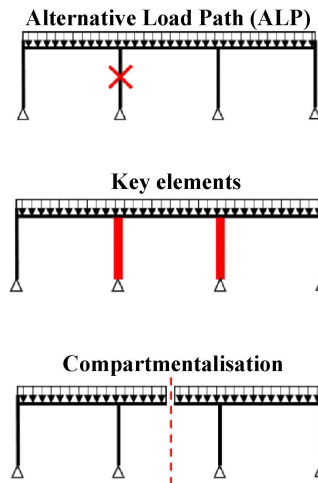
Figure 1.6 Schematic representation of *direct design methods* (Voulpiotis et al., 2022).

This method relies on three possible approaches (Figure 1.6):

- alternative load path (ALP) analysis: this approach consists in explicitly compute the ability of the structure to redistribute the load when a specific local damage occurs. Practically speaking, the structure is deprived from a supporting structural element, independently from the threat causing the

element removal. The element to be removed in case of buildings is in general a supporting column. This approach is widely accepted from codes (EN1991-1-7; ASCE/SEI 7-16; GSA2013; UFC 4-023-03; DoLG2010);

- key elements design (or local resistance method): this approach aims at increasing the resistance capacity of structural elements when damaged by abnormal loads. In this way, local damage is prevented and, thus, no attention is paid on the possible transfer of local damage as in the ALP method. This method, widely recommended in codes (EN1991-1-7; UFC 4-023-03; DoLG2010), is in general recommended when ALP methods are insufficient;

- compartmentalization: this method is based on the isolation of the structure where the local damage occurs in order to avoid its spread on other parts of the structure. This is obtained in two ways: by designing strong elements that stop the collapse of weak elements of the compartment, or by designing weak elements which collapse and disconnect the damage part from the rest.

Threat-specific or threat-independent design method

In threat-specific approach the engineer directly accounts for the threats that could possibly endanger the structure. The evaluation of these risks should be performed by a specific risk-assessment approach and their effects on the structure should be investigated. This approach is considered unfeasible (Starossek, 2009) since it is not possible to account for all the possible abnormal events and their quantification. In addition, their effects are not straightforward to be quantified.

On the other hand, threat independent approach aims at providing a minimum level of collapse resistance without quantifying nor identifying the original cause. Thus, the approach relies on the quantification of nominal loads or national removal of an element.

1.4.2 Design strategies according to EN1991-1-7

Eurocode EN1991-1-7 Annex A defines a flowchart to be followed in case of accidental design situations, as illustrated in Figure 1.7. In detail, accidental actions can be identified or unidentified.

In the first case (i.e., identified accidental actions), the mitigation is reached by applying the following approaches:

- applying prescriptive approaches to increase robustness by guaranteeing minimum requirements (e.g., three-dimensional tying, minimum level of ductility for structural members);
- preventing or reducing the severity of the accidental action by adopting protecting measures (e.g., protective bollards or safety barriers);
- assume that the accidental load will damage the structure, but it is designed in such a way to sustain the local damage (i.e., providing sufficient ductility, strength and redundancy or key element design).

For the unidentified accidental loads, a wide range of possible events are covered in order to mitigate the risk of accidental loads. Also, in this case there are three possibilities:

- provide enhanced redundancy by alternative load path method;
- designing key element on which the damage will occur such that it is able to sustain the application of the accidental load;
- applying prescriptive rules and detailing to provide acceptable robustness for the structure (i.e., providing sufficient ductility, strength and redundancy or key element design).
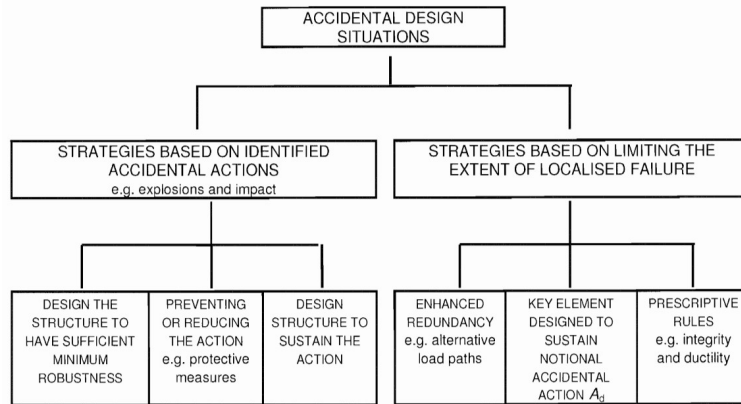
Figure 1.7 Strategies for accidental design situations (EN1991-1-7 Annex A).

Regarding the evaluation of the accidental load, EN 1990 – Basis of structural design gives a specific load combination in case of accidental design scenario. This combination should be adopted when the designer has to verify the robustness of a structure by computing the load bearing capacity against the accidental load (e.g., in case of notional member removal or key element method). The accidental combination reads as follows:

$$\sum_{j\geq1} G_{k,j} \;"+"\; P \;"+"\; A_d \;"+"\; \psi_{2,1} Q_{k,1} \;"+"\; \sum_{i\geq1} \psi_{2,i} Q_{k,i} \qquad (1.3)$$

where "+" and Σ implies "combination", $G_{k,j}$ are the characteristic values of the permanent loads, P is the prestressing load, A_d is the design value of the accidental load, $Q_{k,1}$ is the characteristic value of the leading variable load, $Q_{k,i}$ are the characteristic values of the other variable loads, $\psi_{2,1}$ is the factor for the quasi-permanent value of the leading variable load $Q_{k,1}$, $\psi_{2,i}$ are the factors for the quasi-permanent value of the i-th variable load $Q_{k,i}$.

1.4.3 Design strategies according to ISO2394:2015

In Annex F of ISO2394 an overview of the design strategies for robustness is provided, to be applied where a risk and reliability-based approach is not required. In particular, robustness measures can be classified in:

- event control (EC): it is an indirect method that aims at reducing the probability of occurrence $P(H)$ and/or the intensity of the accidental load by means of monitoring, quality control during construction maintenance and repair, corrective and preventing measures. Specifically, preventing measures can be: installation of fire suppression systems, smoke detectors and alarms, control and limiting of fire loads and ignition sources, prohibition of storage of explosive, use of structural health and monitoring system, installation of protective systems against impacts. In addition, care should be taken on the location of the structure;
- specific load resistance (SLR): this is an approach that aims at reducing the probability of local damage due to the occurrence of the event $P(LD|H)$ by enhancing strength and stiffness, relying on strain hardening and ductility of materials, guaranteeing ductile behavior of members, using mechanical devices. In general, this approach is suitable for structures with a limited number of key elements or when ALP is not applicable.
- alternative load path method (ALP), it is a direct method that aims at reducing the probability of spread damage due to the occurrence of a local damage $P(C|LD)$, relying on redundancy, capacity design, sacrificial and protective devices, continuity and ductility, enhancing strength and stiffness.
- reduction of consequences: this is an indirect approach that aims at reducing the consequence of progressive or disproportionate damage, relying on segmentation and compartmentalization, redundancy of the services of the facility, warnings, interventions and rescue. In practice, this is obtained by means of electro-mechanical equipment, backup facility, emergency planning, automatic sprinkler systems, video-monitoring systems.

1.5 Measure of Structural robustness

Although qualitative evaluation of structural robustness allows a definition of the response of a structure against progressive collapse, quantification is needed when the purpose is to estimate the safety level in decision making.

According to Starossek (2018) and Lind (1995), to quantitatively estimate the robustness, the following criteria should be respected:

- *objectivity*, for which a robustness measure should be independent from the decisions of the user;
- *expressiveness*, for which the measure should guarantee differences between robust and non-robust structures;
- *calculability*, meaning that the computational cost to derive the robustness measure should be relatively low;
- *simplicity*;
- *generality*, meaning that the measure can be applicable to any kind of structure.

A robustness index is in general a scalar that goes from 0 and 1. The lower limit indicates that the structure has any reserve of strength after the initial damage, while the opposite occurs for the upper limit (i.e., the structure is not sensitive to the abnormal load).

In the following, the most common indices to measure structural robustness are given, distinguishing between deterministic, reliability-based calculations and risk-based. Going from the first to the last approach, the complexity of the calculation increases.

1.5.1 Deterministic measures for robustness

The large part of deterministic indices is threat independent, meaning that they provide dimensionless factor that are not function of the specific threat which induces an eventual progressive collapse. In the following, the most common deterministic-based indices for the evaluation of structural robustness are listed (Table 1.3).

Table 1.3 Deterministic-based measures for structural robustness.

Measure	Formulation	Reference
Robustness factor	$R = \dfrac{L_{damaged}}{L_{design}}$	Frangopol and Curley (1987)
Residual influence factor	$RIF_i = \dfrac{RSR_{fail,i}}{RSR_{intact}}$	Chen et al. (2016)
Robustness index	$\rho = \dfrac{\|\bar{s}\|}{\|\bar{s}^*\|}$	Biondini and Frangopol (2008)
Energy-based robustness measure	$R_e = 1 - \max_j \dfrac{E_{r,j}}{E_{f,k}}$	Starossek and Haberland (2011)
Overload factor	$OF = \dfrac{L_u}{L_d}$	Khandelwal (2011)
Pushdown based robustness measure	$\lambda = \dfrac{C_V}{D_V}$	Parisi and Augenti (2012)
Relative robustness index	$RRI = \dfrac{L_{damaged} - L_{design}}{L_{intact} - L_{design}} = \dfrac{\lambda_{damaged} - 1}{\lambda_{intact} - 1}$	Fallon et al. (2016)
Stiffness-based robustness measure	$R_S = \min_j \dfrac{\det K_j}{\det K_0}$	Starossek and Haberland (2011)

Where:

- $L_{damaged}$ is the load bearing capacity of the damaged system;
- L_{design} is the design load;
- $RSR = R_c/S_c$ is the reserve strength ratio obtained from the characteristic value of base shear capacity R_c and the design load corresponding to ultimate limit state S_c;
- $RSR_{fail,i}$ is the reserve strength ratio for the i-th member under failure;
- RSR_{intact} is the reserve strength ratio for intact system;
- $\bar{s}$ is the displacement vector of the intact system;

- $\bar{s}^*$ is the displacement vector of the damaged system;
- $E_{r,j}$ is the energy released during the initial failure of the j-th element and contributing to damage a k-th element;
- $E_{f,k}$ is the energy required to damage the k-th element;
- L_u is the ultimate capacity of the system;
- L_d is the nominal gravity load;
- C_V is the vertical load-bearing capacity of the damaged structure after member removal;
- D_V is the vertical design load in accidental combination;
- $\lambda_{damaged}$ is the maximum load multiplier of the damaged system;
- λ_{intact} is the maximum load multiplier of the intact system.

1.5.2 Reliability-based or risk-based measures for robustness

Reliability-based and risk-based quantification approaches explicitly consider uncertainties associated with an accidental design situation, related to both material and load properties. In addition, while deterministic approaches consider deterministically the removal of an element, a probabilistic approach allows to account for the probability of losing more than one component as a consequence of a single event.

Although the larger computational effort, this approach can provide a more comprehensive evaluation of the structural robustness. In the following, the most common reliability-based and risk-based indices are listed (Table 1.4).

Table 1.4 Reliability-based and risk-based measures structural robustness.

Measure	Formulation	Reference
Robustness index	$\beta_r = \dfrac{\beta_{intact}}{\beta_{intact} - \beta_{damaged}}$	Frangopol and Curley (1987)
Redundancy index	$RI = \dfrac{P_{f(dmg)} - P_{f(sys)}}{P_{f(sys)}}$	Fu and Frangopol (1990)
Vulnerability index	$V = \dfrac{P(r_d, S)}{P(r_i, S)}$	Lind (1995)
Robustness index	$ROI = \min_i \dfrac{P_{f0}}{P_{fi}}$	Maes et al. (2006)
Robustness index	$I_{rob} = \dfrac{R_{dir}}{R_{dir} - R_{ind}}$	Baker et al. (2008)
Robustness index	$I_{rob} = \dfrac{\beta_{damaged}}{\beta_{intact}}$	Sørensen (2011)

Where:

- β_{intact} is the reliability index for the intact system;
- $\beta_{damaged}$ is the reliability index for the damaged system;
- $P_{f(dmg)}$ is the probability of the damage occurrence;
- $P_{f(sys)}$ is the failure probability of the system;

- $P(r_d,S)$ is the failure probability of the structure as function of the resistance of damaged structure r_d and the action S;
- $P(r_i,S)$ is the failure probability of the structure as function of the resistance of the intact structure r_i and the action S;
- P_{f0} is the failure probability of the undamaged structure;
- P_{fi} is the failure probability of the structure due to the damage on the i-th member;
- R_{dir} is the direct risk associated with the localized damage;
- R_{ind} is the indirect risk of progressive collapse.

1.6 Structural robustness for reinforced concrete buildings

Compared to other type of structures, cast-in-situ reinforced concrete buildings can ensure an adequate level of structural performance under extreme events thank to many advantages. In fact, ductility at the sectional level can be guaranteed by proper reinforcement detailing, structural continuity is easy to be designed, buckling of columns is not common since the size of the columns is large enough and membrane effects of beams and slabs can strongly improve structural robustness.

However, the large masses that characterize RC buildings are difficult to be born by the structural elements when the alternative load path has to be reached. In addition, brittle failures due to an inadequate shear reinforcement detailing can occur, not guarantying a ductile mechanism. For this reason, an approach similar to capacity design principles (Paulay and Priestley, 1992) proper of the seismic design is welcome, in order to reach a hierarchy of strengths between brittle and ductile behavior (Castaldo and Miceli, 2024; Castaldo et al., 2022; Gino et al., 2023).

In the following, some key aspects of the mechanical behavior of RC buildings in case of robustness evaluation are deepened.

1.6.1 Membrane effects in RC structures

One of the advantages of RC buildings is the possibility of exploiting the membrane action effects. Membrane effects can be distinguished between those related to beam-like elements and those regarding slab-type elements. More precisely, in case of beam-types members it is better to identify them as axial stress conditions rather than membrane effects (which involve tangential and radial stresses)

In general, these effects strongly depend on the following parameters:

- slenderness of the members;
- ratio between the length of the element and the height of the cross-section;
- reinforcement ratio;

- mechanical properties of steel;
- mechanical properties of concrete.

Membrane stresses in *beam-type elements* arise under bending behavior when large displacements are involved. This is not only the case of removal of a supporting element (i.e., Figure 1.8b), but also when excessive vertical loads are applied to the structural system (i.e., Figure 1.8a). The structural response in both cases can be described by evaluating the load-deflection curve, as shown in Figure 1.8c. By comparing the curve obtained when membrane stresses are involved with the one where those effects are not present, it is possible to observe an increase in the resistance of the structure for the first case. In fact, the curve related to the response without membrane forces, is obtained by disregarding the geometrical non-linearities as well as the membrane effects.

In the first stage, this effect determines compressive axial actions due to the cracking of concrete and consequent elongation of the beam, which is constrained by the presence of the lateral columns that compress the beam itself. In general, this behavior is more marked if the span length is lower, and it is influenced by the cracking state of concrete as well as the effects of shrinkage and creep. Then, tensile actions arise due to the plasticization of the cross-sections and thanks to the presence of longitudinal reinforcement that acts as a tie. Contrary to the compressive behavior, the tensile one, also called catenary effect, is more enhanced for larger spans, and it is not influenced by the state of the concrete but only by the ultimate strain of longitudinal reinforcement as well as its geometrical ratio.

Furthermore, the axial actions are strongly influenced by the constraint conditions: the larger the stiffness of the lateral constraints, the larger the catenary effect.
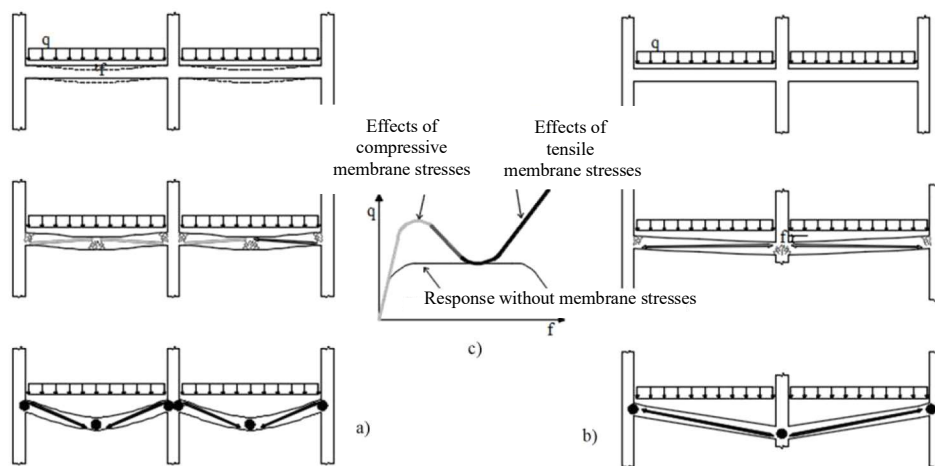
Figure 1.8 Axial effects in beam-like elements (modified from CNR, 2018): (a) due to excessive loads; (b) due to removal of a supporting element; (c) displacement load curve.

In case of *slab-type elements*, membrane effect consists in the arise of radial and tangential stresses that contribute to an increase of the flexural shear and punching resistance.

This phenomenon is due to the cracking of the extrados in the plane of the slab (Figure 1.9), in a section close to the column (where maximum negative bending moment is present). This causes a difference in stiffness between the uncracked and cracked part, causing the former to be a constraint to the radial expansion for the latter. Thus, a tangential stress ring forms which equilibrates the radial compressive condition.
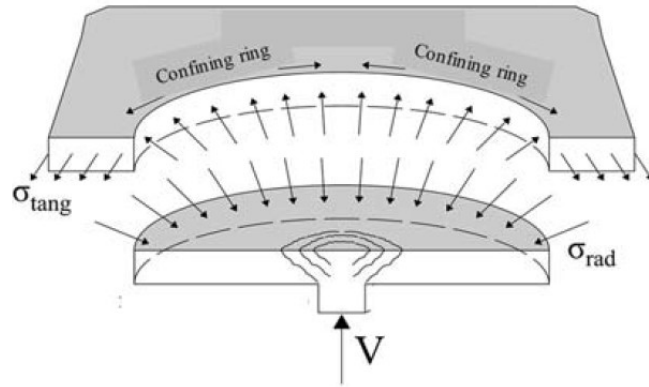
Figure 1.9 Compressive membrane forces in slab-type elements (Belletti et al., 2018).

1.6.2 Ties in RC structures

In general, buildings with rectangular plan can be designed with four types of ties (peripheral, internal, horizontal and vertical ties). In codes, two formulations are present regarding the modelling of ties in RC buildings: the first is the approach proposed by Eurocodes 2 (EN1992-1-1) and the second is the one proposed by DoD Guidelines (UFC 4-023-03).

Ties according to Eurocode 2

Eurocode 2: Design of concrete structures – Part 1-1: General rules and rules for buildings defines indications to design ties in reinforced concrete buildings. In detail, ties in floor (Figure 1.10) are designed as follows.

- Peripheral ties (Figure 1.10A): at each floor and roof level a continuous peripheral tie within 1.2 m from the edge is recommended. The resisting tensile force of the ties is:

$$F_{t,per} = 10\,kN/m \cdot L \geq 70kN \qquad (1.4)$$

where L is the length of the final span expressed in m.

- Internal ties (Figure 1.10B): at each floor and roof level a continuous internal tie should be placed in the two orthogonal directions and should be effectively anchored to peripheral ties or to column and walls. The resisting tensile force of the internal ties per unit width in both directions is:

$$F_{t,int/m} = 20 \, kN/m \tag{1.5}$$

In addition, in floors without screeds where ties can not distribute transversely to the direction of the secondary beams of the floor, ties can be placed along the secondary beams or joists, with the following requirement:

$$F_{t,int} = 20 \, kN/m \cdot (L_1 + L_2)/2 \geq 70 \, kN \tag{1.6}$$

where L_1 and L_2 are the length of the spans in meter of the floor slabs on two sides.

- Horizontal ties to columns and walls (Figure 1.10C): at each floor and roof level edge columns and wall should be tied horizontally to the structure. The resisting tensile force per unit meter of facade for each column should be equal to 20 kN/m and the force must not exceed 150 kN per column.

A - peripheral tie   B - internal tie   C - horizontal column or wall tie
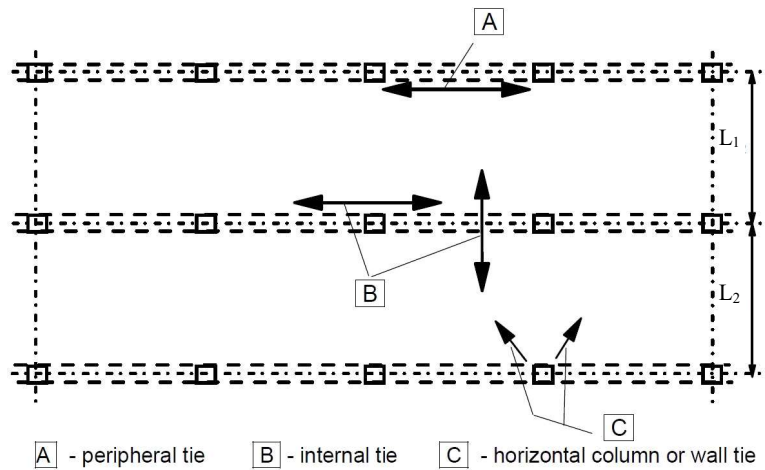
Figure 1.10 Ties design in Eurocode 2 (CEN, 2004).

Eurocode 2 also defines the requirements for vertical ties for cast-in situ buildings, by ensuring continuity of longitudinal reinforcement of the columns. In addition, if the building is divided into portions, the ties should be provided for each portion of the building.

Ties according to General Service Administration

This approach can be applied to framed structure with at least 4 spans in each direction. Ties are defined in order to guarantee a minimum level of ductility, continuity and redundancy.

In particular, a distributed load at the floor level is defined as follows:

$$w_f = 1.2D \cdot 0.5L \tag{1.7}$$

where D is the dead load and L is the variable load.

Then, the following type of ties are considered.

- Peripheral ties in floors: at each floor and roof level a continuous peripheral tie within 1.0 m from the edge is recommended. For framed and two-way load bearing wall buildings, the resisting tensile force of the ties in kN is:

$$F_{t,p} = 6w_f L_1 L_p + 3W_c \tag{1.8}$$

where L_p is equal to 1 m and W_c is equal to 1.2 times the permanent load due to the infill having span length L_1.

- Internal ties in floors: at each floor and roof level a continuous peripheral tie within 1.0 m from the edge is recommended. The resisting tensile force per unit width in the longitudinal or transverse direction:

$$F_{i/m} = 3w_f L_1 \tag{1.9}$$

where L_1 is the largest distance between the columns that support two adjacent floors.

Regarding vertical ties, they are guaranteed by providing continuous longitudinal reinforcement in columns. In addition, the strength is evaluated as function of the design floor load w_f multiplied for the influence area of the column.

1.6.3 Experimental tests on beam-column subassemblies and capacity curve

In the past years, several experimental tests have been performed in order to study the structural robustness of beam-column subassemblies (i.e., systems composed by two-spans beams and two or three columns). The test is usually carried out by simulating the loss of the central column to study the capability of the subassembly to carry out the load, which is applied on the removed column. The pioneers of this type of tests were Sadek et al. (2011) and Lew et al. (2011). The difficulty of this experimental tests is to simulate the constraint conditions of the subassembly as if it was part of the entire frame. For example, Lew et al. (2011) and Yu and Tan (2013) simulated the axial-restraint made by the indirectly-affected frame on the directly-affected one by connecting the subassembly to a steel frame and a reaction wall. This test was conducted on two specimens with different seismic detailing. Yu and Tan (2014) and Yu and Tan (2017) worked on the effects of boundary conditions on two-spans three-columns sub assemblies. In addition, they investigated the possibility to enhance the catenary capacity by modifying the structural detailing. Forquin and Chen (2017) tested four specimens in order to study the influence of sliding and pin connections on the boundary conditions. A different type of loading configuration was adopted by Yu et al. (2014), where the dynamic behavior of a beam-column subassembly with non-seismic detailing was studied by causing an explosion.

Other researchers were mainly focused on studying the influence of slab membrane effects on beam-slab-column specimens. In Ren et al. (2013) and Lu et al. (2013) specimens with and without the presence of the slab were tested in order to compare the results.

Structural behavior in case of a supporting column loss

To better understand the structural behavior of a beam-column subassembly in case of a supporting column loss, the test of Lew et al. (2011) is considered. In detail, the experimental work focuses on two beam-column assemblies composed by three columns and two beams. The subassemblies were extracted from the second floor of two ten-story concrete moment-resisting frame buildings and for two seismic design categories (SDC) (i.e., SDC C and SDC D according to American Concrete Institute Building Code 318-02).
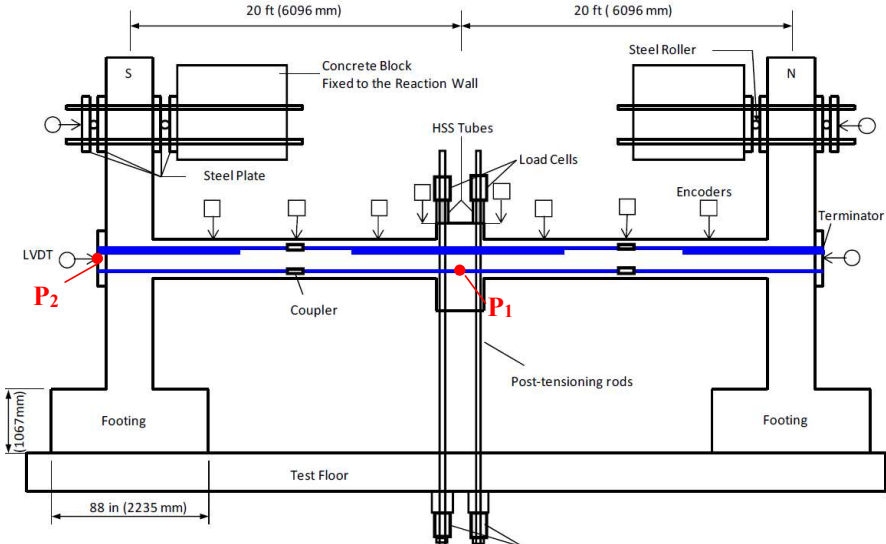
Figure 1.11 Test setup of the specimen IMF (modified from NIST, 2011).

In detail, the specimen IMF was extracted from an intermediate frame of the SDC C building, while the specimen SMF was extracted from a special moment of the SDC D building. In the following, the results and considerations for the IMF prototype are given but similar conclusions can be drawn also for the SMF configuration. More details on both tests and on numerical results are given in NIST Technical Note 1720 (2011).

The test setup of IMF specimen is given in Figure 1.11. The test consisted in the application of a monotonic increasing vertical displacement on the unsupported central column (i.e., point P_1 in Figure 1.11) by means of hydraulic jacks, up to reaching collapse. Regarding the constrain conditions, the tops of the two end columns were restrained from horizontal movement by a two-roller constraint. One roller was placed on the interior (beam side) face of the column and the other on the exterior face. These rollers could slide on 51 mm steel plates which were fixed to the interior and exterior faces of the column. Steel plates were anchored to the

columns by means of 32 mm post-tensioning bars, which were anchored to a reinforced concrete block on the reaction wall.

By analyzing the load-deflection curve (Figure 1.12a) in the point of displacement application (i.e., point P_1 in Figure 1.11), after reaching the initial peak load, a softening was observed. Then, the load started to increase again up to failure. The vertical displacement at which this increase was registered coincided with around the depth of the beam. Failure occurred because of fracture of the beam lower longitudinal reinforcement close to the central column. The ultimate load was larger than the one reached in the first peak.
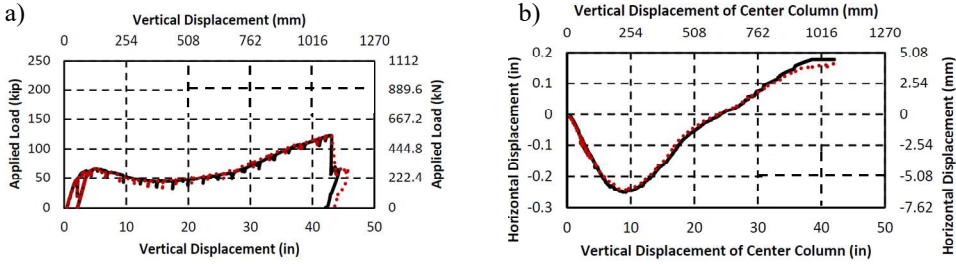
Figure 1.12 Results of the experimental test IMF (modified from NIST, 2011): (a) Load-deflection curve on P_1; (b) Horizontal displacement on P_2 vs deflection on P_1. The two colors refer to mirror positions of the transducers.
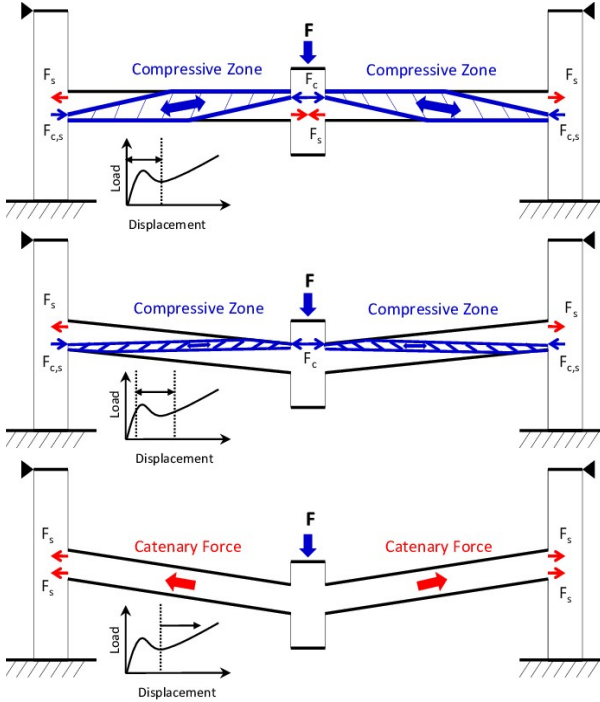
Figure 1.13 Stages of the structural behavior of beam-column subassemblies under supporting column loss scenario (NIST, 2011).

Regarding the horizontal displacement in correspondence of the beam-column node (i.e., point P_2 in Figure 1.11), the behavior is shown in Figure 1.12b. At first,

the columns move towards the internal part and then, when the load started to increase again, the movement was shifted to the opposite direction.

This behavior can be described by recognizing three different stages (Figure 1.13):

- *flexural stage (a)*: where the beam is first subjected to a flexural behavior, causing the increasing in load up to formation of plastic hinges at the beam column connections. Because of the cracking of concrete, the beams tend to elongate while the columns constrain this elongation causing the development of compressive arching forces on the beams. In this stage, point P_2 tends to move horizontally in the outward direction because of the beams elongation caused by cracking;
- *softening stage (b)*: characterized by a decrease of the carrying capacity of the structure caused by the yielding of reinforcement and crushing of concrete. In this phase, the compressive arching forces reduce, implying a shift in the direction of the horizontal movement of the columns.
- *catenary stage (c)*: where tensile axial forces are fully exploited, and the resisting mechanism is fully born by catenary action, because the flexural beam contribution is almost zero. In this stage the load is carried by the longitudinal reinforcement which acts as a tie. The horizontal displacement of the column changes sign, implying that the columns are displaced outward due to the catenary activation.

In the following, the peak of the capacity curve in the flexural stage is identified as $P_{MAX,FL}$, while the ultimate resistance is indicated by P_{ULT}. It should be emphasized that the third stage is possible only if the longitudinal reinforcement is continuous over the support in correspondence of the lost column, otherwise the catenary force can not be mobilized, and the failure occurs during the softening stage.

1.6.4 Design considering the removal of a column

The bearing capacity of a framed system in case of progressive collapse can be modelled in a simplified way by assuming the hypothesis of pure flexural or pure membrane behavior.

In detail, the maximum load in bending regime (i.e., $P_{MAX,FL}$) can be computed as:

$$P_{MAX,FL} = \frac{2(M_{PL}^+ + M_{PL}^-)}{L} \tag{1.10}$$

where, the plastic moments at the sections of the beams close to the beam-column nodes can be computed neglecting the reinforcement in compression as follows:

$$M_{PL}^+ = 0.9 \cdot A_s^+ \cdot f_{yd} \cdot d \tag{1.11}$$

$$\mathrm{M}_{PL}^{+} = 0.9 \cdot A_s^{-} \cdot f_{yd} \cdot d \qquad (1.12)$$

where A_s^{-} and A_s^{+} are, respectively, the tensile reinforcements in the sections close to the beam-column connection for negative and positive bending moment, d represents the effective depth of the beam and f_{yd} is the design value of the yielding strength for the steel reinforcement. It should be underlined that this computation neglects the presence of normal compressive forces which would increase the flexural peak as well as the presence of reinforcement in the compressed area. However, current and past literature studies (Jian et al., 2014; Naji, 2017; Pham and Tan, 2017; Li et al., 2011) are developing methods to predict the behavior of beam-column sub-assemblages by comparison with experimental results. These investigations try to capture the non-linear effects allowing the derivation of the vertical load and displacement corresponding to the formation of plastic hinges, the displacement at the onset of catenary effect as well as the yielding and rupture of longitudinal reinforcement.

Regarding the ultimate load at the end of the catenary effect (i.e., P_{ULT}), it can be computed as:

$$P_{ULT} = \frac{2\delta}{L} \cdot A_{s,cont} \cdot f_t = 2\theta_u \cdot A_{s,cont} \cdot f_t \qquad (1.13)$$

where δ is the displacement of the point where the column is accidentally removed, θ_u is the ultimate chord rotation, L is the span length of the beam and $A_{s,cont}$ is the continuous reinforcement over $2L$, f_t is the failure stress of reinforcement. The ultimate chord rotation should be evaluated according to experimental results as mentioned above.

1.6.5 Structural modelling to simulate progressive collapse

The progressive collapse of a RC structure is a dynamic phenomenon involving a sudden modification of the structural configuration from intact to damaged. This transition involves non-linearities which should be taken into account. In fact, the transition from elastic to non-linear field allows to dissipate a quantity of energy which is released during the progressive collapse scenario.

In principles, four types of analysis can be performed:

- Linear static analysis: in this analysis the dynamic phenomenon is modelled by statically amplifying the load. This type of analysis has the advantage that can be managed in a simpler way also by non-expert engineers. At the same time, it is not possible to account for both geometrical and material non-linearities, catenary or membrane effects and redistribution of internal stresses.
- Non-linear static analysis: in this case both geometrical and material non-linearities as well as catenary or membrane effects can be accounted for.

31

However, constitutive laws for material as well as non-linear behavior of the connections should be properly modelled. This requires to be expert in the field of modelling because the different choices are fundamental to capture the structural behavior. A drawback of this approach is that the dynamic effects can be taken into account only in a simplified way by considering proper load amplifications.

- Linear dynamic analysis: this method has the same disadvantage of the linear static analysis since it neglects the non-linearities but accounts for the dynamic effects.

- Non-linear dynamic analysis: this method represents the most complete for accounting for both non-linear and dynamic effects involved in a progressive collapse scenario. At the same time, the required expertise is large and the computational effort increases, especially, when large structures are studied.

Non-linear pushdown analysis

Considering the improvements of numerical codes during the past years, non-linear analysis is for sure required to better understand progressive collapse phenomena. The capacity of absorbing and dissipating the energy during a progressive collapse is strongly dependent on the constitutive laws of materials and on the connections of the structural elements forming the structural system. At the same time, dynamic analysis is not always necessary since it requires a step-by-step integration which not only is time consuming but affected by numerical convergence problems. For this reason, an equivalent static approach, also called pushdown analysis, can be thought as the proper compromise between computational effort and accuracy of the results.

Pushdown analysis can be performed by applying two possible methods:

- Load Controlled Pushdown Analysis (LC-PD): this method is the one proposed by the U.S. General Service Administration Guidelines. It consists in increasing step-by-step the gravity load in case of a column removal scenario. In this case, the load factor gives the amount of gravity load that the structure is able to sustain in case of column removal. The drawback of this approach is that it is not possible to capture the softening behavior of the structure.

- Displacement-Controlled Pushdown Analysis (DC-PD): this method is similar to the previous one, but the step-by-step evolution is applied to the displacement history. In this case, the softening behavior can be captured.

Chapter 2

Structural reliability

2.1 Introduction

When repeating the measurement of a physical phenomenon, it never gives back always the same result. Multiple results arise and some outcomes appear to be more frequent than the others. The occurrence of multiple results for a given phenomenon is identified by the term *uncertainty* or *randomness*.

Uncertainties affect all the fields of engineering problems. For example, in structural engineering the ultimate tensile strength of a bar under uniaxial tensile testing is not always the same even if the "same" bar is tested. Thus, the ultimate capacity of a reinforcement bar has to be treated as a *random variable* (i.e., a parameter that is subjected to a certain degree of uncertainty).

The primary goal of any engineering problem is that the capacity (or resistance or supply) should satisfy at least the demand. For example, in structural or geotechnical engineering the supply is intended as the resistance or the strength of a member while the demand is the load or any of its effects. However, the majority of the parameters involved in the evaluation of both demand and capacity are subjected to many sources of uncertainty. Thus, the performance cannot be satisfied entirely but a satisfactory level of acceptance should be defined. In this context, reliability defines the probabilistic assurance of the performance that a structure should guarantee.

European Guidelines define structural reliability as the "*ability of a structure or a structural member to fulfil the specified requirements, including the design working life, for which it has been designed*".

In this chapter, the basic concepts behind the reliability problem formulation are discussed. At first, the basics of probabilistic analysis are given. Then an overview of the main uncertainties affecting the structural engineering problems follows. After that, the definition of the limit state function and the performance requirements to be guaranteed in case of new structures is evaluated. Finally, the different reliability methods (i.e., level III, level II, level I and level 0) are discussed.

2.2 Basics of probability theory

Before entering in the details of reliability theory, a brief overview of the basic aspects behind probability theory are herein given. Specifically, it is necessary to give an explanation of the following key concepts:

- *experiment* is defined as the realization of a certain set of conditions "π" and can be repeated an indefinite number of times. The result of an experiment allows to declare unequivocally "occurrence" or "non occurrence". In this context, it is always important to declare the set of conditions "π" in order to interpret correctly the results of an experiment;
- *random events* refer to experiments that are not unequivocally determined by the set of conditions "π". In this case, the results of such experiments could, but not necessarily, occur when the conditions "π" are met. In general, random events are represented by a capital letter (e.g., *A* or *B*). When an event is certain to occur every time, the condition are met, it is usually identified with the capital letter *U*, otherwise an impossible event is defined with the capital letter *V*.
- *sample space of a random experiment Λ* is the ensemble of the events that can be an outcome of the experiment and can be finite or infinite.

If an event *B* occurs every time the condition "π" is met, as a result of which another event *A* occurs, it is said that the event *A* implies *B* (i.e., $A \subset B$). It two events occurs simultaneously when the condition "π" is met, then the result is an intersection of the events (i.e., $A \cap B$). If at least one of the events *A* or *B* occurs at every realization of "π", the result is the union of the two events (i.e., $A \cup B$). The opposite of an event *A* represents its complementary and it is indicated as $\bar{A}$. Thus, the union between an event and its complementary is the certain event (i.e., $A \cup \bar{A} = U$), while the intersection is the impossible event (i.e., $A \cap \bar{A} = V$). A system of events A_i forms a complete system of events if their union gives the certain event *U*.

Random events obey to commutative, associative and distributive laws, as follows, respectively:

$$A \cap B = B \cap A, A \cup B = B \cup A \tag{2.1}$$

$$(A \cap B) \cap C = A \cap (B \cap C), (A \cup B) \cup C = A \cup (B \cup C) \tag{2.2}$$

$$(A \cap B) \cup C = (A \cup C) \cap (B \cup C), A \cup (B \cap C) = (A \cup B) \cap (A \cup C) \tag{2.3}$$

In this context, *Probability* is identified as the occurrence of a certain random event. There are many ways of defining probability (i.e., classical definition, geometrical definition, statistical definition and axiomatic definition).

According to the axiomatic definition, *Probability* is identified as a real function *P* defined in a sample space *Λ* and having the following properties:

$$P(A) \geq 0 \qquad (2.4)$$

$$P(U) = 1 \qquad (2.5)$$

$$P\left(\bigcup_{i=1}^{\infty} A_i\right) = \sum_{i=1}^{\infty} P(A_i) \qquad (2.6)$$

where A_i are mutually exclusive events.

2.2.1 Basics rules and theorem for the computation of the probability

In this subsection, the main theorems useful for probability analysis are discussed. Before that, some basics on the mathematics behind probability analysis are given.

Considering two events A and B that should not necessarily be mutually exclusive, the *principle of summation* of probabilities reads as:

$$P(A \cup B) = P(A) + P(B) - P(A \cap B) \qquad (2.7)$$

where it follows that the probability of the sum of two mutually exclusive events is only the sum of the probabilities of the single events, being the intersection null.

In addition, the conditional probability of the event A under the complementary condition that B has occurred, is identified as *conditional probability*. The conditional probability is computed as:

$$P(A \mid B) = P(A \cap B) / P(B) \qquad (2.8)$$

Then, two events are said *mutually exclusive* if the conditional probability $P(A|B)$ is null, and also $P(A \cap B) = 0$. In addition, two events A and B are *collectively exhaustive*, if they build up the space of all possibilities (i.e., $P(A \cup B) = 1$).

In addition, two events A and B are independent if the occurrence of the event B does not influence the occurrence of the event A, and thus $P(A \mid B) = P(A)$. From Eq. (2.7), it holds that if A and B are independent: $P(A \cap B) = P(A) \cdot P(B)$, which can be deducted also from Eq. (2.8).

Total probability theorem

The Total Probability Theorem (TPT) applies to a set of events A_i, with $i=1,2,...,n$, which are both *mutually exclusive* and *collectively exhaustive*. Thus, the basic assumption behind the TPT is that:

$$P(A_i \cdot A_j) = 0, i \neq j \tag{2.9}$$

$$P(A_1 + A_2 + \ldots + A_n) = \sum_{i=1}^{n} P(A_i) = 1 \tag{2.10}$$

Then, the Total Probability Theorem reads as follows:

$$P(B) = \sum_{i=1}^{n} P(A_i) P(B \mid A_i) \tag{2.11}$$

Bayes theorem

The Bayes or Bayesian theorem applies to the computation of the probability of the individual hypothesis A_i assuming that B has occurred (i.e., the conditional probability $P(A_i \mid B)$). Specifically, imagine that A_i is a set of *mutually exclusively* and *collectively exhaustive* hypothesis statements, while B is a statement regarding observed data. The Bayes theorem follows from the Total Probability Theorem and reads as:

$$P(A_i \mid B) = \frac{P(A_i) P(B \mid A_i)}{\sum_{j=1}^{N} P(A_j) P(B \mid A_j)} \tag{2.12}$$

where:

- $P(A_i \mid B)$ is called "a posteriori" or "posterior probability" and represents how probable is the hypothesis A_i given that the observed data B is known.
- $P(A_i)$ is the "a priori" or "prior probability" and indicates how probable is the hypothesis A_i.

2.3 Uncertainty

When dealing with construction works, many sources of uncertainty are encountered which can not be eliminated. Therefore, it is necessary to recognize them and properly account for their inclusion in the design (Miceli et al. 2024a, Bertagnoli et al. 2024, Ferrara et al. 2024, Gino et al. 2024). Usually, the origin of uncertainties in structural engineering are:

- lack of knowledge regarding the material behavior in real structures;
- human errors in the execution and operation;
- inaccurate evaluation of the performance of a facility;
- simplification on the actual behavior of the structure;
- statistical uncertainty due to missing data;
- inherent uncertainty of loads, materials and geometry.

In general, uncertainty can be distinguished as function of its source: if cognitive (qualitative) or noncognitive (quantitative).

Cognitive sources or qualitative sources come from the attempt to model the reality from intellectual abstractions. In detail, they can come from:

- skill and expertise of the workers and designers;
- definition of certain parameters (e.g. performance);
- quality and deterioration;
- other human errors.

Non cognitive sources have the advantage that can be quantified. In detail, they can be distinguished in three categories:

- *inherent uncertainty* of the physical observation: this uncertainty depends on the fact that the repeat of a measurement on the same physical properties does not give the same result due to many factors (e.g., quality of the instrumentation, test procedure, ambient noise, human observer). The inherent randomness can be reduced if many data are collected. In this way, information on the variability and probabilistic distribution of the data is obtained. However, the number of measurements can not be infinite, and it is limited by the availability of money or time;
- *statistical uncertainty*: this uncertainty depends on the number of samples used to statistically characterize a certain physical property or, in other words, it determines the uncertainty in the variability of physical property;
- *model uncertainty*: this uncertainty derives from the attempt to capture the characteristics of a system by means of simplified models that consist in mathematical laws or numerical models. By comparing the outcome of a numerical model with the corresponding "real" behavior, it is possible to probabilistically characterize the model uncertainty.

Concerning structural reliability analysis, the scientific literature distinguishes between two sources of uncertainties that can be treated in a separate way since they can be assumed to be independent: *aleatory* and *epistemic* uncertainties. The aleatory uncertainty is related to inherent randomness of a physical quantity, while the epistemic one is caused by the lack of knowledge behind each assumption.

In structural reliability analysis, the *aleatory* uncertainty collects the inherent variability of material, geometrical and load properties while the *epistemic* uncertainty is related to human errors, model uncertainty and statistical uncertainty. In the following, the methods to evaluate both aleatory and epistemic uncertainty is explained.

In general, for selecting the distribution type to account for the physical uncertainty the following procedure is followed:

- select a set of possible distributions based on the experience for similar types of physical quantity;

- consider a sample of observations representative of the physical quantity ensuring homogeneity and representability;
- adopt appropriate methods to evaluate the statistical characteristics of the physical property (e.g., maximum likelihood estimation (MLE) method, moment estimates, least-square fit);
- compare the sample data with the resulting distributions by means of appropriate methods both graphically (e.g., histogram or probability paper plots) or though goodness-of-fit tests (e.g., Chi-square, Aderson-Darling, Kolmogorov-Smirnov).

The probabilistic representation of a physical quantity is probably the most effective way to reduce the uncertainty of a physical quantity. In the following, the most common assumptions behind the probabilistic distributions adopted for the resistance and load models are given.

Resistance models

Material properties are defined as function of specific tests having specific characteristics, sampled according to specific rules and so on. Materials are defined by means of stress-strain laws whose basic parameters are: modulus of elasticity, strength of the material, yield stress (if present), limit of proportionality and strains at peak and rapture stress. In the following, the basic assumptions behind the two main materials for reinforced concrete structure are given as treated in JCSS Probabilistic Model Code 2001, part III.

- *Probabilistic models for concrete*
  The cylinder concrete compressive strength is assumed as a random variable f_c distributed as $\sim LN(f_{cm}; V_c)$, where LN stands for lognormal distribution, f_{cm} is the mean value of the concrete compressive strength obtained by testing results or code prescriptions and V_c is the coefficient of variation equal to 0.15 if no experimental or inspection results are available. The other mechanical properties (i.e., young modulus E_c, concrete tensile strength f_{ct}, peak strain ε_c) of concrete can be indirectly computed from the expression given in EN1992-1-1 and *fib* Model Code 2010 or probabilistically modeled in line with JCSS 2001.

- *Probabilistic models for steel reinforcement*
  For the steel reinforcement properties, the yielding strength f_y is modeled as $\sim LN(f_y; V_y)$, where LN stands for lognormal distribution, f_{ym} is the mean value of the steel yielding strength obtained by testing results or code prescriptions and V_y is the coefficient of variation equal to 0.05 if no experimental or inspection results are available. Regarding the steel elastic modulus E_s, it is distributed as a lognormal variable with mean value E_{sm} that can be taken as 205 GPa and coefficient of variation V_{Es} equal to 0.03. The ultimate strain can be assumed according to *fib* Model Code 2010 or probabilistically modeled in line with JCSS 2001.

Load models

Loads can be classified according to their type as follows: self weight of structures, occupancy loads, actions caused by industrial activities, action caused by transport, climatic actions, hydraulic actions and action from soil or rock including earthquake.

A similar classification regards their variations in time, such that three categories can be distinguished:

- *Permanent actions*: their variation in time around the mean value is small and slow, or it is monotonically tending to a limiting value.
- *Variable actions*: their variation in time is frequent and large.
- *Exceptional actions*: whose magnitude is very large, but the occurrence probability is very low.

In general, the following assumptions are considered for the probabilistic distribution of the main loads:

- Normal distribution for self weight.
- Normal distribution for other permanent loads.
- Extreme Value distribution (Gumbel or rarely Frechet) for variable actions. In fact, in case of variable loads, the probabilistic distribution accounts for the largest extreme load occurring during a certain reference period (e.g., lifetime or annual).

2.4 Limit state

The concept of reliability is strictly related to the performance requirements for which the structure is designed during its reference period. These requirements are identified as limit states, which stands for a condition behind which the structure is not considered reliable anymore. Thus, the structure can be either identified as satisfactory (i.e., safe or serviceable) or unsatisfactory (i.e., failed or unserviceable) if the design criteria are respected or not, respectively. Limit states can be distinguished between Ultimate Limit State (ULS) and Serviceability Limit State (SLS).

The ULS is related to the safety of people and/or the structural integrity of a facility and it is defined as function of the bearing capacity of the structure. If the capacity is overcome, the structure or part of it is considered to fail. The ULSs account for:

- loss of equilibrium (e.g., turn over, sliding, push up, etc.);
- formation of a mechanism;
- collapse due to rupture, fatigue or excessive deformations or crushing;
- instability.

The SLS is related to the performance, the comfort and the visual aspect of a structure during its use. SLS can be irreversible, if the critical value remains after removal of the load (e.g., permanent local damage or deflection), or reversible, if the critical value is no longer present after removal of the load (e.g., cracks in prestressed concrete, excessive vibrations). In case of irreversible limit states, the criteria adopted are the same for the ULS. In case of reversable limit states, alternative serviceability requirements are adopted which are different from the load combinations approach.

In general, SLSs require the following verifications to be performed:

- deformations that can affect visual aspects and comfort of users;
- vibrations that can affect the comfort and functionality of a facility;
- local damages, including cracking, that can influence visual aspects, durability and use.

The limit state is identified by the *performance function* or *limit state function* which represents the mathematical relationship between the basic variables X_i in defining the performance of a structure or a component. The *limit state function* is usually identified in an implicit form as:

$$Z = g(\bar{X}) = 0 \tag{2.13}$$

where $\bar{X}$ is the vector of the n basic variables. The basic variables include the actions, the mechanical properties, the geometrical data and the model uncertainty.
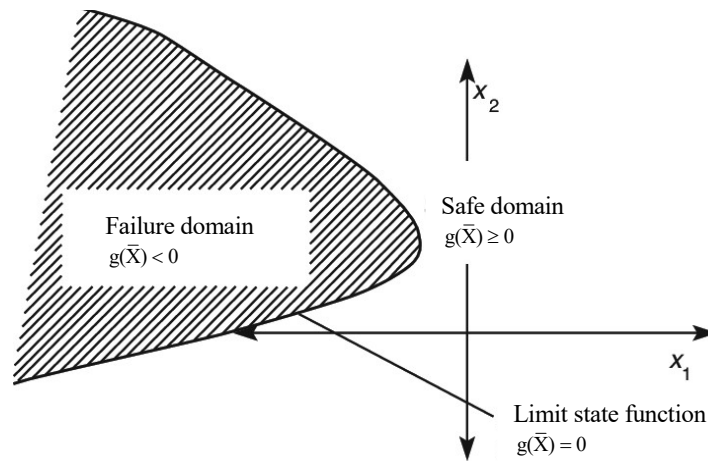
Figure 2.1 Representation of the *limit state function* with two basic variables X_1 and X_2.

Each basic variable should be characterized in probabilistic term. If it has a negligible variation in time or space, the basic variable is considered deterministic.

Since $g(\bar{X})$ is a mathematical function of basic variables, the *limit state function* is a basic variable itself. Furthermore, the *limit state function* determines the condition of satisfactory or unsatisfactory of a structure. In particular, when

$g(\overline{X}) \geq 0$ the structure is considered safe, while if $g(\overline{X}) < 0$ the structure is considered unsafe (Figure 2.1).

For most limit states, the probability of failure is computed as the probability that the *limit state function* is lower than zero:

$$P_f = P\{g(\overline{X}) < 0\} \tag{2.14}$$

By assuming that the basic variables contained in the vector $\overline{X} = [X_1, X_2, ..., X_n]$ are described by time-independent joint probability density function $\varphi_{\overline{X}}(x)$, the probability of failure can be written as:

$$P_f = \int_{g(\overline{X})<0} \varphi_{\overline{X}}(x)dx \tag{2.15}$$

where the integration is performed over the failure region (i.e., where the *limit state function* is lower than zero).

Then, the complementary to 1 of the failure probability allows to compute the probability of success P_s, as follows:

$$P_s = 1 - P_f \tag{2.16}$$

Thus, the reliability problem consists in solving Eq. (2.15) in order to find the failure probability associated to a certain limit state or performance level. The issue is that the joint probability density function of the random variables is very difficult to be expressed as well as the resolution of the integral in Eq. (2.15). In the next section, the methods to solve this integral are illustrated.

An equivalent way of expressing the failure probability is the reliability index β, which is defined as the negative value of a standard normal variable corresponding to the failure probability P_f. The mathematical expression of the reliability index is:

$$\beta = -\Phi_U^{-1}(P_f) \tag{2.17}$$

where $\Phi_U^{-1}(P_f)$ represents the inverse standard normal distribution function.

Table 2.1 Mutual correspondence between failure probability and reliability index.

P_f	β
10^{-1}	1.3
10^{-2}	2.3
10^{-3}	3.1
10^{-4}	3.7
10^{-5}	4.2
10^{-6}	4.7
10^{-7}	5.2

The failure probability and the reliability index represent equivalent reliability measures with one-to-one mutual correspondence as shown in Table 2.1.

The actual codes provide target reliability β_t values (i.e., minimum requirements for the reliability indices in order to respect the performance requirements associated with certain limit states). These values are based on optimization procedures that accounts for quality assurance and quality management measures.

Regarding the ULS, the target reliability indices are given in Table 2.2 and Table 2.3 for, respectively, 1 year and 50 years of reference period.

Table 2.2 Target reliability indices (and corresponding failure probability) for 1 year reference period and ULS (ISO 2394).

		Minor consequences of failure $\rho<2$	Moderate consequences of failure $2\leq\rho<5$	Large consequences of failure $5\leq\rho<10$
Relative cost of safety measure	Large (A)	3.1 ($P_f\approx10^{-3}$)	3.3 ($P_f\approx10^{-4}$)	3.7 ($P_f\approx10^{-4}$)
	Normal (B)	3.7 ($P_f\approx10^{-4}$)	4.2 ($P_f\approx10^{-5}$)	4.4 ($P_f\approx5\cdot10^{-6}$)
	Small (C)	4.2 ($P_f\approx10^{-5}$)	4.4 ($P_f\approx10^{-6}$)	4.7 ($P_f\approx10^{-6}$)

Table 2.3 Target reliability indices (and corresponding failure probability) for 50 years reference period and ULS (*fib* Model Code 2010).

Low consequences of failure	Medium consequences of failure	High consequences of failure
3.1 ($P_f\approx10^{-3}$)	3.8 ($P_f\approx5\cdot10^{-5}$)	4.3 ($P_f\approx10^{-5}$)

As one can observe, the target reliability is function of the consequence of failure and the cost of safety measure.

The consequence of failure is computed according to cost analysis and are based on the ratio ρ between the total costs (i.e., given by the sum between the construction and the failure costs) and the construction costs. Minor consequences are associated to structures where the risk to life conditioned to the failure occurrence is small or negligible (e.g., silos, agricultural structures). Moderate consequences regard medium risk to life and considerable economic consequences (e.g., office or residential or industrial buildings). Finally, large consequences are related to high risk to life and significant economic consequences (e.g., hospitals, bridges, high rise buildings, theaters). In addition, consequence classes are related to the type of failure, which can be classified in: ductile failure with reserve strength capacity, ductile failure with absence of strength capacity, brittle failure. Thus, structures prone to a brittle failure should be designed with a larger target reliability.

The evaluation of the cost of safety measures determines three different classifications: large (A), normal (B) and low(C). The normal class is in general

associated to medium variability of the loads and resistances (i.e., coefficient of variations between 0.1 and 0.3).

The target reliability β_t increases if the cost of safety class is reduced and the consequences classes are larger since the failure becomes less probable. The most common design situations consider a moderate consequence class and a normal relative cost of safety (i.e., β_t equal to 4.2).

As for the SLS, failures are not related to loss of human life but to the performance related to the use of the structure. Target values for those limit states depend on the fact that the state is reversible or irreversible. As anticipated, the reversable serviceability limit states require proper considerations that go behind the scope of this dissertation. For the irreversible serviceability limit states, the target values for the reliability index are given in Table 2.4.

Table 2.4 Target reliability indices (and corresponding failure probability) for one year reference period and irreversible SLS (ISO 2394).

		Target index
Relative cost of safety measure	High	1.3 ($P_f \approx 10^{-1}$)
	Normal	1.7 ($P_f \approx 5 \cdot 10^{-2}$)
	Low	2.3 ($P_f \approx 10^{-2}$)

2.5 Elementary reliability theory

The basic purpose of the structural reliability formulation is to determine the probability of failure associated with a certain limit state. This failure probability can be estimated with refined methods or by means of simplified approaches. In general, four different reliability methods can be distinguished (listed from the most refined to the least):

- *level III* method;
- *level II* method;
- *level I* method;
- *level 0* method.

2.5.1 *Level 0* method

The level 0 method follows a deterministic approach which adopts deterministic or nominal values for the basic variables and one empirical global safety factor. In particular, the basic verification is the following:

$$R_{nom} \geq \gamma E_{nom} \qquad (2.18)$$

where R_{nom} and E_{nom} are respectively the nominal value of the capacity and the nominal value of the demand. This method is nowadays not used anymore because it quantifies the level of reliability, both in assessment and design, with a certain

degree of underestimation. Nowadays, probability-based methods are more reliable and substitute the deterministic ones.

2.5.2 *Level I* method

The level I method is a semi-probabilistic approach that is currently adopted in Eurocodes and that was first introduced in EN 1990. The probabilistic distribution of basic variables is accounted for in a simplified way by considering their design values. In this formulation, S stands for the action effect and R for the structural resistance and the corresponding design values S_d and R_d are determined considering the design values of all the basic variables involved in the problem formulation. According to this approach, the structure is considered safe if the following relation is respected:

$$g(\overline{X}) = R_d(\overline{X}) - S_d(\overline{X}) > 0 \tag{2.19}$$

where $\overline{X}$ is a vector of design parameters.

Specifically, the design values of the action and the resistance are obtained as:

$$\begin{aligned} S_d &= S\{F_{d1}, F_{d2}, ...a_{d1}, a_{d2}, ...\theta_{d1}, \theta_{d2}\} \\ R_d &= R\{X_{d1}, X_{d2}, ...a_{d1}, a_{d2}, ...\theta_{d1}, \theta_{d2}\} \end{aligned} \tag{2.20}$$

where subscript *"d"* stands for the design value, F denotes the actions, X the material properties, a the geometrical parameters and θ the model uncertainty.

In order to compute the design values of the basic variables X_d and F_d, it is necessary to define the representative values of the basic variables related to resistances (i.e., X_{rep}) and actions (i.e., F_{rep}).

Representative values for resistances X_{rep}

The representative values for materials are defined by their characteristic values X_k which in general correspond to a specific percentile. Since the resistance should be lowered to be on the side of safety, in general a quantile of 5% is assumed for the representative value of the material properties, meaning that the 5% of the population is lower than X_k.

Representative values for actions F_{rep}

In case of loads it is necessary to distinguish between the permanent and the variable actions:

- when the action refers to the self weight, the corresponding characteristic value G_k coincides with mean unit weight of the material;
- when the action refers to a variable load, the representative value of the variable load Q_{rep} is defined as function of the load combination to be adopted, as follows: i) characteristic value Q_k, ii) combination value $\psi_0 Q_k$,

iii) frequent value $\psi_1 Q_k$, iv) quasi-permanent value $\psi_2 Q_k$. In general, the characteristic value corresponds to a 95% or 98% quantile.

Then, in order to compute the design values, the following relations should be adopted:

$$E_{d,i} = \gamma_S S\left[G_{d,i}; Q_{d,i}; \overline{a}_d\right]$$
$$R_d = \frac{R\left[X_d; \overline{a}_d\right]}{\gamma_R} \tag{2.21}$$

where:

- $\overline{a}_d$ is the design value for the geometry;
- X_d are the design value of the resistance parameters;
- $G_{d,i}$ are the design values of the permanent actions ("i" defines the i-th action)
- Q_d are the design values of the variable actions ("i" defines the i-th action);
- γ_R is the partial factor related to model uncertainty for the resistance model;
- γ_S is the partial factor related to uncertainty in the modelling of the actions and in the effects of the actions.

The design values of the resistance parameters are obtained as follows:

$$X_d = \eta \frac{X_k}{\gamma_m} \tag{2.22}$$

where:

- η is the conversion factor which accounts for the effects of the load duration, temperature, moisture, scale effects;
- X_k is the characteristic value of material parameter as previously defined;
- γ_m is the partial factor related to material parameters.

The design values of the load parameters are obtained as follows:

$$G_d = \gamma_G G_k$$
$$Q_d = \gamma_Q Q_{rep} \tag{2.23}$$

where:

- G_k is the characteristic value of permanent loads as previously defined;
- Q_{rep} is the representative value of variable loads as previously defined as function of the considered combination;
- γ_G is the partial factor related to permanent loads;
- γ_Q is the partial factor related to variable loads.

2.5.3 *Level II* method

The level II method is a probabilistic approach that is based on the First-Order Reliability Methods (i.e., FORM) to approximate joint probability density function given in Eq. (2.15). In detail, between the different approaches, the following ones are described:

- first-order second-moment (FOSM);
- advanced first-order second-moment (AFOSM);

In the former case, the information on the distribution of random variables is not considered, while in the latter case it is accounted for.

First-order second-moment (FOSM)

In this approach, the *performance* or *limit state function* is linearized by means of a first-order Taylor series approximation, adopting only the second-moment statistics (i.e., means and covariances) of the random variables. For this reason, this method is called "second-moment".

The original formulation derives from Cornell (1969) adopting a two-variable approach. Specifically, by defining R and S as statistically independent normally distributed random variables for resistance and load, respectively, the limit state function $Z=R-S$ is as well a random variable normally distributed. Specifically, in the assumption of normal distribution, the mean value μ_Z and standard deviation σ_Z of Z are simply computed as follows:

$$\mu_Z = \mu_R - \mu_S$$
$$\sigma_Z = \sqrt{\sigma_R^2 + \sigma_S^2} \tag{2.24}$$

where μ_R and μ_S are, respectively, the mean values of the resistance and the load, while σ_R and σ_S are, respectively, the standard deviation of the resistance and the load, assuming that both are normally distributed and independent random variables.

Then, the reliability index or safety index or Cornell index is obtained as:

$$\beta = \frac{\mu_Z}{\sigma_Z} = \frac{\mu_R - \mu_S}{\sqrt{\sigma_R^2 + \sigma_S^2}} \tag{2.25}$$

An alternative approach is the one formulated lately from Rosenbleuth and Esteva (1972), where it is assumed that the resistance and load random variables are both lognormally distributed. This is a more realistic assumption since for physical reasons in general the random variables are positive quantity. In this case, the load and the resistance are lognormal basic variables having mean values equal to, respectively, λ_S and λ_R and coefficient of variation equal to, respectively, ξ_S and

ξ_R. Hence, another random variable Y is introduced such that $Y=R/S$. Thus, the following relationship is valid in such a way that Z is a normal distribution:

$$\ln Y = Z = \ln R - \ln S \qquad (2.26)$$

In this case the reliability coefficient is computed as:

$$\beta = \frac{\lambda_R - \lambda_S}{\sqrt{\xi_R^2 + \xi_S^2}} \qquad (2.27)$$

Both the previous two formulations can be generalized if many random variables are involved in the reliability problem, by considering a Taylor series expansion of the performance function as follows:

$$Z = g(\mu_{\bar{X}}) + \sum_{i=1}^{n} \frac{\partial g}{\partial X_i}\left(X_i - \mu_{X_i}\right) + \frac{1}{2}\sum_{i=1}^{n}\sum_{j=1}^{n}\frac{\partial g}{\partial X_i}\frac{\partial g}{\partial X_j}\left(X_i - \mu_{X_i}\right)\left(X_j - \mu_{X_j}\right) + \cdots \qquad (2.28)$$

where μ_{X_i} is the mean value of X_i. Then, the two quantities to be substituted in Eq. (2.25) in order to compute the reliability index are obtained by truncating the series at linear terms, as follows:

$$\mu_Z \approx g(\mu_{X_1}, \mu_{X_2}, \dots, \mu_{X_n})$$
$$\sigma_Z^2 \approx \sum_{i=1}^{n}\sum_{j=1}^{n}\frac{\partial g}{\partial X_i}\frac{\partial g}{\partial X_j}Cov\left(X_i, X_j\right) \qquad (2.29)$$

where $Cov\,(X_i,X_j)$ is the covariance of X_i and X_j.

The drawbacks of this approach are that when the *limit state function* is non-linear, since a linearization approach is adopted, it could be possible to make large errors on its evaluation. In addition, by adopting this approach, different values of the reliability index can be obtained even if two mechanically equivalent formulations of the same performance function are elaborated.

Advanced First-order second-moment (AFOSM)

This method is also called Hasofer-Lind (H-L) method, inspired by Hasofer and Lind (1974). It is based on a transformation of the performance limit state $g(\bar{X}) = 0$ in a reduced performance limit state $g(\bar{X}') = 0$ by introducing the generic reduced variable as follows:

$$X_i' = \frac{X_i - \mu_{X_i}}{\sigma_{X_i}}(\mathrm{i} = 1, 2, \dots, \mathrm{n}) \qquad (2.30)$$

where $X_i^{'}$ is a random variable with zero mean and unit standard deviation. If X_i is normal, then $X_i^{'}$ is a standard normal variable.
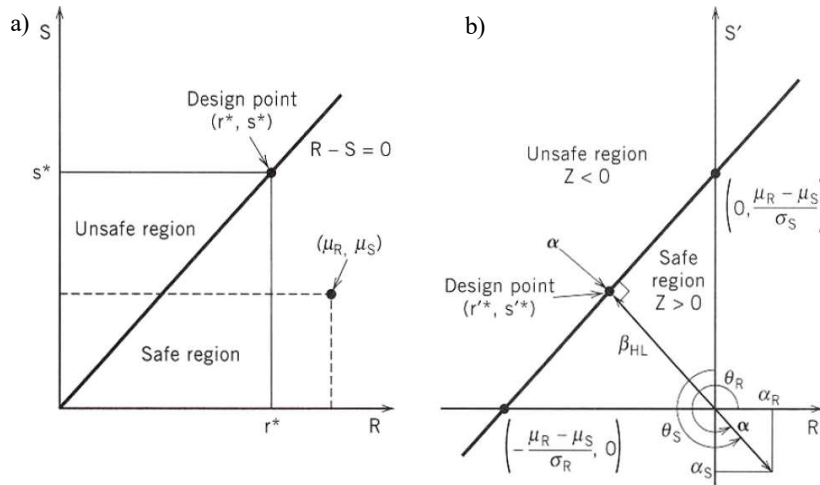
Figure 2.2 Representation of the HL method in case of two-variable approach: a) original coordinate system; b) reduced coordinate system (modified from Hasofer and Lind, 1974).

Adopting this transformation, a new coordinate system is obtained, called transformed or reduced coordinate system. Then, the reliability index according to H-L method is equal to:

$$\beta_{HL} = \sqrt{\left(\overline{x}^{'*}\right)^{'}\left(\overline{x}^{'*}\right)}$$

(2.31)

where β_{HL} represents the minimum distance from the origin of axes to the limit state surface in the reduced coordinate system. This minimum distance is also called checking point or design point and it is identified by the vector $\overline{x}^{*}$ in the original coordinate system and by the vector $\overline{x}^{'*}$ in the reduced reference system. In Figure 2.2, a schematic representation of this method is presented.

2.5.4 *Level III* method

The level III method is a probabilistic approach that aims at solving the integral of Eq. (2.15) in order to exactly calculate the probability of failure P_f and, thus, the corresponding reliability index β.

In this case, the reliability estimation is obtained with a simulation technique both for explicit and implicit limit state functions. In particular, each random variable is sampled many times in order to represent its real distribution according to its statistical characterization. The computation of the integral can be performed by means of:

- numerical solutions;
- simulation techniques.

Exact solution for two random variables

As already mentioned, level III methods allow to explicitly calculate the integral given in Eq. (2.15). This can be done analytically when it is possible to explicitly evaluate the joint probability density function $\varphi_{\bar{X}}(x)$. This is the case when two independent basic variables are considered in the problem formulation and lead to a linear limit state function.

In detail, let consider the resistance variable R and the load variable E as the two independent random variables. The limit state function can be written as $Z = g(\bar{X}) = R - E = 0$.
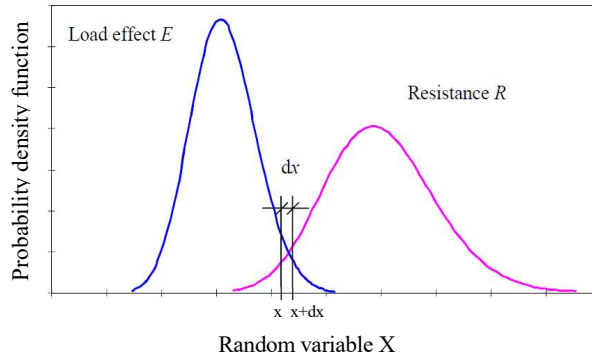
Figure 2.3 Representation of reliability problem in case of two basic variables (modified from Leonardo da Vinci Pilot Project, 2005).

With reference to Figure 2.3, let define A as the event of occurrence of the action effect E in the differential interval $< x, x + dx >$, such that the probability of occurrence of the event A can be computed as:

$$P(A) = P(x < E < x + dx) = \varphi_E(x)dx \qquad (2.32)$$

Then, let define B as the probability that the resistance R occurs in the interval $< -\infty, x + dx >$, such that its probability can be computed as:

$$P(B) = P(R < x) = \Phi_R(x) \qquad (2.33)$$

Where in the previous equations, $\varphi_E(x)$ is the probability density function (PDF) of E evaluated in x and $\Phi_R(x)$ is the cumulative density function (CDF) of R evaluated in x. Then, the differential of the failure probability is:

$$dP_f = P(A \cap B) = P(A)P(B) = \Phi_R(x)\varphi_E(x)dx \qquad (2.34)$$

By integrating the differential relationship, the analytical formulation of the probability of failure in case of two independent random variables is:

$$P_f = \int_{-\infty}^{+\infty} \Phi_R(x)\varphi_E(x)dx \qquad (2.35)$$

This integral, usually defined as *convolution integral*, can be solved by numerical integration or using simulation methods.

Monte Carlo simulation technique

This method derives its name from the place where gamblers take risks (i.e., Monte Carlo). The first time this approach was used was during the II World War as a code word for nuclear weapons in Los Alamos National Laboratory of Mexico.

Supposing the sample dimension is equal to N, this method is made of several steps that can be summarized as follows:

i.   definition of all the random variables involved in the reliability problem;

ii. definition of the statistics for all the random variables in terms of probabilistic distribution and its parameters;

iii. generation of the values of each random variable. Specifically, this task is different if the distribution is related to a continuous or a discrete random variable.

- *Continuous random variables*

   The sampling is performed by first generating in a random way N numbers between 0 and 1. This numbers are called pseudo random numbers and are denoted as u_i where $i=1,2,...,N$. Then, the inverse cumulative density function (i.e., CDF) method is used, meaning that the CDF $F_X(x_i)$ of the sampled random variable x_i is equated to the pseudo random number u_i as follows:

$$x_i = F_x^{-1}(u_i) \qquad (2.36)$$

- *Discrete random variables*

   If X is a discrete random variable, the approach is similar to the previous one but the CDF $F_X(x_i)$ should be evaluated by considering the summation of individual PMF (probability mass function). Then, a numerical search procedure is needed to compute the i-th realization of the discrete basic variable as follows:

$$F_X(\mathrm{x}_{j-1}) < u_i < F_X(\mathrm{x}_j) \qquad (2.37)$$

iv. evaluation of the problem in a deterministic manner by associating the sampled value of the random variable for each set of realization. In particular, the reliability problem will be solved N times deterministically;

v. extract the probabilistic information from all the N solutions of the problem (i.e., if failure or success is obtained);

vi. evaluation of the failure probability by dividing the numbers of failures N_f for the total numbers of realizations (i.e., N), as follows:

$$P_f = \frac{N_f}{N} \tag{2.38}$$

vii. evaluation of the accuracy and efficiency of the failure probability by means of the computation in Eq. (2.38). The accuracy depends on the number of samplings that are performed. Of course, the larger N the more accurate will be the computation of the failure probability. In order to numerically evaluate the accuracy, the coefficient of variation (i.e., COV) of the estimated probability of failure can be evaluated as follows, according to Ayyub and Haldar (1985):

$$COV(P_f) = \frac{\sqrt{\dfrac{(1-P_f)P_f}{N}}}{P_f} \tag{2.39}$$

where the estimation is based on the assumption that each sampling is a Bernoulli trial, and the number of failures can be considered to follow a binomial distribution.

As a general consideration, the number of simulations cycles in order to reach a desired level of accuracy depends on the order of magnitude of the failure probability to be estimated. In many engineering problems, failure probability is around 10^{-5}, therefore, only 1 out of 100'000 realizations would fail. This means that N should be larger that at least 100'000 in order to obtain at least one fail. Thus, 10 times this minimum value is an accurate number for N in this case in order to obtain enough accuracy on the estimation of the failure probability.

Variance reduction techniques

As mentioned in the previous section, the accuracy of the evaluation of the failure probability is an important issue in Monte Carlo simulation technique. This issue can be solved if a large number of cycles is performed. In case of variance reduction techniques, the accuracy is increased by reducing the variance or the error of the estimation without changing its expected value or increasing the number of samples. However, this approach is more difficult from a computational point of view.

VRTs can be adopted both to constraint the sample to be representative for the estimation or for elaborating strategies to achieve (positive or negative) correlation between random observations. The former approaches are called *sampling methods* (i.e., importance sampling, systematic sampling, stratified sampling, Latin Hypercube sampling, adaptive sampling, conditional expectation). The latter are

called *correlation methods* (i.e., common random numbers, antithetic variates, control variates).

In the following, the importance sampling method and the Latin Hypercube methods will be described. For more details, reference is made to Haldar and Mahadevan (2000).

Importance sampling method

The importance sampling method (Harbitz, 1986) is used to concentrate the distribution of samples in a region that mainly contributes to the failure probability evaluation.
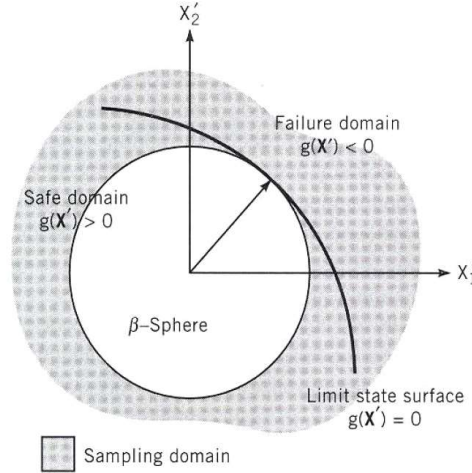
Figure 2.4 Importance sampling method representation (Harbitz, 1986).

This approach is schematically represented in Figure 2.4, where it is shown how the sampling occurs outside the β-sphere since it corresponds to the area where no failure occurs. According to this approach, an indicator function is introduced as follows:

$$I_g(\overline{X}) = \begin{cases} 0 & \text{if } g(\overline{X}) > 0 \\ 1 & \text{if } g(\overline{X}) < 0 \end{cases} \tag{2.40}$$

Then, a new PDF $f_1(\overline{X})$, called sampling density function, is introduced in order to obtain samples in the desired regions. Thus, the failure probability of Eq. (2.15) can be re-written as:

$$P_f = \int\limits_{g(\overline{X})<0} \left[I_g(\overline{X}) \frac{f_X(\overline{X})}{f_1(\overline{X})} \right] f_1(\overline{X}) \, d\overline{X} \tag{2.41}$$

In case of Monte Carlo simulation approach, the estimated value of the failure probability is obtained as follows:

$$P_f = \frac{1}{N} \sum_{i=1}^{N} I_g(\overline{X}) \frac{f_X(\overline{X})}{f_1(\overline{X})} \qquad (2.42)$$

Latin Hypercube sampling technique

In this sampling technique, introduced first by Mckey et al. (1979), the range of the basic variable X_i is subdivided into *n* partitions of equal marginal probability of *1/n*, and the basic variable is sampled in each of partition. After the sampling, the realizations are successively randomly combined. This method appears to be advantageous when the output (i.e., failure probability) is dominated by few of the basic variables involved in the reliability formulation.

In this approach, if *n* is the number of basic variables the following steps are followed:

i. each variables X_i is associated to a probability interval from 0 to 1 that is subdivided into *n* non-overlapping equiprobable sub-intervals having boundaries h_{inf} and h_{sup};

ii. a single value is sampled from each sub-interval and the corresponding basic variable is computed according to the CDF method as previously described;

iii. a random combination between the *n* sampled values for each X_i basic variable is performed in order to randomly combine the results.

As a rule of thumb, the size of the sample should be 10 times the number of probabilistically independent design variables in order to have the population's mean value to be close to the mean value of the requested distribution range.

Chapter 3

Design of multistorey RC buildings and FEM modelling validation and assumptions

3.1   Introduction

This chapter deals with the description of the case studies where the design improvements are applied and discussed in the following chapters. At first, a brief description of the design procedure for the multistorey RC buildings is given. In particular, two buildings are designed: one with regular seismic resistant frames in both directions and the other with both seismic resistant frames and secondary ones, with columns and beams having different cross sections. Then, the finite element modelling assumptions to carry out the non-linear analyses on different frames of the buildings are described. These assumptions have been validated by reproducing the results of the beam-column sub-assembly tested by Lew et al. (2011). In addition, the approach to calibrate equivalent springs at each beam-column node of the frame is deepened, in order to account for the contribution of the orthogonal framed system in the transverse direction with respect to the plane of the studied frame. This approach is applied to calibrate both elastic and non-linear constitutive laws of the springs.

3.2   Design of multistorey RC building

In this thesis, two different ordinary reinforced concrete buildings are designed:

- the first building is as much as regular as possible in terms of beams and columns sizes in order to conduct preliminary analyses and study the robustness of a RC frame both in case of a deterministic and a probabilistic approach;

- the second building is characterized by different column and beam sizes, including both deep and wide beams, in order to study the three-dimensional effects on the robustness of a RC structure as well as to investigate different failure scenarios.

Both buildings are located in a high seismicity area (i.e., L'Aquila in Italy), at 714 m from the sea level, and are designed according to Italian and European code rules (i.e., MIT, 2018; MIT, 2019; CEN, 1993; CEN, 2007). For both cases a high ductility class is assumed. The materials adopted are C25/30 for concrete and B450 for reinforcing steel.

In the following, the two seismic designs are shown, illustrating an overview on the actions, dimensioning of the structural elements and reinforcement detailing.

3.2.1 First building

The building is characterized by 5 stories with an inter-story height of 3 m and 4 spans of 5 m in both directions (Figure 3.1). The building is regular both in plan and in elevation. In detail, the study is conducted on an internal frame of this building, as shown in Figure 3.1b.

The design reference period is of 50 years and assuming an exposure class XC2 and a structural class S2, the clear concrete cover is equal to 3.5 cm for all the structural elements.
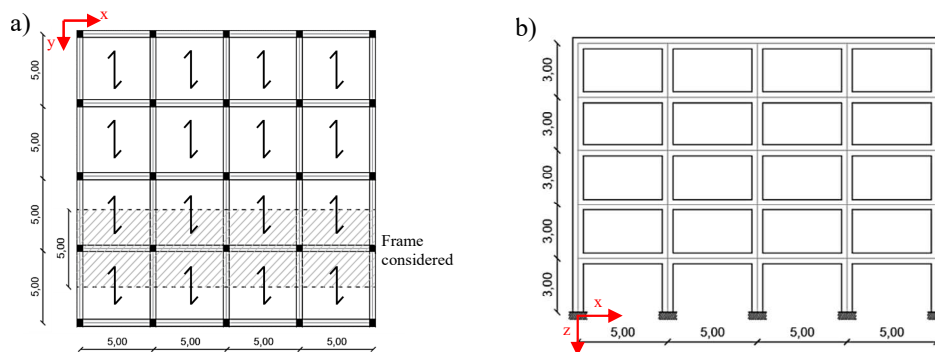
Figure 3.1 Geometry of the first building: (a) in plan view with joists disposition direction; (b) lateral view. Measures in m.

The considered actions are: permanent loads (G) (including permanent structural G_1 and non structural loads G_2), variable loads (Q) (considering live loads Q_1, wind Q_2 and snow Q_3) and seismic action (E). In particular, a brick concrete one-way slab of 30 cm is used.

Table 3.1 resumes the characteristic or mean values of the actions considered in the design. Regarding the seismic action, the following assumptions are adopted:

- Design reference period V_N=50 years.
- Ground type: B "*Deposits of very dense sand, gravel, or very stiff clay, at least several tens of min thickness, characterized by a gradual increase of mechanical properties with depth*".

- Topography class: T_3 "*Location of the intervention at the crest of a relief with an average slope of less than or equal to 30°*".
- Damping factor of 5%.
- Behavior factor q=5.85 assuming high ductility class (A), α_u/α_1=1.3 for multi-story multi-bay frames and k_w=1 for frame systems.

Table 3.1 Summary of the actions considered for the first building.

Action	Type of action	Value	
Permanent structural load (G_1) (mean value)	Beam and column self-weight	Assuming a specific weight of 25 kN/m^3	
	Slab self-weight	3.2 kN/m^2	
Permanent non-structural load (G_2) (mean value)	Screed, pavement and plaster	1.4 kN/m^2	
	Internal partition	1.2 kN/m^2	
Live load (Q_1) (characteristic value)	Floors	2 kN/m^2	
	Roof	0.5 kN/m^2	
Snow (Q_2) (characteristic value)	Roof	2.17 kN/m^2	
Wind (Q_3) (characteristic value)	Height	Upwind	Downwind
	3 m	0.72 kN/m^2	-0.36 kN/m^2
	9 m	0.72 kN/m^2	-0.36 kN/m^2
	15 m	0.79 kN/m^2	-0.36 kN/m^2

In Figure 3.2 the design spectrum together with the elastic one are shown. The peak ground acceleration is equal to 0.104g considering the Operational Limit State and 0.261g considering the Life Safety Limit State according to the Italian guidelines (MIT, 2018).
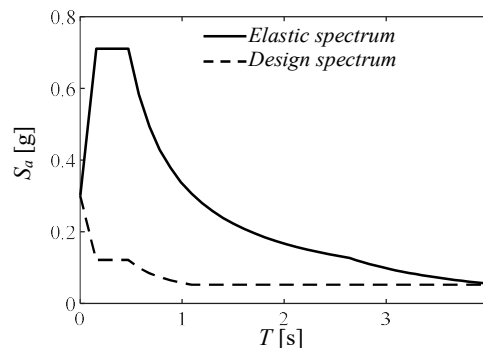
Figure 3.2 Comparison between design spectrum and elastic spectrum for the life safety limit state (LSLS) for building 1.

Summary of design characteristics

The ultimate limit state (ULS) and serviceability limit state (SLS), combined with the capacity design principles have led to the following design choices:

- Column cross sections: 60x60 cm^2.
- Beam cross sections: 40x50 cm^2.

The choice for a large height of the beam is in line with the need of achieving a larger bearing capacity in flexural stage, as demonstrated in the experimental tests of Ren et al. (2016), Lu et al. (2017) and Adam et al. (2020). This can be beneficial to reach earlier the performance point in terms of energetic equivalence proposed by Izzuddin et al. (2008). Furthermore, a quite large height-to-width ratio of the beam equal to 80% is due to the need of facilitating a more ductile behavior in the post-peak stage to reach the activation of the catenary effect, as seen in Di Trapani et al. (2020).

As for the detailing, 18 mm bars are adopted for the longitudinal reinforcement of the beams, 20 mm for the one of the columns and 8 mm bars for the transverse reinforcement for all the structural elements. In Table 3.2 the summary of the reinforcement detailing is shown. No distinction between dissipative and non-dissipative zone is made in the columns, while the extension of the dissipative area in the beams is equal to 1 m from the column axis. It should be noted that these characteristics are valid for the frames in both directions of the 3D building. Finally, all the beam-column nodes have a spacing of the stirrups equal to 5 cm.

It should be noted that the detailing in terms of longitudinal reinforcement of the beams respect the ties criteria of Eurocode 2 (i.e., EN1992-1-1).

Table 3.2 Reinforcement detailing of the building.

	Floor	Size [mm^2]	Longitudinal bars *	Stirrups *
Beams	1st-2nd 3rd	400x500	$3\phi_u 18 + 3\phi_l 18$(D), $2\phi_u 18 + 3\phi_l 18$ (ND)	2-leg$\phi 8/100$
	4th	400x500	$4\phi_u 18 + 3\phi_l 18$(D), $2\phi_u 18 + 3\phi_l 18$ (ND)	2-leg$\phi 8/100$
	5th	400x500	$5\phi_u 18 + 3\phi_l 18$(D), $2\phi_u 18 + 3\phi_l 18$ (ND)	2-leg$\phi 8/100$
Columns	all	500x600	$10\phi 20$	4-leg$\phi 8/100$
Nodes	all			4-leg$\phi 8/50$

*D indicates the dissipative area, ND the non-dissipative area, ϕ_u and ϕ_l are, respectively, the longitudinal reinforcement in the upper and lower chords. The units of measure are mm.

3.2.2 Second building

The building is characterized by 5 stories with an inter-story height of 3.5 m and 4 spans of 5 m in x-direction and 3 spans of 5 m in y-direction (Figure 3.3).

The building is regular both in plan and in elevation.

The design reference period is of 50 years and assuming an exposure class XC2 and a structural class S4, the clear concrete cover is equal to 3 cm for all the structural elements.

The considered actions are: permanent loads (G) (including permanent structural G_1 and non structural loads G_2), variable loads (Q) (considering live loads Q_1, wind Q_2 and snow Q_3) and seismic action (E). Specifically, a brick concrete one-way slab of 30 cm is used.
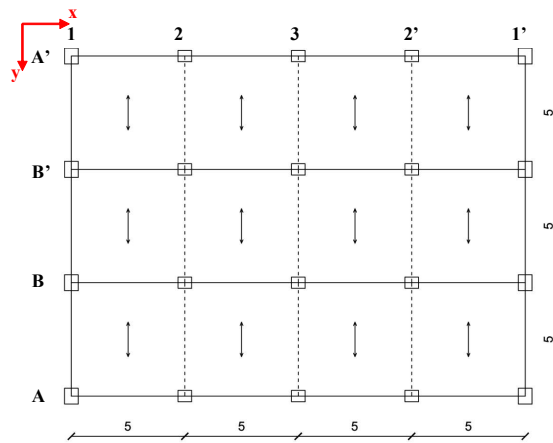
Figure 3.3 In plan view of the second building with joists disposition direction. Measures in m.

Table 3.3 resumes the characteristic or mean values of the considered actions.

Table 3.3 Summary of the actions considered for the second building.

Action	Type of action	Value	
Permanent structural load (G_1) (mean value)	Beam and column self-weight	Assuming a specific weight of 25 kN/m^3	
	Slab self-weight	3.2 kN/m^2	
Permanent non-structural load (G_2) (mean value)	Screed, pavement and plaster	1.4 kN/m^2	
	Internal partition	1.2 kN/m^2	
	Infill walls	6.4 kN/m	
Live load (Q_1) (characteristic value)	Floors	2 kN/m^2	
	Roof	0.5 kN/m^2	
Snow (Q_2) (characteristic value)	Roof	2.17 kN/m^2	
Wind (Q_3) (characteristic value)	Height	Upwind	Downwind
	3 m	0.72 kN/m^2	-0.36 kN/m^2
	9 m	0.72 kN/m^2	-0.36 kN/m^2
	14 m	0.77 kN/m^2	-0.36 kN/m^2
	17.5 m	0.85 kN/m^2	-0.36 kN/m^2

Regarding the seismic action, the following assumptions are adopted:

- Design reference period V_N=50 years
- Ground type: B "*Deposits of very dense sand, gravel, or very stiff clay, at least several tens of min thickness, characterized by a gradual increase of mechanical properties with depth*".
- Topography class: T$_3$ "*Location of the intervention at the crest of a relief with an average slope of less than or equal to 30°*".
- Damping factor of 5%.
- Behavior factor q=5.85 assuming high ductility class (A), α_u/α_1=1.3 for multi-story multi-bay frames and k_w=1 for frame systems.

In Figure 3.4 the design spectrum together with the elastic one are shown.
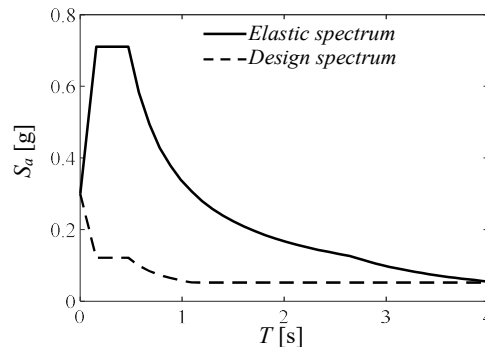
Figure 3.4 Comparison between design spectrum and elastic spectrum for the life safety limit state (LSLS).

Summary of design characteristics

The ultimate limit state (ULS) and serviceability limit state (SLS), combined with the Capacity Design principles have led to the following design choices:

- Beams cross sections of the frames in x-direction: 40x50 cm^2.
- Beams cross sections of the frames in y-direction: beams of 40x50 cm^2 for the perimetral frames and wide beams of 60x23 cm^2 for the internal ones.
- Columns cross-sections: 70x60 cm^2 for the perimetral frames in y-direction and 50x60 cm^2 for the remaining columns.

Table 3.4 Reinforcement detailing of the second building.

Element	Plan location	Floor	Size [mm^2]	Longitudinal bars *	Stirrups *
Beams	A1-A1'	1st-3rd	400x500	4ϕ_u18+3ϕ_l18 (D) 2ϕ_u18+3ϕ_l18 (ND)	2-legϕ8/100(D), 150(ND)
		4th-5th	400x500	3ϕ_u 18+3ϕ_l18 (D) 2ϕ_u18+3ϕ_l18 (ND)	2-legϕ8/100(D), 150(ND)
	B1-B1'	1st-3rd	400x500	5ϕ_u18+3ϕ_l18(D) 2ϕ_u18+3ϕ_l18 (ND)	2-legϕ8/100(D), 150(ND)
		4th-5th	400x500	4ϕ_u18+3ϕ_l18 (D) 2ϕ_u18+3ϕ_l18 (ND)	2-legϕ8/100(D), 150(ND)
	A2-A'2 A3-A'3	1st-5th	230x600	2ϕ_u14+2ϕ_l14	2-leg ϕ8/100
Columns	A1,B1	all	600x500	10ϕ20	4-legϕ8/100 (D), 150(ND)
	A2,A3, B2,B3	all	600x700	16ϕ20	4-legϕ8/100(D), 150(ND)
Nodes	all	all			4-legϕ8/50

*D indicates the dissipative area, ND the non-dissipative area, ϕ_u and ϕ_l are, respectively, the longitudinal reinforcement in the upper and lower chords. The units of measure are mm.

The perimetral beams in y-direction are treated as seismic-resistant elements while the remaining in y-direction (i.e., the shallow or wide beams) are considered as secondary elements. For this reason, no distinction is made between dissipative and non-dissipative area for the wide beams. In addition, the largest dimension of the columns is oriented towards the y-direction for the perimetral frames along y

and towards the x-direction for the remaining columns, as qualitatively shown in Figure 3.3.

As for the reinforcement, 18 mm bars are adopted for the longitudinal reinforcement of the beams, 20 mm for the one of the columns and 8 mm bars for the transverse reinforcement for all the structural elements. In Table 3.4 the summary of the reinforcement detailing is listed with reference to the plan location shown in Figure 3.3 and considering the symmetry (e.g., frame A1-A1' is symmetrical with respect to frame A'1-A'1' and so they have the same mechanical and geometrical characteristics). The extension of the dissipative area in the beams (excluding the wide beams) is equal to 1 m from the column axis, while in the columns is equal to 0.6 m from the beam axis. Finally, all the beam-column nodes have a spacing of the stirrups equal to 5 cm.

It should be noted that the detailing in terms of longitudinal reinforcement of the beams respect the ties criteria of Eurocode 2 (i.e., EN1992-1-1).

3.3   Numerical modelling validation

In this thesis, the finite element (FE) models have been performed by means of the software *ATENA 2D* v5 (Cervenka Consulting s.r.o., 2014).

The adoption of a FE software, instead of a fiber-based one, is to have the possibility of studying the non-linear response of a reinforced concrete frame including both brittle and ductile mechanisms from a global and local point of view. In addition, this work focuses on bidimensional (i.e., 2D) analysis, rather than 3D, because of the need of improving the design of plane frames from a robustness point of view. This is a safe design scope for buildings, and if we consider RC slabs having one-way joists (as usually occurs in Italy) the disregard of the membrane effects (i.e., effects along the out-of-plane direction) can be considered on the safe side.

In order to give a predictive value to the numerical analyses of the present dissertation, a numerical model was elaborated to reproduce the experimental results of the sub-assembly already discussed in Chapter 1 (Section 1.6.3). The model hypotheses were then used for all the numerical analyses of the present dissertation.

In detail, the sub-structure is extracted from a 10-story building designed in Seismic Category D according to ACI 318 Building Code and it is an intermediate moment frame (IMF). As shown in Figure 3.5, the sub-assembly is composed by two beams of around 5.5 m and two columns of around 4.5 m.

The beams have 71.12×50.8 cm^2 cross-sections. Their longitudinal reinforcement is composed of 2 bars of 28.65 mm diameters in the lower chord and 4 and 2 bars of 25.4 mm in the upper chord close to the beam column joints and the midspan, respectively. As for the transverse reinforcement of the beams, the dissipative area, whose length is of 1.83 m, is composed by 2-leg stirrups of 12.7 mm at 10.16 cm step, while the non-dissipative area is composed by 2-leg stirrups of 12.7 mm at 22.8 cm step.

The columns have 71.12x71.12 cm² cross-sections. Their reinforcement is composed of 12 bars of 25.4 mm longitudinally and 4-leg stirrups of 12.7 mm diameter with a step of 10.16 cm.

Regarding the constraint conditions, the tops of the end columns were restrained from horizontal movement using a two-roller fixture, with one roller on each face of the column. These rollers interacted with 51 mm steel plates attached to the column faces via cement hydrostone. Horizontal movement of the steel plates on the exterior face was constrained by four 32 mm post-tensioning bars anchored to a reinforced concrete block with a total clamping force of 2669 kN.

The loading scheme consisted of a displacement-controlled application at a rate of approximately 25 mm/minute. The load was applied by means of 4 hydraulic rams in order to have control of any in-plane rotation of the center column. Also, out-of-plane movement of the specimen was restrained by four steel rods fixed to the reaction wall.
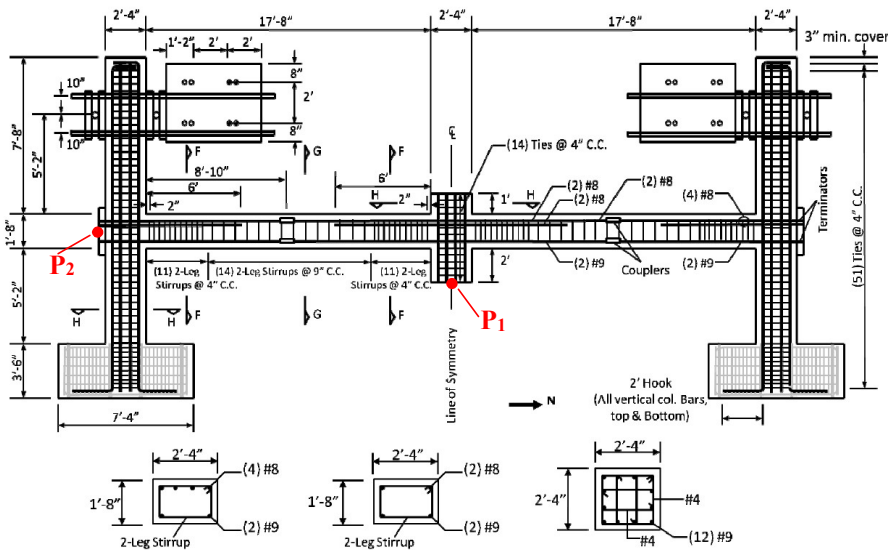
Figure 3.5 Structural details of the experimental test for specimen IMF (modified from NIST, 2011).

Regarding the materials, the mean values of the mechanical properties of both steel and concrete were determined by means of testing. In particular, the mean value of the concrete compressive strength is assumed to be 32 MPa, while the tensile strength is equal to 3.1 MPa. Regarding the steel, four different constitutive laws are considered depending on the bar diameter and structural use, as reported in Table 3.5.

Type	Bar size [mm]	Yield strength [MPa]	Ultimate strength [MPa]	Ultimate strain [-]
Top bars of the beams	25.4	476	648	0.21
Bottom bars of the beams	28.65	462	641	0.18
Bars of the columns	28.65	483	690	0.17
Stirrups	10.16	524	710	0.14

As shown in Figure 3.6, half of the structure was modeled in order to take advantage of the symmetry of the problem and placing rollers with horizontal axis in correspondence of the center line. In addition, in order to model the two-rollers fixture of the column, two springs were placed in correspondence of the joints of the top column, considering a stiffness properly calibrated according to the reaction and the displacement that have been monitored during the test. Specifically, an elastic stiffness equal to 200 MPa was considered, with a length of the spring equal to 5 cm and an area equal to 0.07112 m^2. Finally, the bottom of the column was fully restrained in correspondence of half of the RC rigid footing.
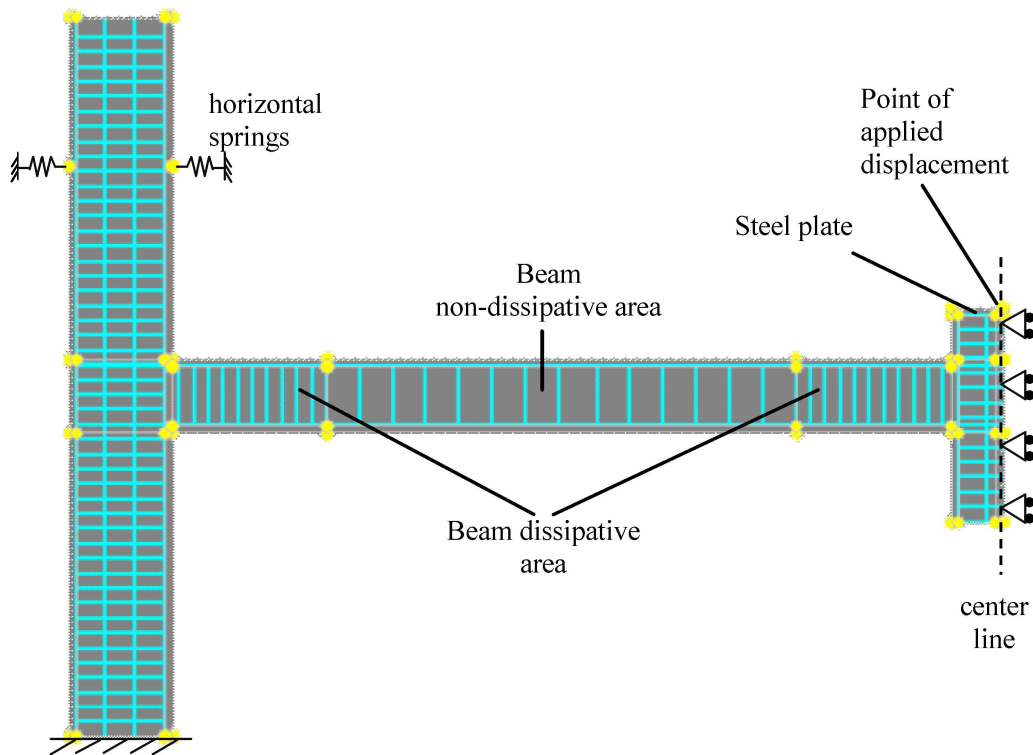
Figure 3.6 FE modelling of the sub-assembly considering joints, macro-elements and discrete bars.

A quadrilateral finite element named "CCIsoQuad" is adopted, which consists of an isoparametric element integrated by Gauss integration at 4 integration points. Those elements are based on bilinear interpolation. A mesh size of 10 cm was selected after an iterative procedure to reach numerical accuracy.

The loading scheme consisted of the application of the self weight and then an imposed vertical downward displacement of 1 cm in correspondence of the loading point, as indicated in Figure 3.6. To better redistribute the stresses due to the application of the imposed displacement, a plate of 5 cm was modeled on top of the accidental lost column. The load deflection curve to be compared with the experimental one was of course deprived from the displacement due to the application of the self weight.

The solution of the equations is obtained by means of a standard Newton-Raphson approach, which fixes the load increment and iterates displacements until the equilibrium is satisfied, according to the tolerances. The maximum number of iterations to reach numerical convergence is equal to 2500 and the tolerances are set equal to (Hendriks et al., 2019):

- 1.0% for the norm of displacement error;
- from 1.0% to 2.5% for the norm of residual force error;
- from 1.0% to 2.5% for the maximum error of residual forces;
- 1.0 ‰ for the out-of-balance energy error.

The solution is reached when all the four criteria are satisfied.

As for the concrete material, the non-linear behavior both in tension and in compression is modelled adopting a *SBeta* material, which is suitable for plane stress 2D analysis. In Figure 3.7a, the equivalent uniaxial constitutive law for concrete in compression is shown in a qualitative representation. Regarding the compressive behavior before the peak stress (i.e., the ascending branch), the formula recommended by CEB-FIP Model Code 90 is adopted. The input values are the secant elastic modulus at the peak stress E_c, the strain at the peak stress ε_c and the compressive strength at the peak f_c. This formulation is suitable both for normal and high strength concrete. For what concerns the behavior after the peak stress, the softening law is a linear descending branch up to zero strength. The parameter that governs the post-peak branch is the compression softening parameter, which is equal to the ratio between the post peak modulus E_d and the secant elastic modulus E_c. Regarding the tensile behavior, the constitutive model adopted is the one in Figure 3.7b. In detail, the behavior in tension without cracks is assumed linear elastic, with elastic modulus equal to E_c and effective tensile strength f_t, while the descending branch of the stress-strain diagram is defined by a linear softening up to the strain c_3 corresponding to zero stress, assumed equal to $10\varepsilon_1$. In this way, it is accounted for the tension stiffening effect (Massicotte et al.,1990), to include the contribution of cracked concrete to the tensile stiffness of reinforcing bars.
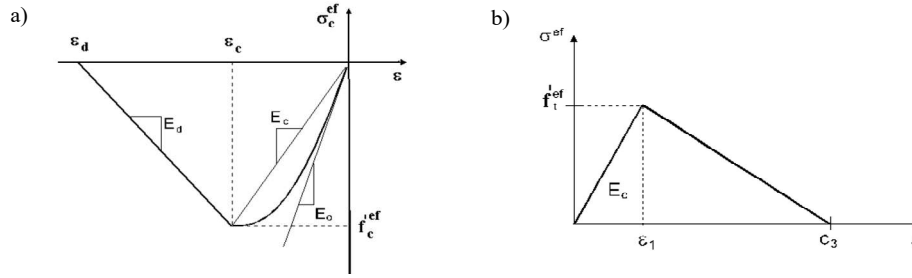
Figure 3.7 Stress-strain diagram of concrete for *SBeta* material (modified from Cervenka Consulting s.r.o., 2014): (a) compressive behavior; (b) tensile behavior.

In addition, the reduction of the compressive strength due to cracks is included by means of a factor equal to 0.45, which represents the maximal strength reduction under large transverse strain, in line with Dyngeland (1989). The shear stiffness decrease after cracking is modelled adopting a variable shear retention factor which evolves with the formation of cracks (Kolmar, 1968). Specifically, the smeared crack approach is adopted, for which the crack forms when principal stress exceeds the tensile strength, and a fixed crack model is assumed. This means that the crack direction is constant and equal to the principal stress direction at the moment of crack initiation (Cervenka, 1985; Darwin and Pecknold, 1974).

In order to account for the confinement effects on concrete due to the influence of transverse reinforcement, the value of the secant elastic modulus at the peak stress E_c, the strain at the peak stress ε_c, the compressive strength at the peak f_c as well as the ultimate strain are defined according to the Saatcioglu and Razvi (1993) model.

Specifically, according to Saatcioglu and Razvi (1993), the triaxial strength of confined concrete f_{cc} can be expressed as function of the unconfined strength f_{co} as function of a k_1 coefficient and the equivalent uniform pressure f_{le}, as follows:

$$f_{cc} = f_{c0} + k_1 f_{le} \tag{3.1}$$

where the coefficient k_1 and the lateral pressure are computed as:

$$k_1 = 6.7 \left(f_{le} \right)^{-0.17} \tag{3.2}$$

$$f_{le} = \frac{f_{lex} b_{cx} + f_{ley} b_{cy}}{b_{cx} + b_{cy}} \tag{3.3}$$

In the previous expression, the equivalent lateral pressure is expressed as the weighted average of the lateral pressure acting on the perpendicular direction of the core dimensions b_{cx} and b_{cy}. In detail, the expressions to compute the lateral pressures on the two main directions are the following:

$$f_{lex} = k_{2x}f_{lx}; \quad f_{lx} = \frac{\sum A_{sy}f_y \sin\alpha}{b_{cx}s}; \quad k_{2x} = 0.26\sqrt{\left(\frac{b_{cx}}{s}\right)\left(\frac{b_{cx}}{s_{lx}}\right)\left(\frac{1}{f_{lx}}\right)} \leq 1.0 \quad (3.4)$$

$$f_{ley} = k_{2y}f_{ly}; \quad f_{lx} = \frac{\sum A_{sx}f_y \sin\alpha}{b_{cy}s}; \quad k_{2y} = 0.26\sqrt{\left(\frac{b_{cy}}{s}\right)\left(\frac{b_{cy}}{s_{ly}}\right)\left(\frac{1}{f_{lx}}\right)} \leq 1.0 \quad (3.5)$$

where s is the stirrups step, s_l is the distance in transverse direction between two consecutive longitudinal bars, A_s is the area of the stirrups leg, α is the angle between the stirrup's legs (usually equal to 90°) and f_y is the yielding strength of the steel reinforcement.

In addition, to evaluate the strain at the peak stress ε_c, the following relationship is adopted:

$$\varepsilon_c = \varepsilon_{01}(1+5K) \quad (3.6)$$

where ε_{01} is the strain corresponding to the peak stress for the unconfined concrete (usually 0.002). Finally, the slope of the descending branch in the post-peak phase E_d is determined by the slope of the branch connecting the peak of the curve and the value corresponding to a stress equal to 85% of the peak one. The deformation ε_{85}, identified as the strain in correspondence of the 85% of the peak stress is given as:

$$\varepsilon_{85} = 260\rho\varepsilon_1 + \varepsilon_{085} \quad (3.7)$$

where ε_{085} is the strain in correspondence of the 85% of the peak stress in case of unconfined concrete (usually 0.0038) and the coefficient ρ is given by:

$$\rho = \frac{\sum A_s}{s(b_{cx}+b_{cy})} \quad (3.8)$$

It should be underlined that the reason to account for the confinement effects also for the beams is that they are subjected to compressive arching forces during the initial phase of the removal of a supporting column (NIST, 2011). Furthermore, confinement effects in beams are crucial when dealing with seismic design as in the case of the frames analyzed in the present dissertation (Miceli et al., 2024b). In addition, when catenary effects starts and the beam is subjected to tensile axial forces, the concrete is not anymore contributing to the resistant mechanism since the load is beard only by the tying behavior of the longitudinal reinforcement of the beams.

For this reason, confined constitutive laws have been considered to reproduce the experimental test. Specifically, different materials have been used to model the

concrete of the beams in the dissipative area (beam D), the beams in the non-dissipative area (beam ND), the column and the concrete cover (equal for all the structural elements), as shown in Figure 3.8, where also the tensile response of concrete is illustrated.
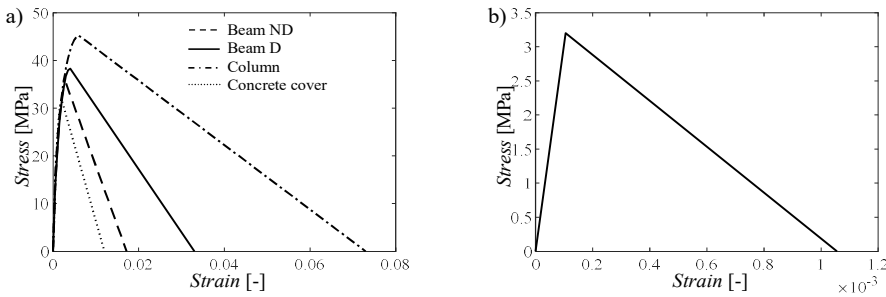
Figure 3.8 Stress-strain diagram of concrete adopted in the FE model: (a) compressive behavior; (b) tensile behavior.

As for the steel reinforcement, a *Reinforcement* material is used adopting a discrete approach (i.e., the reinforcement is modelled through reinforcing bars consisting in truss elements). Perfect bond with the concrete is assumed. A bi-linear law is considered both in tension and in compression including the hardening effects. The constitutive laws of the four different types of steel reinforcement are reported in Figure 3.9. It should be noted that, during experimental investigations related to progressive collapse, often buckling of reinforcement in the compressive zone is observed. This phenomenon is usually related to the small size of concrete cover (Dhakal RP and Maekawa, 2002). Even if in this experimental investigation no buckling phenomena were declared, this issue should be considered for further improvements.
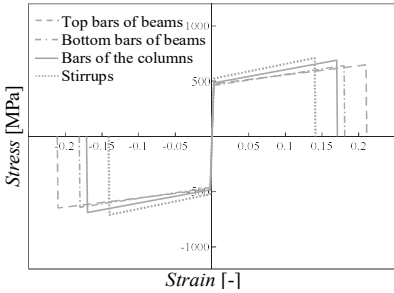
Figure 3.9 Stress-strain diagram of steel reinforcement adopted in the FE model both in tension and in compression.

In the following, the comparison between the numerical and the experimental results is shown in terms of curve load-vertical displacement, horizontal-vertical displacement (Figure 3.10) and considering the crack formation.

It should be noted that not considering the confinement effects in the beams does not allow to capture the increase in resistance as well as the ductility capacity given by the triaxial state of stress enhanced by the presence of transversal reinforcement of the beams together with the compressive arch forces.
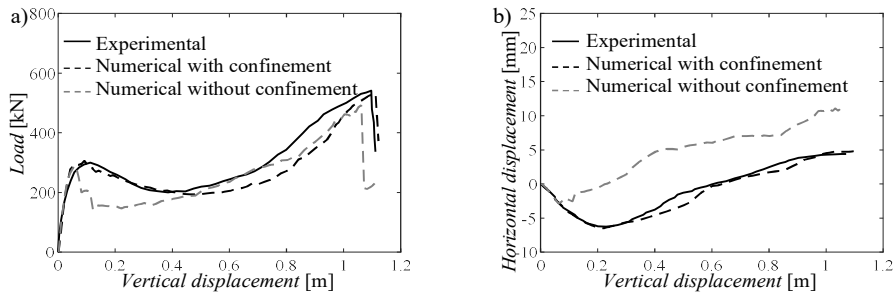
Figure 3.10 Comparison between experimental and numerical results: (a) load vs vertical displacement of point P1; (b) horizontal displacement of Point P2 vs vertical displacement of point P1.

Furthermore, Figure 3.11 shows the trend of the axial load in correspondence of the beam as function of the vertical displacement of point P1. As already anticipated, the removal of a supporting column determines the presence of an axial load of compression in the initial phase up to the softening stage. Then, in correspondence of a displacement of around 20 cm, the transition to catenary effect starts and the normal loads change sign, becoming a tensile action.
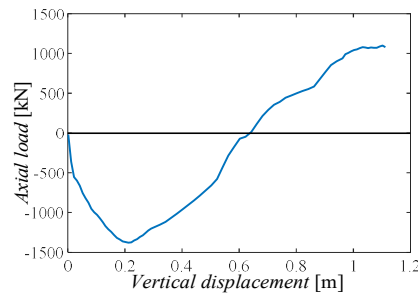
Figure 3.11 Trend of the axial load in the beam as function of the vertical displacement of point P1.

Figure 3.12 shows the comparison between the experimental and numerical results in terms of crack patterns in correspondence of half of the total imposed displacement (i.e., 61.1 cm) and at failure (i.e., 109.2 cm). It should be emphasized that, coherently with the experimental result, failure occurs because of the attainment of the ultimate strain in correspondence of the lower longitudinal bar of the beam close to the central column.
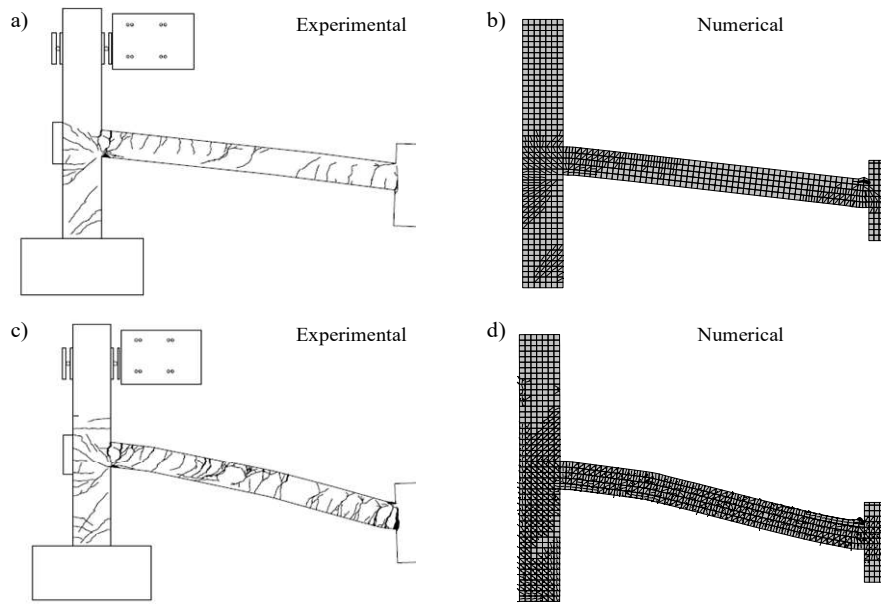
Figure 3.12 Comparison between experimental and numerical results in term of crack pattern for a center column deflection of: (a)-(b) 61.1 cm; (c)-(d) 109.2 cm.

3.4 Numerical modelling of the frame under study

The basic assumptions on the modelling of the experimental tests have been the starting point to model the frames under study. The only difference is that in this case an entire frame has been considered and not only a sub-structure. In Figure 3.13 an example of one of the models considered in this study is reported. In particular, joints, line (i.e., connections between joints), macro-elements (i.e., elements enclosed by four lines) and both shear and transverse reinforcement are shown. The boundary conditions consist of fixed restraints at the base of the columns.
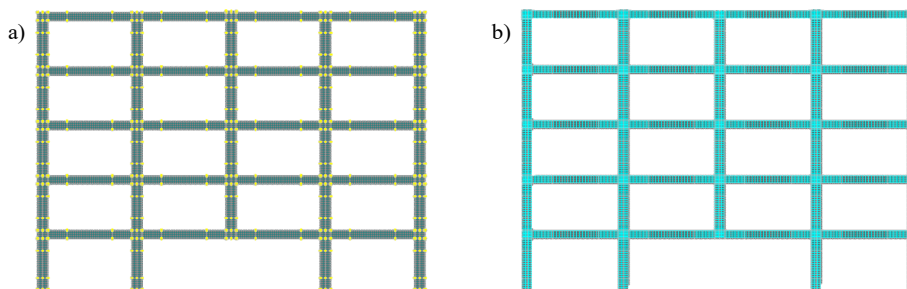
Figure 3.13: Example of a 2D NLFE model: (a) representation of joints, lines, macro-elements and mesh; (b) representation of the longitudinal and transversal reinforcement.

3.4.1 Modelling of equivalent elastic springs

In this dissertation, the contribution of the orthogonal framed system is taken into account in a simplified way by means of equivalent translational springs. The rotational effects are not accounted for since they have a negligible influence on the flexural peak and do not influence the catenary effect, as demonstrated in Zheng et al. (2022) and Pham and Tan (2017), by means of experimental considerations.

Two types of equivalent springs are calibrated: at first by means of elastic analyses (adopted for the analyses in Chapter 4 and Chapter 5) and then by considering also the non-linearities of the materials (adopted for the analyses in Chapter 6).

In both cases, the stiffness of the translational elastic springs has been calibrated for each beam-column node by performing the analyses on SAP2000 (CSI, 2022). In detail, the 3D building is modelled without the accidentally lost column, and considering the axial contribution of the one-way RC slabs by means of 20 cm high joists. The joists are modelled as elastic in both cases.

Elastic 3D analysis

For the elastic analyses only, to account in a simplified way for the non-linear behavior of concrete and according to Avşar et al. (2022), Castaldo and De Iuliis (2014) and ASCE (2000), the following percentages are considered: 0.8 of the torsional stiffness of all the beams, 0.7 of the bending stiffness of all the beams, 0.5 of the bending stiffness of all the columns. In addition, the axial and bending stiffness of beams and the bending stiffness of the columns of the frame under study in the in-plane directions are nullified since their contributions are already considered in the 2D FE model. For the same reason, the axial stiffness of the columns of the frame under study is reduced to 0.5.
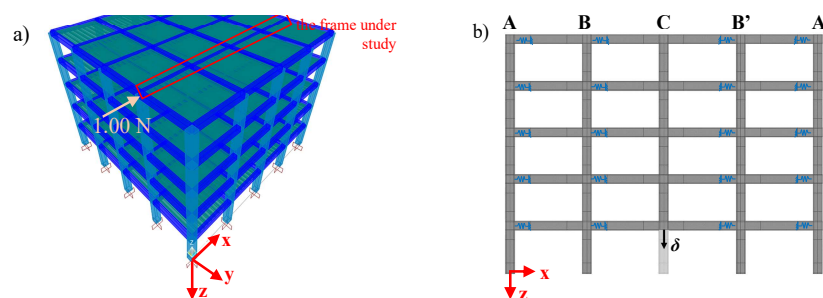
Figure 3.14 Example calculation of the equivalent elastic springs: (a) 3D structure modelled in SAP2000: calibration of the spring stiffness for the last floor, external column; (b) springs positions (in blue) for one of the frame under study modelled in ATENA-2D.

Then, to calculate the stiffness at each beam-column node, a unitary horizontal force in the in-plane direction of the frame under study is applied and the corresponding displacement is computed. An example of the spring calibration in SAP2000 is shown in Figure 3.14a. By dividing the unitary force for the displacement, the corresponding stiffness is calculated. This approach has been

repeated for each beam-column node apart from the ones of the removed column. Finally, the equivalent elastic spring is modelled for each beam-column node in ATENA 2D as shown in Figure 3.14b as a *Spring* element applied at the center line of each beam-column node (in order to better distribute the local stresses).

More details on the numerical values of the equivalent elastic springs will be given in Chapter 4.

Non-linear 3D analysis

For this type of modeling, a difference with respect to the previous case is that the non-linear behavior of both steel and concrete is accounted for. First, the supporting column is removed to simulate the specific failure scenario and the axial and bending stiffness of beams and columns of the frame under study are reduced back to zero since their contributions are already accounted for in the planar FE model. The non-linear behavior of the structure has been modeled using fiber-based plastic hinges placed at specific points in the columns and beams. The length of the plastic hinges is obtained based on ASCE, 2000 and Panagiotakos et al. 2001, considering the geometric properties of the cross-sections of the structural elements. The number of fibers for each cross-section is determined through an iterative process to ensure numerical accuracy. Specifically, the fiber plastic hinges are of "P-M2-M3" type, accounting both for the two orthogonal bending moments and the axial force. This assumption is fundamental when column loss scenario is involved since beams are subjected to axial forces. Within the 3D simulations, the geometrical non-linearities are also considered.
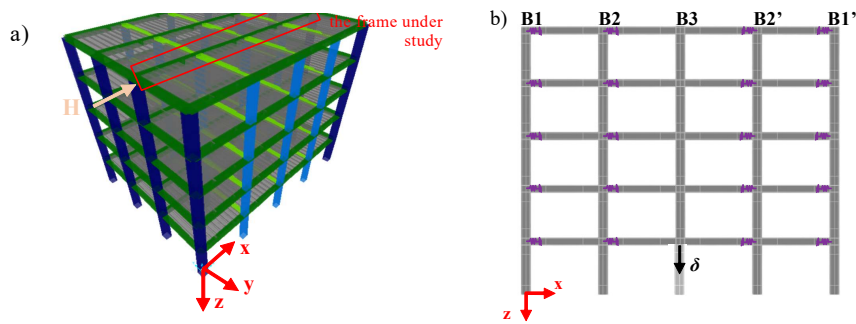
Figure 3.15 Calculation of the equivalent non-linear springs: (a) 3D structure modelled in SAP2000: example of calibrating the spring stiffness for the last floor, external column; (b) springs positions (in purple) for one of the frame under study modelled in ATENA-2D.

Then, differently from the previous calibration, displacement-controlled numerical analyses have been carried out by imposing, in the node, a horizontal displacement (H) in the out-of-plane direction of the orthogonal frame (e.g., x-direction for the example reported in Figure 3.15a, by adopting steps of 1 cm. Shear failure was never reached, respecting all the shear verifications. Then, by dividing the displacement for the reaction, the non-linear force displacement curve representing the constitutive model of the spring is obtained. This process has been reiterated for each beam-column node in all the columns except the one experiencing collapse. A maximum imposed horizontal displacement of 200 mm

was considered since the beam-column nodes do not experience larger displacement during the collapse scenario, as demonstrated in the next Chapters. A schematic representation of the approach to compute the equivalent non-linear springs is shown in Figure 3.15a. Then, the equivalent non-linear spring is modelled for each beam-column node in ATENA 2D as shown in Figure 3.15b as a *Spring* element applied at the center line of each beam-column node (in order to better distribute the local stresses). More details on the non-linear constitutive models will be given in Chapter 6.

As an important remark, it should be underlined that the application of a unit load (or force) at the beam-column node does not influence the calculation of the remaining nodes. In fact, the axial and bending stiffness of beams and the bending stiffness of the columns of the frame under study in the in-plane directions are nullified in the 3D model. This interaction is taken into account in the 2D NLFE model.

Chapter 4

Robustness improvements and deterministic FEM analyses

4.1 Introduction

This chapter deals with the discussion and deterministic evaluation of the design improvements in order to enhance the structural robustness of a reinforced concrete (RC) building located in a high seismicity area. At first, a discussion of code provisions, literature studies, and new proposals for the design of RC buildings under column removal scenario is carried out. Then, these improvements are applied to the building described in Section 3.2.1. (i.e., first building). In particular, a parametric analysis on an internal 2D RC moment resisting (MR) frame is performed by modifying the arrangement of the longitudinal reinforcement, always respecting the capacity design code provisions (CEN, 1998). The goal is to improve the seismic design exploiting the catenary effect as well as increasing the bearing capacity of the structure against an accidental removal of a supporting column.

4.2 Design improvements to enhance structural robustness

At present, the approaches to the design of structures following robustness criteria are mainly deterministic or semi-probabilistic. Regarding the European code rules, two strategies are proposed in EN 1991-1-7:2006. The first strategy is based on the identification of extreme events and on how to reduce the intensity of the action as well as to avoid the damage initiation. The second strategy is based on mitigating the damage extension by means of redundancy, key elements design and prescriptive rules such as integrity and ductility. In particular, redundancy measures aim at finding alternative paths by means of vertical and horizontal ties (traction anchors) and structural elements design performed in order to bear the accidental

load. This accidental load should be computed according to the accidental combination prescribed in EN 1990:2002. In addition, Eurocodes suggest performing a risk assessment under the decision of authorities and/or stakeholders (and not as a prescription) for structures in Consequence Class 3 (i.e., high rise building, grandstands, stadia etc.). The United States regulations (i.e., ASCE 7-10), provide two ways of designing: direct and indirect measures. In direct design, resistance to progressive collapse is explicitly considered during the design process by means of alternative load path method. The indirect design approach incorporates minimum levels of strength, continuity, and ductility implicitly during the design process. This is achieved through ties, load-bearing interior walls, catenary action of floor slabs, redundant structural systems, ductile detailing, providing additional reinforcement and compartmentalization.

Regarding literature studies, many authors have explored various parameters in order to enhance the robust design of reinforced concrete (RC) buildings: the increase of longitudinal reinforcement to improve load-bearing capacity, the reduction of stirrup step to mitigate flexural-shear interaction and prevent brittle failure (Parisi and Augenti, 2012; Ribeiro et al, 2024), the symmetric arrangement of longitudinal reinforcement to increase the bending capacity of beams (Brunesi et al., 2015), the increase in the height of the beam to enhance beam behavior (Ren et al. 2016 and Zhang et al. 2016). In addition, the beneficial effects of RC slab strips as well as transverse beams, particularly in developing catenary actions, are discussed in many works (Belletti et al., 2019; Fascetti et al., 2015; Wang et al., 2022; Brunesi and Parisi, 2017; Feng et al., 2022). Also the presence of infills was demonstrated to enhance the bearing capacity of the structure, as discussed in Di Trapani et al. (2020) and Feng et al. (2022).

In this section, design improvements for robustness enhancement will be discussed and motivated. Notably, reference is made to moment resisting MR frames (i.e., designed according to seismic guidelines). Then, a new analytical approach to calibrate *side face rebars* is proposed.

In this thesis, the design improvements will mainly focus on the arrangement of beam longitudinal reinforcement. In detail, distinction is made between some indications already present in literature studies or code rules and new proposals suggested and investigated in this thesis.

4.2.1 Literature and code rules suggestions

As already anticipated, different code rules and literature study suggest increasing the robustness of RC MR frames by providing:

- *support continuity:* it is intended as arranging the longitudinal reinforcement continuously over the beam-column nodes. In fact, because of standard design and seismic design at ULS, usually beams are conceived with a non-constant arrangement of the longitudinal reinforcement in order to consider the different value and sign of the bending moment across different sections of the beams. In this way, the reinforcement is larger in

the most stressed sections. However, when a supporting column is removed, the presence of a continuous longitudinal reinforcement over the supports can increase the tying capacity of the beams and enhance a robust behavior. As already anticipated, this suggestion is present in many code rules and provisions, such as: GSA2003, DCLG2010, ASCE 7-02, CNR2018;

- *section symmetry (S):* it is intended as having the same amount of longitudinal reinforcement between the upper and lower chord of the cross section. The reason for this is similar to what explained for the previous criterion: because of gravitational loading, the upper chord is subjected to tensile forces close to the supports and the opposite occurs close to the midspan of the beams. However, when a supporting column is removed, the lower chord of the section close to that column is subjected to a shift in the moment sign. This suggestion is present in GSA (2003) as well as studied in some literature works like Brunesi et al. (2015);

- *elastic springs:* this suggestion is intended as including lateral constraints in the beam-column nodes of the frame in order to simulate the presence of the orthogonal structural system. As a general consideration, the presence of the slab as well as the torsional and horizontal flexural-shear response of the beams in the out-of-plane direction can enhance a robust behavior because of the constraint actions on the main frame. These concepts have been studied by many authors such as Belletti et al. (2019), Xuan and Tan (2013), Tan et al. (2022), Wang et al. (2022), Belletti et al. (2018), Botte et al. (2015), Cantone et al. (2016), Avşar et al. (2014). In this work, since planar (i.e., 2D) NLFE model are studied, only the contribution of the horizontal flexural-shear response of the orthogonal beams combined with the one-way joists of the slab are modeled in a simplified way in order to reproduce the three-dimensional effect.

4.2.2 New proposals

In this thesis, the previous considerations have inspired the following new proposals (Miceli and Castaldo, 2024), to be applied to RC MR frames:

- *Continuity (C):* this criterion is inspired by the *support continuity* but is characterized by an increase in the length of the continuous longitudinal reinforcement until the 30% of the span length of the beam, from the column axis and at each beam-column node, in addition to the anchorage length. The reason for this is that when a supporting column is accidentally removed, the extension of the bending moment in the upper chord of the beam is larger and thus, an increase of the continuity length is needed. This helps in avoiding plastic hinges concentrations in cross-sections usually characterized by a lower bending resistance and ductility;

- *global floor equality (E)*: this suggestion consists in applying the same quantity of reinforcement (i.e., the largest one) in all the floors. The reason behind this suggestion is that the longitudinal reinforcement amount in the

beams of the lower floors is usually larger because of larger internal actions are obtained in the lower floors in accordance to the seismic combinations. However, when a supporting column is lost, due to the very large axial stiffness of the columns, all the floors are subjected to similar internal stresses. Thus, this suggestion is based on the idea of exploiting a Vierendeel behavior of the beams in all the floors.

- *partial floor equality (P)*: this proposal is similar to the previous one but consists in applying in the last floor the same amount of reinforcement of the lower one (i.e., the largest amount). Again, this is done to exploit a Vierendeel behavior.

- *side face rebars*: the presence of *side face rebars* can be beneficial in anticipating the tying effect and activating the catenary behavior. In fact, being close to the barycenter of the section, *side face rebars* are not subjected to large stresses during the initial phase (i.e., flexural stage) of the collapse scenario. On the other hand, after the softening stage, beams are subjected to tensile forces and *side face rebars* can provide an important contribution, reducing the mechanical effort required for the other longitudinal bars.

It should be underlined that the design of *side face rebars* in the present dissertation has been carried out by evaluating the tie demand under a progressive collapse mechanisms of the RC sub-assemblages, as discussed in CNR (2018).

Table 4.1 Summary of the different types of NLFE analyses.

	Model	Support-continuity	Continuity	Section symmetry	Elastic springs	Global floor equality	Partial floor equality	Side face rebars
Literature and code rules suggestions	*Code*	●						
	C	●	●					
	CS	●	●	●				
	CS+springs	●	●	●	●			
New proposals	*CSE+springs*	●	●	●	●	●	●	
	CPE+springs	●	●		●		●	
	CSE+springs +rebars	●	●	●	●	●	●	●
	C+springs +rebars	●	●		●			●
	CPE+springs +rebars	●	●		●		●	●

In this thesis, some of these suggestions and proposal are combined in order to investigate the capacity of the frame in terms of flexural behavior and catenary effect. In Table 4.1, all the combinations between the different suggestions and proposals are summarized. These combinations will be evaluated by performing a deterministic approach and analyzing the results of non-linear finite elements

pushdown analysis for different collapse scenario and structural configurations (i.e., Chapter 4 and Chapter 6) and also by means of a probabilistic approach in order to compute the reliability associated with a single column removal scenario (Chapter 5).

It is important to underline that a modification in the beam longitudinal reinforcement should be verified according to the capacity design principles (CEN, 1998), since an increase in the amount of longitudinal reinforcement determines an increase in the shear action on the dissipative area of the beams. A cycling approach is thus needed after each robustness enhancement in order to account for all the verifications, as graphically shown in Figure 4.1.
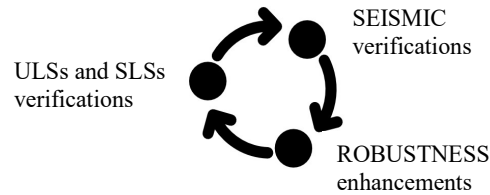
Figure 4.1 Schematic representation of the cyclic design procedure for robustness enhancement (Miceli and Castaldo, 2024).

4.3   FEM modelling

The different frames studied in this chapter are modeled in ATENA 2D following the modeling assumptions described in Section 3.3 and 3.4 and performing pushdown analyses. Specifically, displacement-controlled non-linear analyses are considered, by modeling the frame without the accidentally lost column, applying a monotonically increasing vertical displacement in the point of column removal and monitoring the capacity in terms of reaction given by the structure in the same point.

For all the numerical model, the mean values of the mechanical properties are adopted. Notably, for the C25/30 concrete, the confinement effects are included by means of the Saatcioglu and Razvi (1993) model. Considering the different configurations of the transverse reinforcement, distinction is made between the constitutive models of: concrete in dissipative area of beams ("beam D"), concrete in non-dissipative areas of beams ("beam ND"), concrete in columns, concrete in beam-column nodes and unconfined concrete (i.e., effective concrete cover). Thus, the concrete elastic modulus as well as the compressive strength and strain in correspondence of the peak and the ultimate strain are function of the confinement effects. Hence, the constitutive laws of concrete differ depending on the design assumptions as discussed in the following sections. The tensile behavior of concrete is described by f_{ctm} which is the mean value of the tensile strength (i.e., 2.56 MPa) and E_{cm} representing the mean secant elastic modulus, computed according to Eurocode 2 (CEN, 2004).
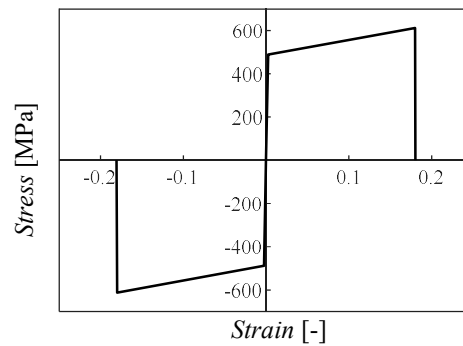
Figure 4.2 Constitutive laws for the steel reinforcement both in tension and compression.

Regarding the B450C steel property, the elastic modulus is assumed equal to 210 GPa, the yielding strength is equal to 489 MPa, while the ultimate strength is equal to 611 MPa (i.e., by considering an ultimate-to-yielding strength ratio equal to 1.25 as suggested by the Italian Guidelines (MIT, 2018). The ultimate strain is equal to 18% (Ren et al., 2016; Lu et al., 2017; Yu and Tan, 2013a-b; Lew et al., 2011), assumed as a nominal value in order to exploit the global response of the frames for large deformation capacity of the steel reinforcement. In Figure 4.2, the constitutive law of the steel reinforcement is shown, and it is equal for all the different design assumptions.
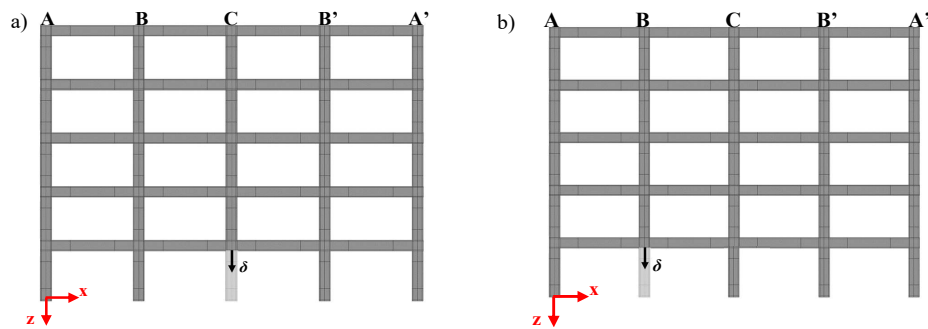
Figure 4.3 Schematic representation of the non-linear pushdown analysis for: (a) first failure scenario; (b) second failure scenario.

In the following, the different configurations of the longitudinal reinforcement are analyzed by means of the capacity curves (i.e., displacement-reaction) considering two failure scenarios (Figure 4.3):

- First failure scenario: removal of the central supporting column.
- Second failure scenario: removal of the second-to-last supporting column.

Only these two failure scenarios are studied since they represent the worst situations in a 3D building when the contribution deriving from infills (Brunesi and Parisi, 2017; Di Trapani et al., 2020; Feng et al., 2022) is not considered.

It should be noted that in this Chapter the capacity of the frame is evaluated by studying the resistance given by the structure against the static application of an imposed increasing vertical displacement. Hence, no loads (included the self weight) are applied in this part of the dissertation. Of course, the application of a concentrated displacement rather than a distributed load (which is closer to reality)

is an assumption. At the same time, the application of a displacement rather than a load allows to investigate the softening response of the structure.

Furthermore, the pushdown analysis is stopped when collapse occurs, consisting of failure at the concrete level or reaching of the ultimate strain of a single reinforcement bar. In the following, the location of the achievement of the ultimate strain of reinforcement bar is clarified for each frame under investigation.

4.4 First failure scenario: removal of the central supporting column

This section focuses on the capacity curves obtained from different NLFE models of the RC MR frame where the first failure scenario is considered (i.e., removal of the central supporting column). Specifically, the following design assumptions will be discussed:

- *Code* model (i.e., according to the conventional design approach).
- Models with *continuity*, *symmetry* and *springs*.
- Models with *global* or *partial equality* and *side face rebars*.
- Models with *minimum* design suggestions.

4.4.1 Code model – first failure scenario

At first, the capacity curve of the model designed according to the actual code rules (i.e., Eurocodes and Italian Guidelines) is analyzed. This design respects only the *support continuity* criterion, meaning that the longitudinal reinforcement is continuous over the supports (i.e., beam-column nodes).
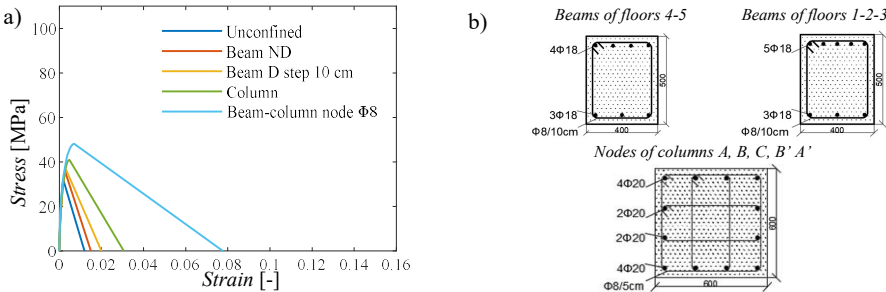
Figure 4.4 *Code model*: (a) concrete constitutive laws in compression; (b) distribution of the longitudinal and transverse reinforcement in the most stressed cross-sections for each floor.

A summary of the constitutive laws of concrete in compression and the different cross-sections in the most stressed parts is presented in Figure 4.4.

The Figure 4.5a shows the NLFE pushdown curve for the frame designed according to the current codes and for the first failure scenario. The peak in the flexural stage, i.e., $P_{MAX,FL}$, is equal to 811 kN. The peak is followed by a very brief softening phase after which failure occurs in correspondence of an imposed displacement of 21 cm and an ultimate resistance i.e., P_{ULT} equal to 738 kN.

As visible from Figure 4.5b, the failure is due to the formation of concentrated curvatures in critical areas, located in the beams, close to the columns B and B', leading to convergence loss. These critical areas are in cross-sections where there is the transition from dissipative to non-dissipative zone and especially where there is a discontinuous longitudinal reinforcement and a change in the step of the stirrups. In these areas, at the last convergence step of equilibrium, the peak value of the strain in the longitudinal reinforcement is equal to around 10% and it is reached in the top bar, while the peak strain of the transverse reinforcement occurs in the first floor, close to the columns B and B', reaching the value of around 6%. Thus, failure occurs at the concrete level. In addition, the shear capacities of the beams close to the column C are equal to around 160 kN and 265 kN in, respectively, the dissipative and non-dissipative area, and are not overcome.

Figure 4.5 Results of the pushdown analyses for the first scenario for the *Code model*: (a) capacity curve; (b) failure mode with the critical regions in terms of crack formation; (c) horizontal displacements of the beam-column nodes; (d) vertical displacements of the beam-column nodes.

By observing the Figure 4.5c-d, it can be deduced that the structure does not show any catenary behavior remaining in the flexural-arching phase. This aspect can be confirmed by analyzing the horizontal displacements monitored on the beam-column nodes of the columns A and B, in correspondence of all the five floors (Figure 4.5c): there is an increasing outward horizontal movement of these columns due to the arching behavior of the beams. By looking at the vertical displacements (Figure 4.5d), the column B, which is the closest to the collapsed area, tends to first move downward due to the flexural behavior and then, because of the arching behavior of the beams, tend to move upward following the rotation of the nodes. On the other hand, being external, the nodes of the column A are less influenced by the initial flexural stage since their movements start when arching behavior causes their upward displacements.

4.4.2 Models with continuity, symmetry and springs – first failure scenario

At first, the modification of reinforcement bars in the frame is evaluated applying the *continuity* criterion and obtaining the *C model*. The new arrangement of the longitudinal reinforcement is continuous along 1.5 m at two edges of the span and it is made of: 3ϕ18 in the lower chord of all the beams of the five floors, 5ϕ18 in the upper chord for the first three floors and 4ϕ18 in the upper chord of the last two floors. As for the ULSs and seismic verifications, the new arrangement of longitudinal reinforcement results verified, meaning that the shear reinforcement of the beams, the longitudinal and shear reinforcement of the columns and of the beam-column nodes remain the same of the *Code model*. The characteristics of this model are reported in Figure 4.6a-b.
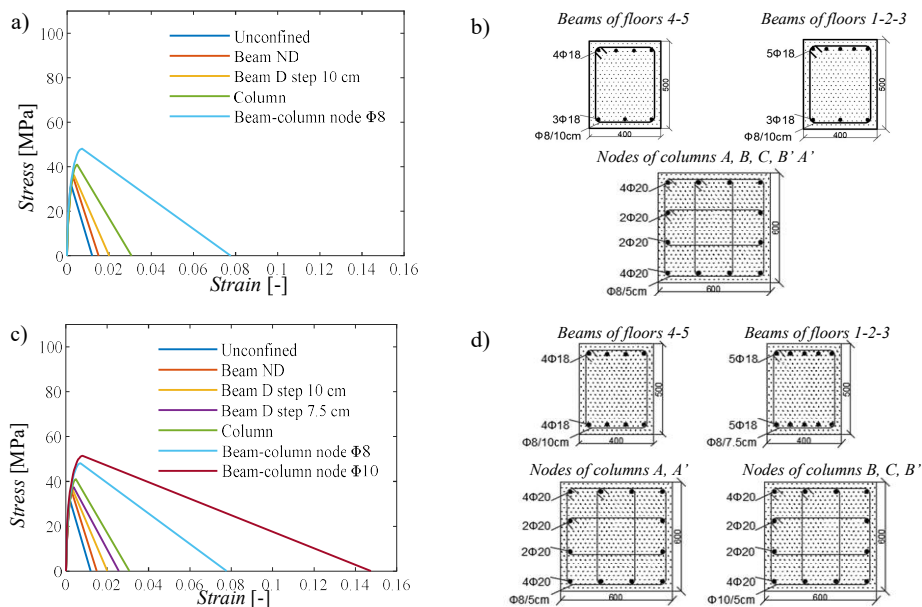
Figure 4.6 (a),(c) concrete constitutive laws in compression; (b),(d) distribution of the longitudinal and transverse reinforcement in the most stressed cross-sections for each floor for, respectively, *C* and *CS* (or *CS+spring*) *models*.

Secondly, while maintaining the *continuity* criterion, the *symmetry* in the cross-sections is adopted, with the aim to have the same quantity of reinforcing bars between the upper and lower chord of the beams and obtaining the *CS model*. This model is characterized by a reinforcing bar arrangement made of 5ϕ18 in both chords of the first three floors and 4ϕ18 in both levels in the last two floors. To respect the capacity design principles, a change of the stirrup steps from 10 cm to 7.5 cm in the dissipative zone for the beams of the first three floors is needed. At the same time, a change in the stirrup diameter from ϕ8 to ϕ10 is necessary for the beam-column nodes of the columns B, C and B', maintaining the step of 5 cm. On the other hand, the longitudinal and transverse reinforcement of the columns remains unchanged. It should be noted that the modification in the stirrup diameter also implies a change of the constitutive law for the confined concrete of the

dissipative zone for both the beams ("beam D step 7.5cm") and for the beam-column nodes ("beam-column node ϕ10"). The characteristics of this model are reported in Figure 4.6c-d.

The third modification consists of considering the contribution of the orthogonal framed system in a simplified way by means of *equivalent elastic springs*. This new model is identified as *CS+spring model*. It should be noted that the mechanical and geometrical characteristics of this frame are the same of the *CS model* and, thus, refer to the characteristics summarized in Figure 4.6c-d.

The approach to calibrate those springs is deepened in Section 3.4.1. In Table 4.2, the numerical values of the *equivalent elastic springs* are listed, while in Figure 4.7 the schematic representation of the spring position is illustrated.

Table 4.2 Elastic spring stiffness for the different floors and for the first failure scenario.

	Spring Stiffness - column A and A' [N/m]	Spring Stiffness - column B and B' [N/m]
1st floor	$9.775 \cdot 10^7$	$9.634 \cdot 10^7$
2nd floor	$7.143 \cdot 10^7$	$7.062 \cdot 10^7$
3rd floor	$5.291 \cdot 10^7$	$5.247 \cdot 10^7$
4th floor	$4.122 \cdot 10^7$	$4.095 \cdot 10^7$
5th floor	$3.291 \cdot 10^7$	$3.270 \cdot 10^7$
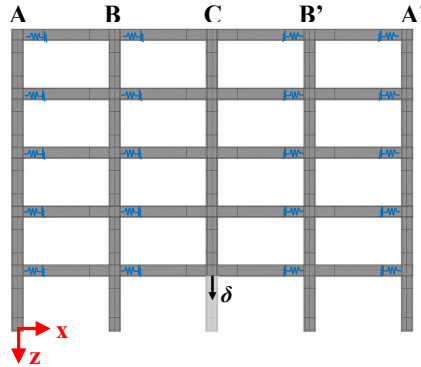
Figure 4.7 Springs positions (in blue) for the first failure scenario.

In the following, the results from the NLFE analysis in terms of capacity curve, vertical and horizontal displacements of the beam-column nodes are shown for: *C model* (Figure 4.8c-d), *CS model* (Figure 4.8e-f), and *CS+springs model* (Figure 4.8g-h). With respect to the *Code model*, adding *continuity* of longitudinal rebars (i.e., *C model*) leads to an increase of the ultimate imposed displacement, equal to 30 cm (Figure 4.8a). In fact, the *continuity* criterion determines a redistribution of stresses along the beam length in a homogenous way (as visible in Figure 4.8b) and, thus, it implies a delay in the ultimate drop of resistance. As a consequence of the increase of the total amount of reinforcement, the flexural peak slightly increases compared to the previous case, reaching a value of $P_{MAX,FL}$ of 846 kN. Another improvement can be observed for the vertical displacement of the column B (Figure 4.8d). The transition from positive (downward) to negative (upward) displacement is herein more pronounced since the presence of a continuous longitudinal reinforcement increases the ductile response. In fact, an important outcome is the

presence of concentrated curvatures in sections closer to the columns (Figure 4.8b) confirming the improvement with respect to what observed in (Figure 4.5b). This result is in line with the observation in CNR (2018), where it is underlined that if the reinforcement is continuous over the lateral columns, the structure shows a larger softening.

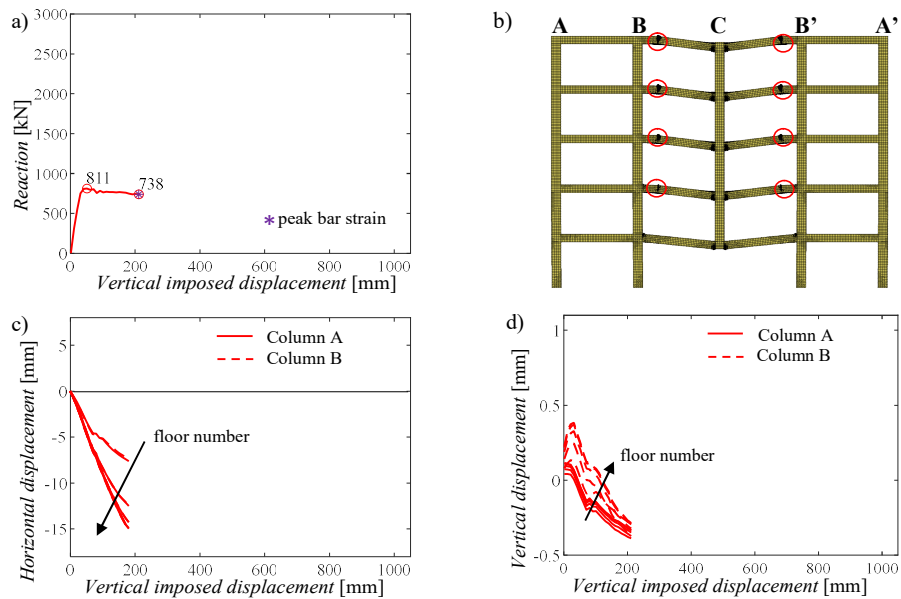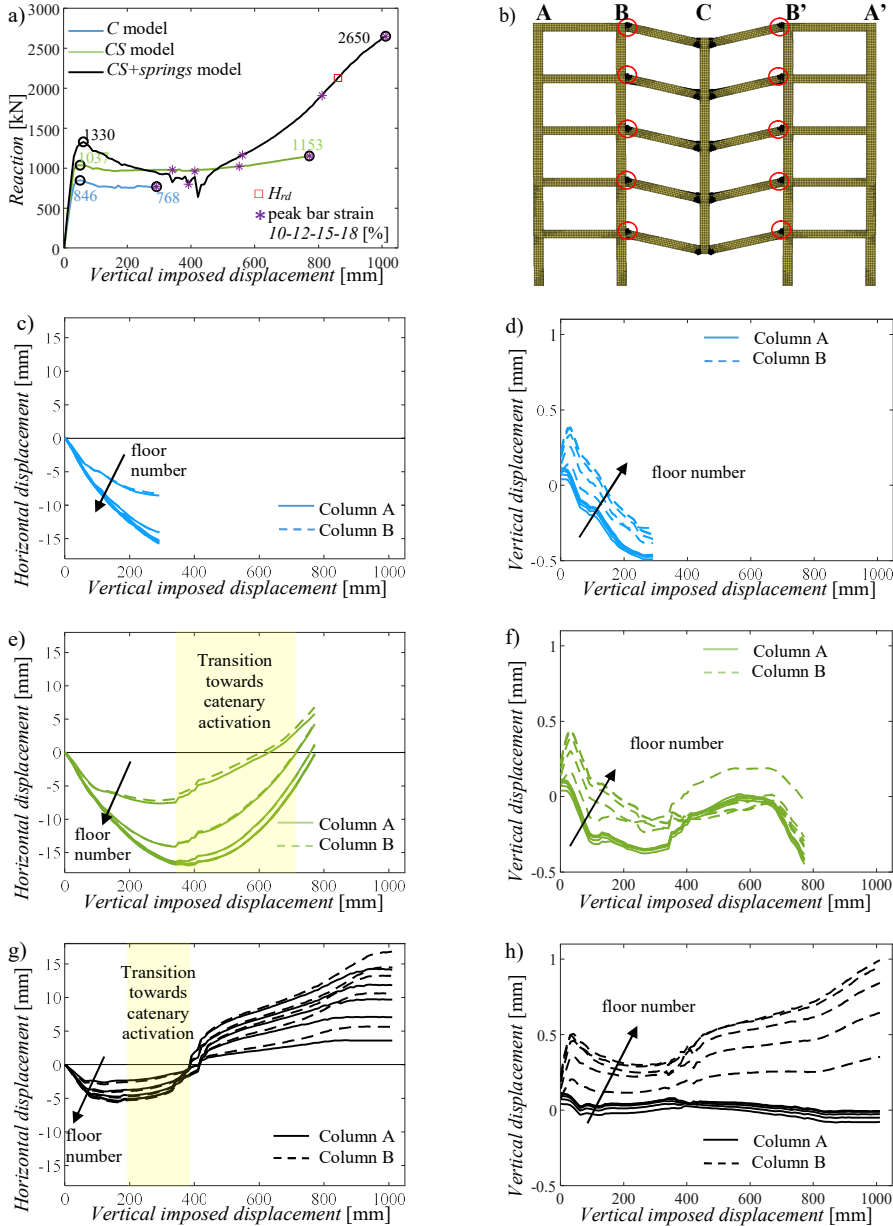**Figure 4.8** Results of the pushdown analyses for the first scenario: (a) capacity curves; (b) failure mode with the critical regions; (c),(e),(g) horizontal displacements of the beam-column nodes; (d),(f),(h) vertical displacements of the beam-column nodes, for *C*, *CS* and *CS+springs models*.

At the last convergence step of equilibrium, the peak tensile strain of the longitudinal bar is equal to 10% and it is reached on the lower reinforcing bars of the beams in correspondence of the central column. Regarding the stirrups peak strain, it is reached in the first floor close to the columns B and B' and it is equal to

around 10%. Even if there is an improvement, no catenary stage occurs: the nodes continue to move outward (horizontal displacements) without any shift in sign (Figure 4.8c), suggesting the persistence of a flexural-arching behavior, also confirmed by the upward increasing displacement of the nodes of the columns A and B (Figure 4.8 d).

As for the adoption of symmetric longitudinal reinforcement (i.e., *CS model*), the main advantage is an important recovery in the strength after the resistance drop during the softening stage. The ultimate resistance P_{ULT} is equal to 1153 kN in correspondence of an ultimate imposed displacement of 77 cm. Furthermore, this ultimate resistance is higher than the flexural peak $P_{MAX,FL}$, equal to 1037 kN. In fact, at a displacement of around 40 cm there is an activation of the catenary behavior for the beams of the frame. The catenary effect activates when the vertical imposed displacement reaches almost one beam depth, as also observed in the experimental test of Lew et al. (2011). The catenary activation is visible from the capacity curve (Figure 4.8a) and from the horizontal (Figure 4.8e) and vertical (Figure 4.8f) displacements of the beam-column nodes. In fact, for the equilibrium of the beam-column nodes, the transition from an arching to a catenary behavior implies the shift from compressive to tensile actions on the beams. Thus, the nodes start to displace inward at an imposed displacement of around 40 cm. At the same time, the transition to catenary behavior implies nodes to move downward. The peak strain reached along the longitudinal reinforcement is equal to the ultimate value of 18% in the upper bars close to the columns B and B'. Regarding the stirrups peak strain, it is reached in the stirrups of the beams of the first floor close to the columns B and B' and it is equal to around 10%.

Finally, the additional presence of lateral springs (i.e., *CS+springs model*) implies an increase in the flexural peak due to the axial loads acting on the beams, with a flexural peak $P_{MAX,FL}$ of 1330 kN. Furthermore, the presence of lateral constraints facilitates the transition to catenary effect at a displacement between 20 cm and 40 cm. The constraints of nodes are also visible in the horizontal displacements shown in Figure 4.8g, for which the outward horizontal displacement of the columns A and B is less pronounced with respect to the inward displacement caused by the tying effect of the rebars. Results in terms of vertical displacements (Figure 4.8h) of the nodes show that the horizontal springs tend to reduce the arching effects of the beams with respect to the previous cases. In fact, the upward movement proper of the arching phase is less pronounced than before, while the downward movement that initiates with the catenary stage is more marked. The loss of resistance registered at a displacement of around 40 cm is due to the crushing of concrete in the sections of the beams close to the column B and B'. The peak strain along the longitudinal reinforcement is equal to the ultimate value of 18% in the lower bars of the beams close to column C. Longitudinal bar failure occurs for the upper ones close to the columns B and B', while the peak strain for the stirrups is around 5%. The important outcome of the adoption of lateral constraints is that the ultimate resistance P_{ULT} of 2650 kN, reached at an ultimate displacement of around 100 cm.

The value of H_{rd} of Figure 4.8a represents the ultimate resistance capacity of the equivalent elastic springs along the horizontal direction corresponding to the ultimate resistance bending moments of the orthogonal beams in the y-z plane. The resistance capacity associated to the horizontal shear resistance of the orthogonal beams in the y-z plane is never overcome, computed according to MIT (2018) and MIT (2019). It should be noted that the structural performance depends on the equivalence between the external work and the internal energy (Izzuddin et al., 2008). The catenary effect guarantees the stability of the performance because it allows to reach the energy equivalence for lower vertical displacements and, thus, for lower rotation angles. Furthermore, in case of large dynamic phenomena as in the case of a progressive collapse, the presence of the catenary behavior is also fundamental to reach an energy equivalence for large displacements to avoid the collapse according to the "near-collapse" limit state. It follows that the two essential requirements are to increase the flexural peak optimizing the amount of the rebars as well as to anticipate the activation of the catenary effect. The possibility of respecting those requirements is investigated in the following section.

4.4.3 Models with global or partial equality and side face rebars – first failure scenario

In this section, alternative proposals are explored concerning both equal reinforcement distribution among the floors and the arrangement of *side face rebars*.

Initially, a frame identified as *CSE+springs model* is considered, where the same amount of longitudinal reinforcing bars across all floors is arranged while adhering to the previous criteria of *continuity*, section *symmetry*, and the presence of *springs*. The goal is to reduce the mechanical stresses in the lower floors and redistribute them evenly among all the structure (i.e., exploiting the Vierendeel behavior). Specifically, 5ϕ18 rebars are symmetrically placed along 1.5 m edges in all beams across all the five floors. To maintain capacity design principles, this modification implies a stirrup step of 7.5 cm in the beam dissipative areas and ϕ10 stirrup diameter with a 5 cm step at beam-column nodes. Longitudinal and transverse reinforcement in columns remains unchanged. The characteristics of this model are shown in Figure 4.9a-b.

Another enhancement involves introducing additional rebars to enhance the tying capacity of longitudinal reinforcement, particularly beneficial in case of column loss. Two levels (placed at around 1/3 and 2/3 of the beam height) of 2ϕ16 *side face rebars* are added to the *CSE+springs model* along each beam length for all floors while maintaining *continuity*, section *symmetry*, and *global floor equality*. This model, identified as *CSE+springs+rebars model*, undergoes verifications without further modifications with respect to the *CSE+springs model*. The characteristics of this model are shown in Figure 4.9c-d.

Another approach involves applying *continuity*, *symmetry*, and *floor equality* criteria only to the first and last floors, while maintaining continuity alone in the three intermediate floors. This new frame, identified as *CPE+springs*, consists in

the following reinforcement arrangement: (5+5)φ18 in the first and last floors, (3+5)φ18 in the second and third floors, and (3+4)φ18 in the fourth floor. To respect all the verifications, a 7.5 cm stirrup step in dissipative areas is provided for the first and last floors and φ10 stirrups only for beam-column nodes in columns B, C, and B' of the last floors are necessary. Modifications to constitutive laws and reinforcement arrangements are outlined in Figure 4.9e-f.
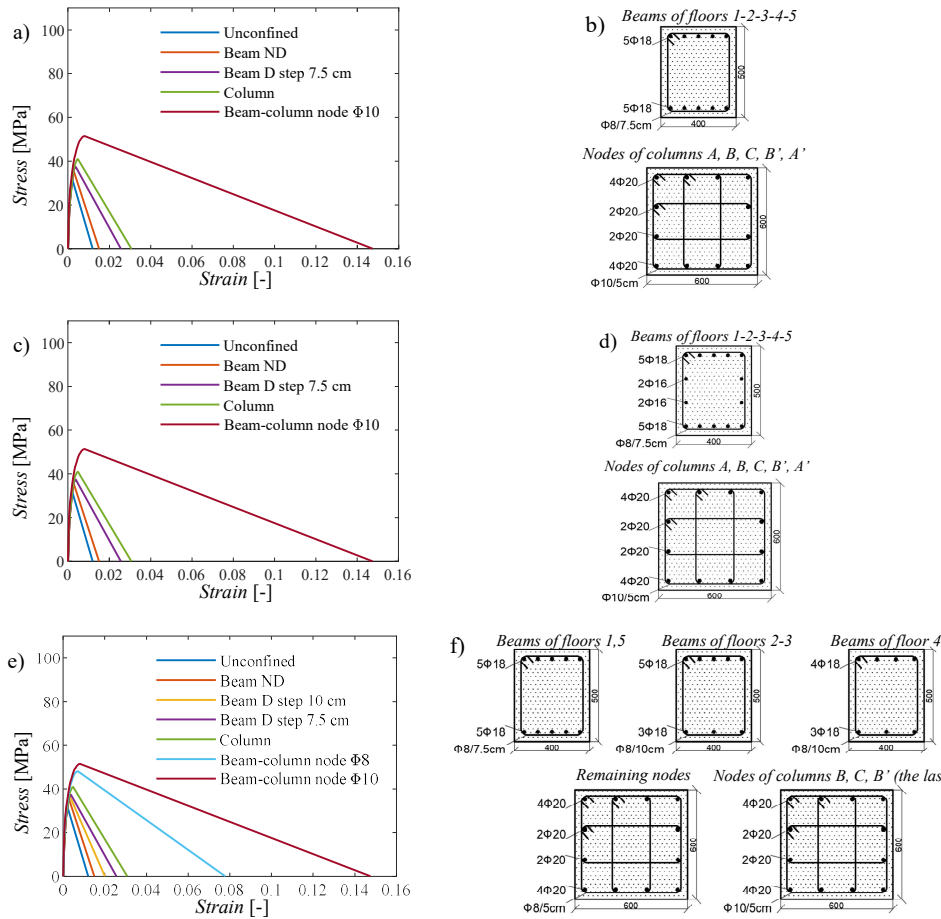
Figure 4.9 (a),(c),(e) concrete constitutive laws in compression; (b),(d),(f) distribution of the longitudinal and transverse reinforcement in the most stressed cross-sections for each floor, for *CS+springs*, *CSE+springs+rebars*, *CPE+springs models*.

Figure 4.10 illustrates the results of these improvements in terms of capacity curves, indicating a transition to catenary effects evident in both horizontal and vertical displacements of beam-column nodes. Notably, the *CSE+springs model* exhibits a resistance drop during the transition from arching to catenary behavior. Conversely, the *CPE+springs model* considerably reduces this resistance drop, although stirrups fail near the central columns at approximately 40 cm. The *CSE+springs model* shows increased flexural and ultimate resistance compared to the *CPE+springs model* and the *CS+springs model*. Moreover, the transition to catenary behavior begins slightly earlier in the *CSE+springs* and *CPE+springs models*, at around 15 cm displacement, with the latter taking advantage from a reduced amount of reinforcement.

However, structural response during the transition phase may be unstable due to resistance drop, especially in the *CSE+springs model*. Incorporating *side face rebars* in the *CSE+springs+rebars model* prevents this drop entirely by reducing the mechanical effort at the concrete level, resulting in reduced damage levels.
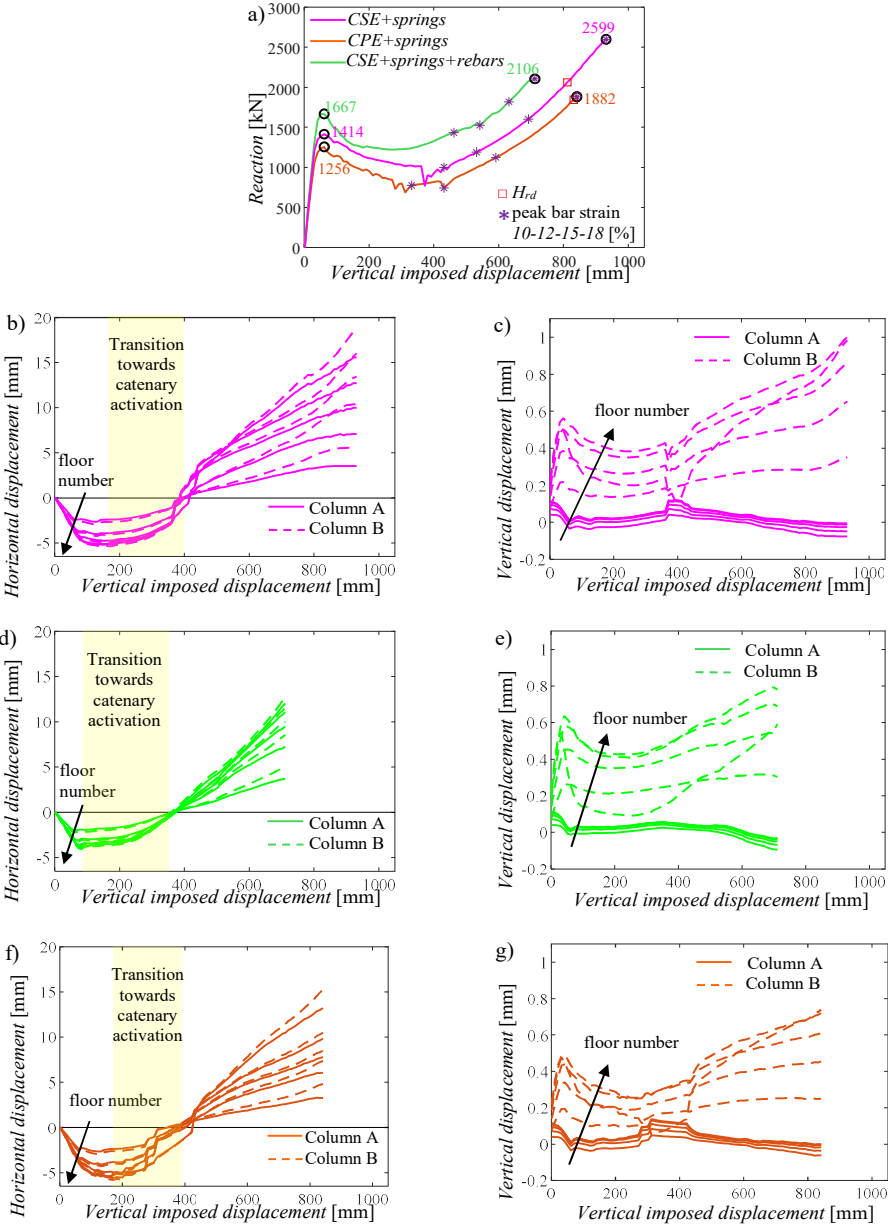
Figure 4.10 Results of the pushdown analyses for the first scenario: (a) capacity curves; (b),(d),(f) horizontal displacements of the beam-column nodes; (c),(e),(g) vertical displacements of the beam-column nodes, for *CSE+springs, CSE+springs+rebars, CPE+springs models*.

Additionally, both flexural peak and ultimate resistance increase, and the transition to catenary effect starts significantly earlier, around an imposed displacement of 10 cm. The ultimate strain for longitudinal reinforcement is reached in different locations depending on the model, with the *CSE+springs* and *CPE+springs models* reaching it in the lower bars close to central column and the

86

CSE+springs+rebars model reaching it in the upper *side face rebars* near columns B and B'. The ultimate bending resistance of orthogonal beams is reached at the end of the catenary path for *CSE+springs* and *CPE+springs models* but is never reached in the *CSE+springs+rebars model*. In addition, the horizontal shear resistance capacity is never exceeded.

4.4.4 Models with minimum design suggestions – first failure scenario

The previous results have highlighted the crucial role of longitudinal reinforcement arrangement in activating the catenary effect and ensuring adequate resistance against accidental column loss. However, the increase in total reinforcement compared to the *Code model* design may conflict with sustainability principles, particularly regarding economic concerns. To address this, various design strategies incorporating different combinations of proposed enhancements are considered in this subsection.
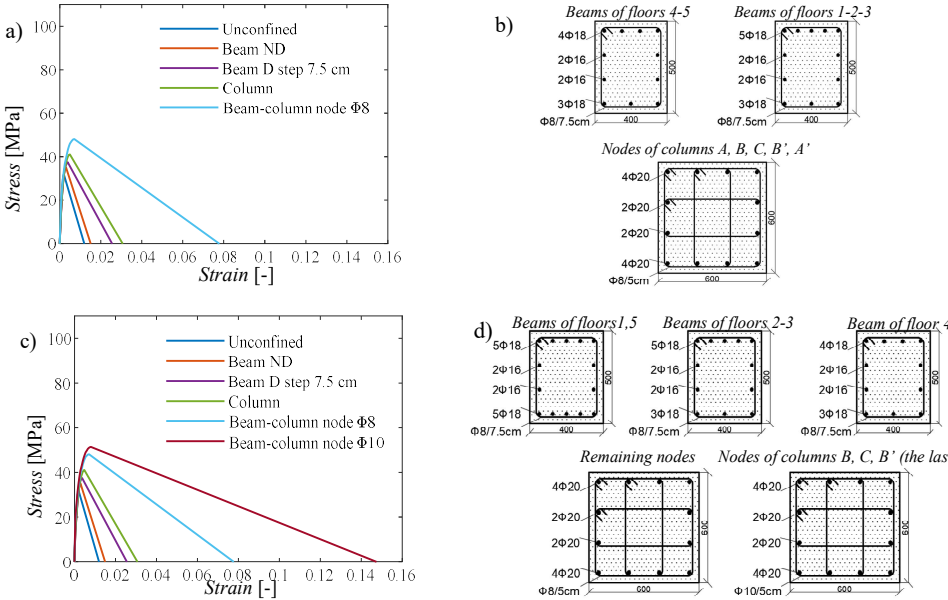
Figure 4.11 (a),(c) concrete constitutive laws in compression; (b),(d) distribution of the longitudinal and transverse reinforcement in the most stressed cross-sections for each floor, for *C+springs+rebars, CPE+springs+rebars models*.

One proposal involves integrating *continuity* together with the inclusion of two levels of 2ϕ16 *side face rebars* at approximately 1/3 and 2/3 of the beam height across all five floors, in addition to lateral springs. This new frame, labeled as *C+springs+rebars model*, necessitates a stirrup step reduction from 10 cm to 7.5 cm in beam dissipative areas across all floors to comply with seismic verification. The other structural elements remain unchanged. These modifications are depicted in Figure 4.11a-b.

Another proposal is to add *side face rebars* across all five floors to the model with *partial floor equality*, designated as the *CPE+springs+rebars model*. In this

case, to respect capacity design principles, the stirrup step in all the floors is adjusted from 10 cm to 7.5 cm. The modifications are illustrated in Figure 4.11c-d.

Figure 4.12 Results of the pushdown analyses for the first scenario: (a) capacity curves; (b),(d) horizontal displacements of the beam-column nodes; (c),(e) vertical displacements of the beam-column nodes for *C+springs+rebars, CPE+springs+rebars models*.

The results of these two new models are depicted in Figure 4.12. In both cases, flexural peaks and ultimate resistances overcome the corresponding values of the *CS+springs model*, while flexural peaks are lower compared to the *CSE+springs+rebars model*. In both models, activation of catenary response enables a stable structural performance. Specifically, the transition to catenary behavior occurs at a displacement of approximately 15 cm with a rotation angle of around 0.03 in both models, similar to the displacement achieved in the *CSE+springs+rebars model*. Stirrup failures close to the collapsed column are recorded during the post-transition phase at an imposed displacement of around 45 cm for the *CPE+springs+rebars model*, subsequent to catenary activation. Figure 4.12 also illustrates varying levels of deformation in the rebars for increasing vertical displacement.

It is worth noting that the presence of *side face rebars* reduces the resistance drop during the transition to catenary action. This is crucial for achieving a stable

energy equivalence, as a smaller gap implies larger internal energy provided by the structure in case of sudden column loss.

These aspects underscore the significant role of *side face rebars* in anticipating catenary effects, facilitating an earlier stable response with potential reduction in concrete damage concerning both "life-safety" and "near-collapse" limit states. Additionally, the combination of *continuity* with *partial floor equality* represents an effective alternative strategy to limit the increase in longitudinal rebars, substituting the *symmetry* suggestion.

The ultimate bending resistance of orthogonal beams is attained at the end of the catenary path for both models, while it is never surpassed if *side face rebars* are considered in the orthogonal frames. At the same time, the resistance capacity associated with horizontal shear resistance is never exceeded.

4.5 Second failure scenario: removal of the second-to-last supporting column

This section deals with the second failure scenario, implying the removal of the second-to-last supporting column (i.e., column B). Some useful robustness suggestions proposed for the first failure scenario are herein analyzed.

In detail, the following design assumptions are discussed:

- Models with *global* or *partial equality* and *side face rebars*.
- Models with *minimum* design suggestions.

The other design assumptions (i.e., *code model* and models with *continuity*, *symmetry* and *springs*) lead to similar considerations with respect to the previous failure scenario and, thus, are not discussed.

According to the procedure explained in Section 3.4.1, the equivalent elastic stiffness of the springs have been re-calibrated and listed in Table 4.3. In addition, the spring position is shown in Figure 4.13.

Table 4.3 Elastic spring stiffness for the different floors and for the second failure scenario.

	Spring Stiffness column A [N/m]	Spring Stiffness column C [N/m]	Spring Stiffness column B' [N/m]	Spring Stiffness column A' [N/m]
1st floor	$7.468 \cdot 10^6$	$9.747 \cdot 10^7$	$1.685 \cdot 10^8$	$9.766 \cdot 10^7$
2nd floor	$7.210 \cdot 10^6$	$7.128 \cdot 10^7$	$1.031 \cdot 10^8$	$7.138 \cdot 10^7$
3rd floor	$6.954 \cdot 10^6$	$5.283 \cdot 10^7$	$6.854 \cdot 10^7$	$5.288 \cdot 10^7$
4th floor	$6.684 \cdot 10^6$	$4.119 \cdot 10^7$	$5.013 \cdot 10^7$	$4.120 \cdot 10^7$
5th floor	$6.309 \cdot 10^6$	$3.288 \cdot 10^7$	$3.837 \cdot 10^7$	$3.289 \cdot 10^7$
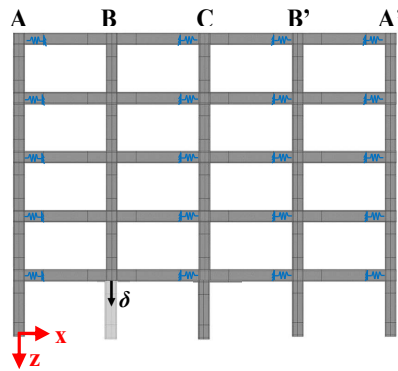
Figure 4.13 Springs positions (in blue) for the second failure scenario.

4.5.1 Models with global or partial equality and side face rebars – second failure scenario

This subsection deals with the pushdown analysis on the models with *global* or *partial floor equality* and *side face rebars*. The models have the same characteristics summarized in Figure 4.9, the only difference is in the failure scenario and, thus, in the modeling of equivalent elastic springs.

The results in terms of capacity curves are shown in Figure 4.14 for *CSE+springs*, *CPE+springs* and *CSE+springs*+rebars models.

Since this column removal implies a lower contribution provided by the orthogonal frames, the flexural peaks are relatively lower with respect to the same models of the first failure scenario as well as the catenary effect is less pronounced and also slightly delayed. As observed in Figure 4.14a, the same deformation levels in the reinforcement rebars are achieved for lower displacements in comparison with the first failure scenario (i.e., Figure 4.10a).

As for the previous analyses, the presence of *side face rebars* determines an increase of the flexural peak and an anticipation of the transition towards the catenary effects. In fact the catenary activates at around 20 cm for the *CSE+springs*+rebars *model* (Figure 4.14d), if compared to the cases where the *side face rebars* are not included, where the catenary effect starts at around 35 cm of imposed displacement (Figure 4.14b,f).

In addition, the stirrups fail close to the removed column at around 45 cm for the *CSE+springs*+rebars *model* and around 40 cm for the *CPE+springs+rebars model*.

Furthermore, in the second failure scenario, the ultimate bending resistance of the orthogonal frame is reached for lower displacements with respect to the first failure scenario. However, if the *side face rebars* are included also in the orthogonal beams, this allows to postpone the failures at larger vertical displacements. The resistance capacity associated to the horizontal shear resistance is never overcome.
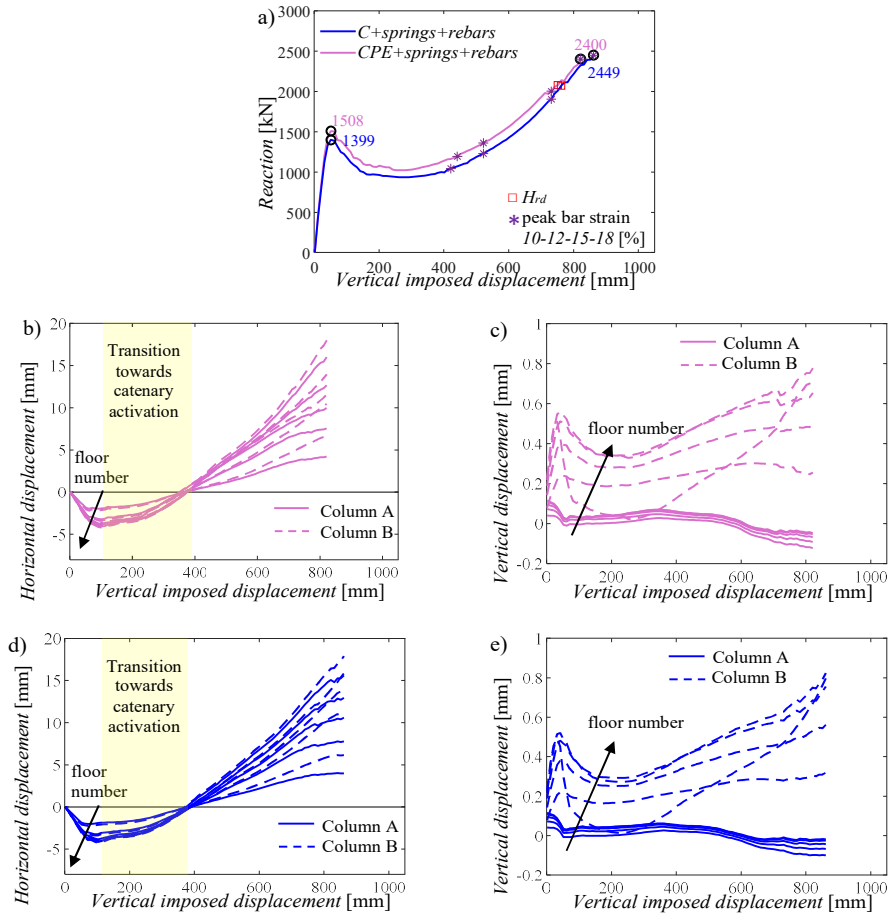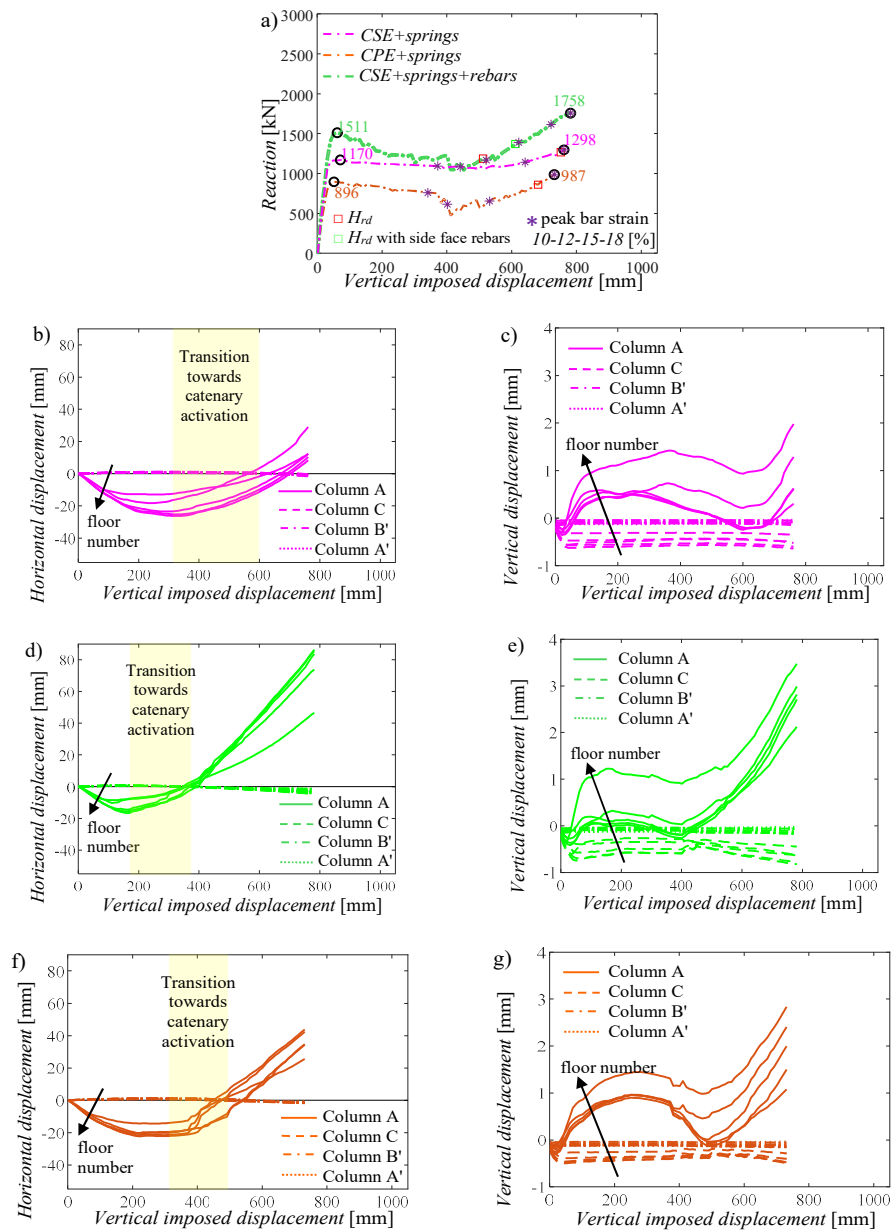
Figure 4.14 Results of the pushdown analyses for the second scenario: (a) capacity curves; (b),(d),(f) horizontal displacements of the beam-column nodes; (c),(e),(g) vertical displacements of the beam-column nodes, for *CSE+springs, CSE+springs+rebars, CPE+springs models*.

4.5.2 Models with minimum design suggestions – second failure scenario

The last investigation regards the adoption of *minimum* design recommendations also for the second failure scenario.

The results of the pushdown analysis are reported in Figure 4.15. The flexural peaks are slightly lower with respect to the *CSE+springs+rebars model* and the transition to catenary occurs for displacements slightly higher than 20 cm for the *C+springs+rebars* and *CPE+springs+rebars models*.

91

In addition, the stirrups fail in the beams close to the collapsed column, at a displacement of around 35 cm for the *C+springs+rebars* model and around 45 cm for the *CPE+springs+rebars* model.

Again, the ultimate bending resistance of the orthogonal frame is reached for lower displacements with respect to the first failure scenario and it is postponed if *side face rebars* are included also in the orthogonal beams. In addition, the ultimate resistance associated to the horizontal shear resistance is never overcome.
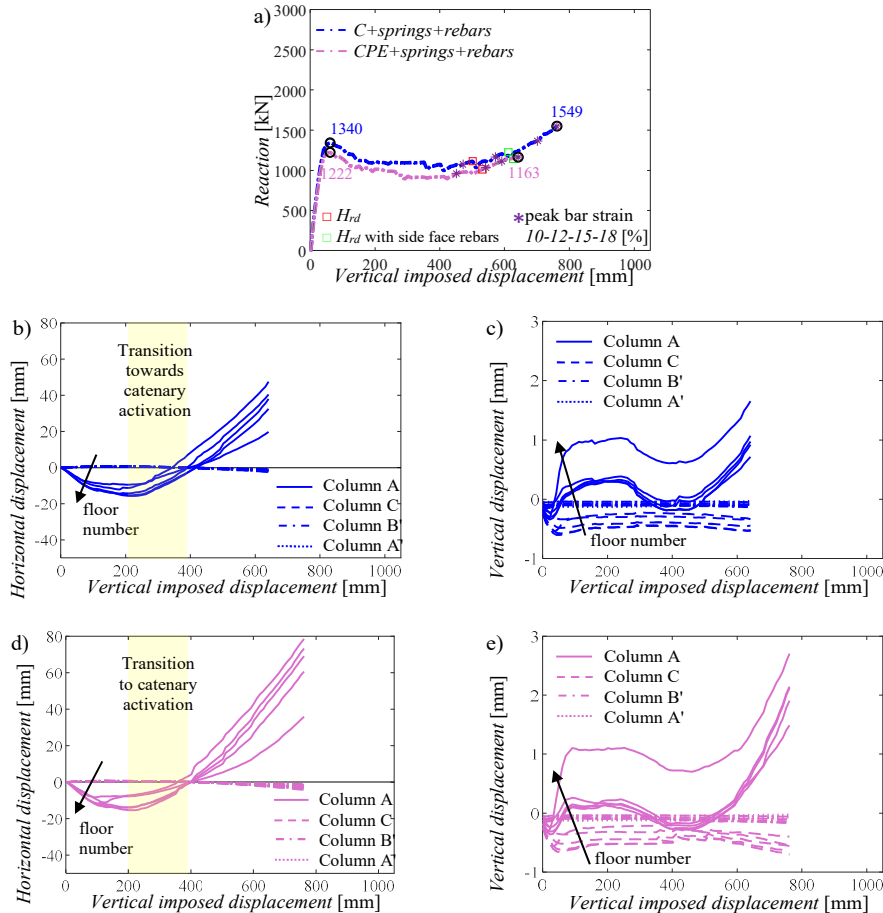
Figure 4.15 Results of the pushdown analyses for the second scenario: (a) capacity curves; (b),(d),(f) horizontal displacements of the beam-column nodes; (c),(e),(g) vertical displacements of the beam-column nodes for *C+springs+rebars, CPE+springs+rebars models*.

As a general observation, it can be deduced both for the first and the second failure scenario that the presence of *side face rebars*, combined with the *continuity* criterion, is a good compromise between robustness and sustainability principles. In fact, it is possible to reach a high flexural resistance and an anticipated catenary behavior adopting a lower amount of reinforcement with respect to other solutions.

It should be noted that the side longitudinal reinforcement in beams of the frames against both vertical and seismic loads is usually not considered to bear the relevant torsion actions. However, the presence of *side face rebars* can also be beneficial in order to bear the torsion due to the progressive collapse phenomenon on the beams belonging to frames not directly involved in the collapse scenario.

Thus, the side face rebars can be both beneficial in the beams directly involved by the collapse in order to bear the flexural and axial loads against progressive collapse and, at the same time, are helpful to bear the torsion of the orthogonal beams.

Chapter 5

Reliability assessment of the robustness improvements

5.1 Introduction

This chapter describes the reliability assessment of the robustness of the most relevant frames analyzed in Chapter 4 by means of a full probabilistic approach (i.e., considering both the aleatory uncertainties in the loads and in the material parameters).

Quantitative risk analysis in probabilistic terms offers the possibility of assessing the safety of LPHC (Low Probability, High Consequence) events, enabling the incorporation of uncertainties inherent in engineering problems. For instance, Botte et al. (2021) conduct a sensitivity analysis to determine the bearing capacity of various reinforced concrete (RC) structural elements when a central supporting component is removed. Brunesi et al. (2015) elaborate fragility analyses for low-rise RC buildings, estimating the likelihood of different damage states following a column loss scenario. Uncertainties in both demands and resisting capacities of connections in moment-resisting (MR) steel frames are studied in Xu and Ellingwood (2011). Meanwhile, Arshian et al. (2016) employs global variance-based sensitivity analysis to investigate key uncertainty sources in the response of RC structures facing sudden column loss. Furthermore, Bhattacharya (2021) computes a reliability-based index for structural collapse during extreme events, focusing on 2D linear elastic truss systems through random load and strength sampling. Stewart (2006) implements probabilistic risk assessment to evaluate various blast scenarios impacts on structural systems, particularly relevant to terroristic attacks. Ding and Yang (2017) undertakes a probabilistic analysis of steel-concrete composite floors against progressive collapse, highlighting potential non-conservative design when using load combinations from GSA Guidelines (2013). Droogné et al. (2018) quantified the reliability and robustness of planar RC frames through a conditional risk-based robustness index and accounting for

membrane actions. The definition of performance limit states for progressive collapse analysis is studied in Parisi et al. (2018), by means of a multilevel sensitivity analysis. Lastly, Zhang and Qiang (2022) examines the reliability of RC frames under different column-loss scenarios, identifying the absence of infill walls in a side column-loss scenario as particularly critical, with failure probabilities ranging from 0.016 to 0.137.

Current code rules do not provide any recommendation regarding progressive collapse risk assessment. Only suggested values of reliability index are recommended in some guidelines (e.g., values larger that 1.5 are suggested by CNR, 2018).

5.2   Framework for the reliability assessment

This chapter proposes a probabilistic robustness assessment of three 2D reinforced concrete moment resisting frames designed in seismic area, considering a central supporting column loss scenario. In particular, based on the results of Chapter 4, the reliability level of three different frames is studied:

- *frame 1*: is the frame designed according to current *code* rules where the presence of lateral *springs* is included (i.e., *Code+springs model*);
- *frame 2*: where the criteria of *continuity* of longitudinal reinforcement and the presence of *side face rebars* are included in the design as robustness enhancement suggestions, as well as the presence of lateral *springs* (i.e., *C+springs+rebars model* of Section 4.2);
- *frame 3*: this frame derives from the *frame 2* but the criteria of the *global equal* reinforcement amount in all the floors and *symmetric* in cross-sections are considered (i.e., *CSE+springs+rebars model* of Section 4.2).

The characteristics of the three frames are summarized in Figure 5.1 in terms of longitudinal and transverse reinforcement in the most stressed cross-sections as well as in Figure 5.2 in terms of constitutive laws of materials (considering the mean values of the mechanical properties).

It should be underlined that in all the three frames the presence of equivalent lateral springs to include the three-dimensional effects of the orthogonal framed system are included. Those springs are calibrated according to the procedure in Section 3.4.1 and assume the same numerical values already described in Chapter 4, Section 4.4.2.
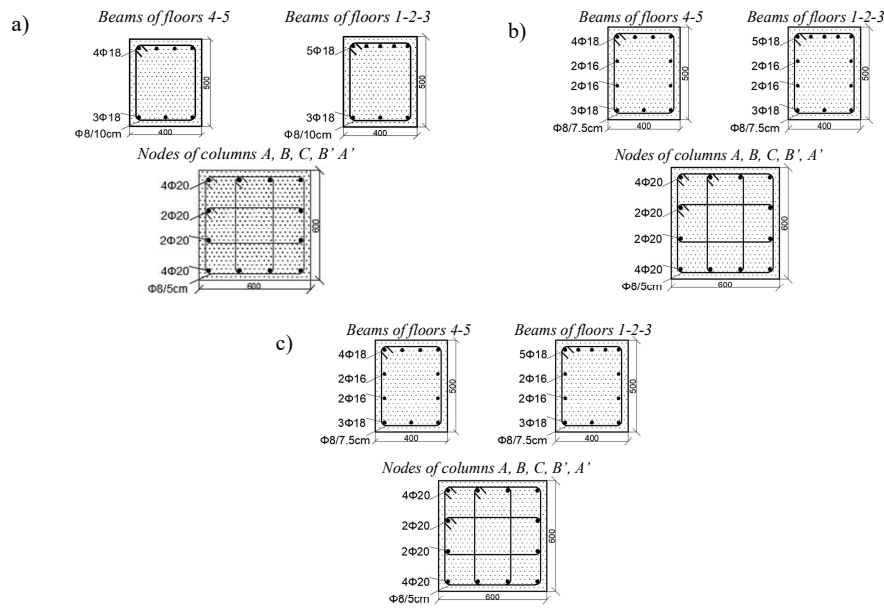
Figure 5.1 Summary of the distribution of the longitudinal and transverse reinforcement in the most stressed cross-sections for each floor for: (a) *frame 1*; (b) *frame 2*; (c) *frame 3*.
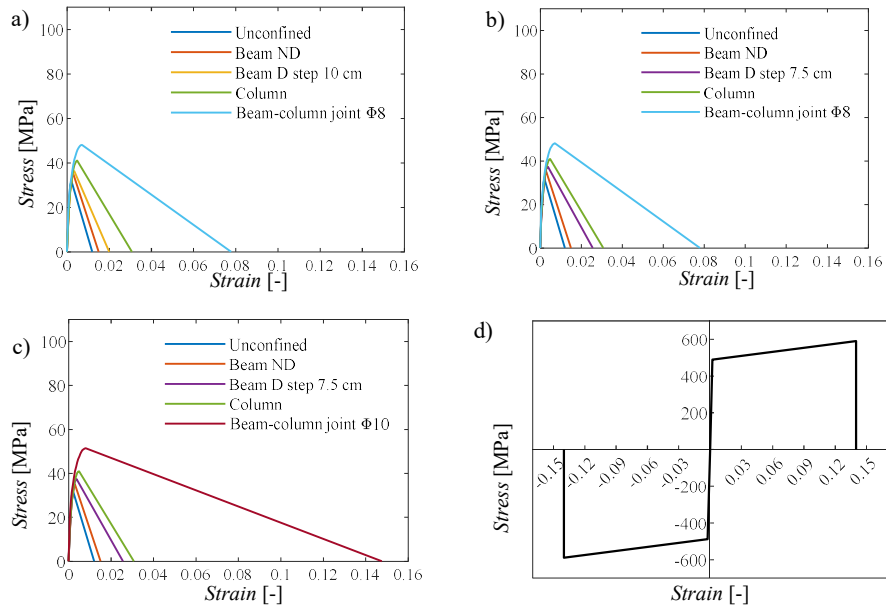
Figure 5.2 Summary of the constitutive laws for: (a)-(b)-(c) concrete in compression for, respectively, *frame 1*, *frame 2* and *frame 3*; (d) steel in tension and in compression for all the frames.

To evaluate the structural robustness in terms of reliability using a comprehensive probabilistic approach, the following 5-step procedure is proposed, drawing inspiration from previous studies (i.e., Izzuddin, 2008; Iman, 2008; Tsai and Lin, 2009; Xu and Ellingwood, 2011):

1. Sample the aleatory properties of materials and loads using Latin Hypercube Sampling (LHS) method (as explained in Section 2.5.4)

2. Conduct a preliminary analysis through displacement-controlled pushdown Non-linear Finite Element (NLFE) simulations. Specifically, the aleatory structure without the supporting column is modelled and a progressively increasing displacement is applied at the point where the column is removed. Then, the reaction at the same point is monitored to define probabilistic capacity curves (i.e., displacement-reaction curves).

3. Compute the Dynamic Amplification Factors (DAFs) using the energy equivalence approach as suggested by Izzuddin (2008). Determine the dynamic displacement and corresponding dynamic gravitational load (P_d) causing that displacement. Evaluate the DAFs as the ratios between dynamic and static gravitational loads.

4. Perform probabilistic static-equivalent NLFE analyses by simulating the removal of the supporting column and amplifying the loads of adjacent spans in each floor using the energy-based DAFs. Maintain the other spans loaded with non-amplified gravity loads.

5. The aleatory results in terms of strains for different materials are probabilistically characterized to assess structural reliability at the ultimate limit state (ULS).

It should be noted that a static-equivalent procedure accounts for the dynamic nature of failure scenarios while avoiding the complexity of dynamic analyses. It enables consideration of both geometrical and material non-linearities in the assessment of structural reliability.

5.3   Probabilistic sampling – step 1

This section deals with the step 1 of the framework described in Section 5.2. In particular, the description of the probabilistic sampling applying the Latin Hypercube Sampling technique (as described in Section 2.5.4) is deepened.

Table 5.1 Probabilistic characterization of the sampled basic variables.

	Distribution	Mean Value	CoV [-]
f_c	Lognormal [2]	31.9 MPa [5,6]	0.15 [2]
E_s	Lognormal [2]	210000 MPa [5,6]	0.03 [2]
f_y	Lognormal [2]	488.6 MPa [5,6]	0.05 [2]
f_u	Lognormal [2]	589.8 MPa [5,6]	0.05 [2]
ε_{su}	Lognormal [2]	0.14 [8-12]	0.09 [2]
ρ	Normal [3,4]	25 kN/m^3 [5,6]	0.05 [3,4]
G_1	Normal [1]	16 kN/m [5,6]	0.05 [1]
G_2	Normal [1]	13 kN/m [5,6]	0.05 [1]
Q_f	Gumbel [1]	7.3 kN/m [7]	0.20 [3,4]
Q_r	Gumbel [1]	1.8 kN/m [7]	0.20 [3,4]
Q_s	Gumbel [1]	4.7 kN/m [7]	0.20 [3,4]

[1] JCSS (2001), [2] JCSS (2002), [3] Slobbe et al. (2020), [4] Baravalle and Köhler (2019), [5] EN (1991), [6] MIT (2018), [7] fib (2016), [8] Ren et al. (2016), [9] Lu et al. (2017), [10] Yu and Tan (2013a-b), Lew et al. (2011) [11] Caprili and Salvatore (2018) [12].

In detail, a total of 11 different basic random variables are sampled:

- 5 variables for the material properties (i.e., concrete compressive strength f_c, reinforcing steel elastic modulus E_s, reinforcing steel yielding strength f_y, reinforcing steel ultimate strength f_u and reinforcing steel ultimate strain ε_{su}).
- 6 variables for the actions (i.e., reinforced concrete specific-weight ρ from which the self weight of the beams and column are computed, other permanent structural load G_1 (i.e., self weight of the slab), permanent non-structural load G_2 (i.e., weight of the screed, pavement, plaster and internal partitions), floor variable loads Q_f, roofing variable loads Q_r and snow load Q_s).

Table 5.2 Correlation matrix for the steel properties.

	f_y	f_u	ε_u
f_y	1	0.85	-0.50
f_u	0.85	1	-0.55
ε_{su}	-0.5	-0.55	1
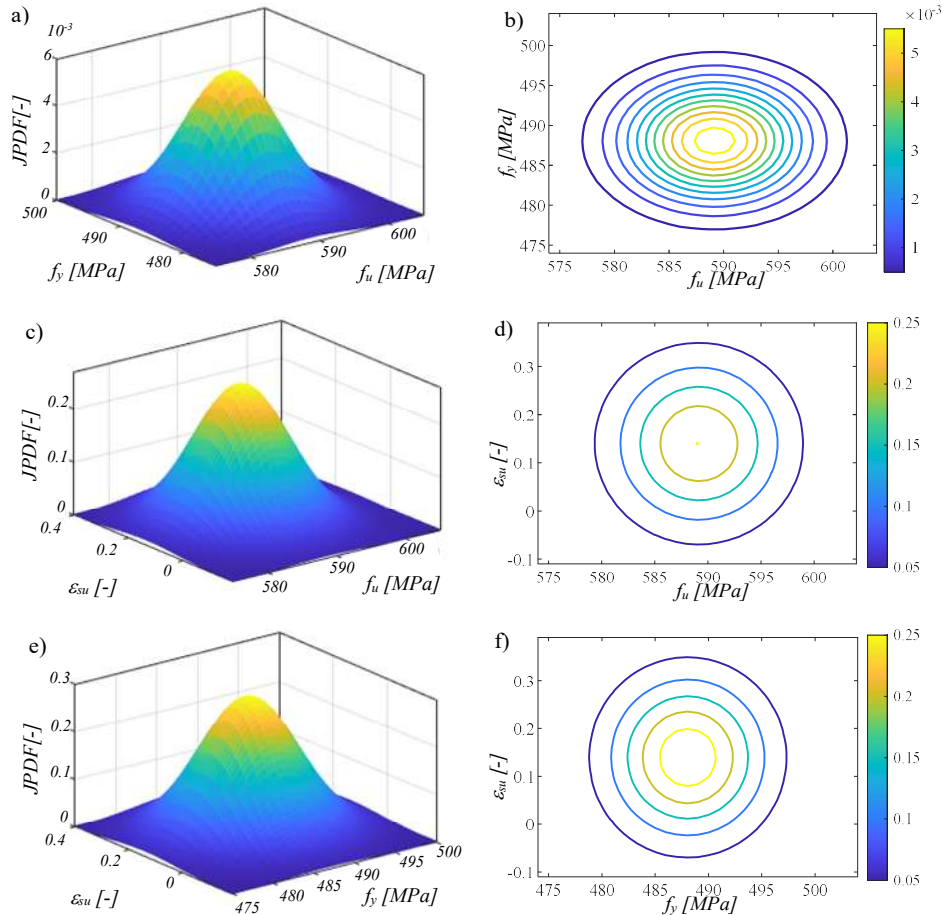
Figure 5.3 Correlation between steel variables JPDFs and contour plots for the following sets of correlated random variables: (a)-(b) f_u and f_y; (c)-(d) f_u and ε_{su}; (e)-(f) f_y and ε_{su}.

In addition, a number of samples equal to 100 has been selected for the purpose of this dissertation, considering that, as a rule of thumb, the sampling size should

be 10 times the number of basic variables (Mckey et al., 1979). Following this rule of thumb, it is possible to obtain a quite stable estimate of both the variance and average value of the output variables.
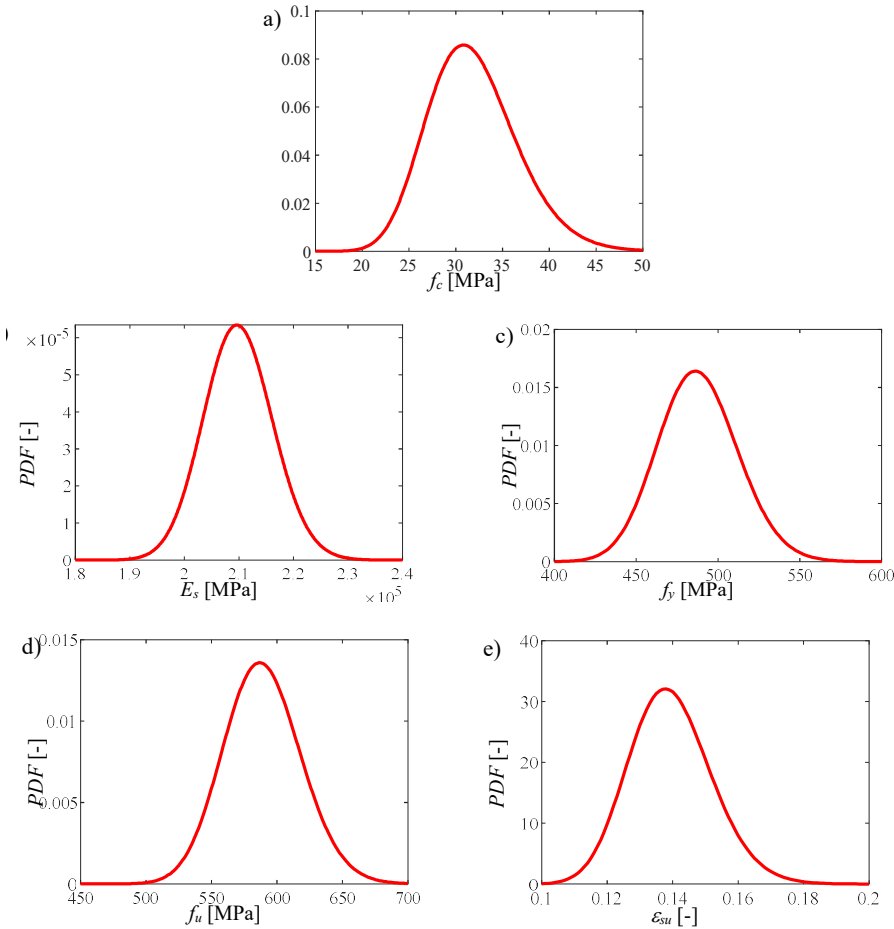
Figure 5.4 Probability Density function for the basic variables related to the material properties.

The probabilistic distributions as well as mean values and coefficients of variation (CoVs) of the random variables are listed in Table 5.1, where also references are given. More precisely, for the permanent loads the mean values coincide with the nominal values computed according to the design of the building described in Section 3.2.1, while for the variable loads the mean values are obtained from the characteristic values according to their distribution and related to a reference period of 50 years. All the other parameters are given from code rules and literature studies.

It should be underlined that a mean value for the ultimate strain of reinforcement steel equal to 0.14 is assumed. Also, the mean value of the ultimate strength of steel reinforcement is given from an ultimate-to-yielding strength ratio equal to 1.21. These last two assumptions are in accordance with different experimental tests analyzing the robustness of RC sub-assemblies (Ren et al., 2016; Lu et al., 2017; Yu and Tan, 2013a-b; Lew et al., 2011) as well as in line with the

results of monotonic tensile tests conducted on a wide range of steel reinforcing specimens (Caprili and Salvatore, 2018).

In addition, the equivalent elastic springs are modified for each of the 100 simulations according to the elastic modulus of concrete in compression of the i-th sampling realization (E_{ci}), where i=1,...,100. In fact, since the equivalent elastic springs are computed according to the procedure explained in Section 3.4.1, within an elastic analysis based on the mean property of concrete material, each spring stiffness for each of the 100 numerical simulation is obtained by multiplying its value for the ratio E_{ci}/E_{cm}, where E_{cm} is the mean concrete elastic modulus.

In this work, the correlation between steel properties is accounted for by means of the correlation coefficients, suggested by JCSS (2001) and listed in Table 5.2.

In Figure 5.3, the joint probability density functions (JPDFs) together with the contour plots for the three sets of the correlated variables are shown.

In the following figures, the probability density function (PDF) of the basic variables for the material properties (Figure 5.4) and the load properties (Figure 5.5) are given.
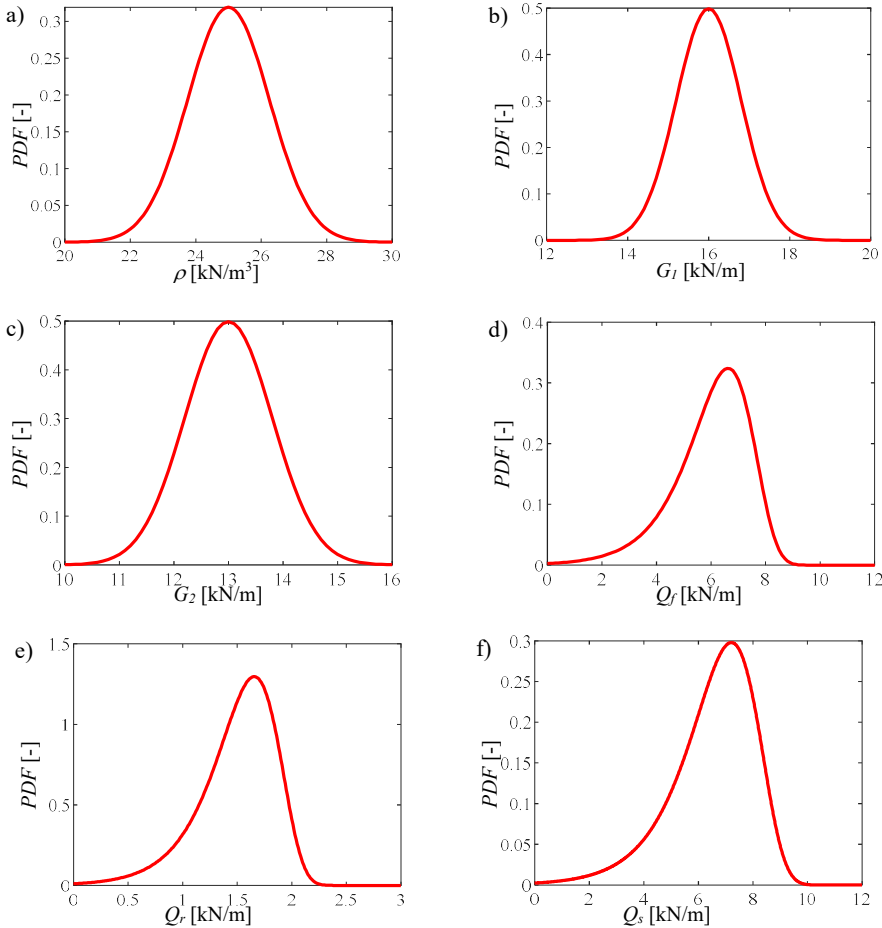
Figure 5.5 Probability Density function for the basic variables related to the load properties.

5.4 Probabilistic capacity curves and dynamic amplification factor – step 2 and step 3

In this section the procedure to compute the dynamic amplification factor (DAF) is described together with the results of the non-linear pushdown analyses. The computation of the DAFs is based on the energy equivalence approach proposed by Izzuddin (2008).

The idea behind this method is that the phenomenon of a sudden column loss is similar to a sudden application of gravity loads on the affected sub-structure, which is the part of the structure directly affected by the accidental phenomenon (i.e., the central spans in this case study). This is true especially when large deformations are involved as in a column loss scenario.

At the beginning of the column loss phenomenon, the gravity load is larger than the static structural resistance, due to the dynamicity of the phenomenon. This causes that the increase in deformations is transformed into additional kinetic energy, causing an increase in the velocities. Since deformations increase more and more, the static structural resistance increases as well overpassing the gravity loading, causing a reduction in the velocities and, thus, in the kinetic energy. The maximum dynamic displacement is reached when its derivative is zero, thus, when the velocity is reduced back to zero. Hence, the displacement at which the kinetic energy is null corresponds to the dynamic displacement and so to the performance point. Physically, the kinetic energy is zero when the work done by the external gravity loads W, equates the energy absorbed by the structure U. The former (i.e., W) is computed by multiplying the static gravity load P_o applied to the point of column removal for the vertical displacement in the same point. Whereas, the latter (i.e., U) is equal to internal energy given by the structural elements which can be evaluated as the area under the capacity curve (i.e., $P(\delta)$).

Specifically, the following applies:

$$W = \lambda_d P_0 \delta_d \qquad (5.1)$$

$$U = \int_0^{\delta_d} P(\delta)d\delta \qquad (5.2)$$

where δ_d is the maximum dynamic displacement corresponding to the performance point, δ is the generic vertical displacement subjected by the point of column removal and λ_d is the dynamic amplification factor. By equating the two quantities and knowing that the dynamic load P_d is evaluated as the load corresponding to the dynamic displacement in the pushdown curve, the following applies:

$$\lambda_d = \frac{P_d}{P_o} \qquad (5.3)$$

Within the application of this approach, two cases are possible:

- the work done by the external loads never equals the internal energy given by the structure for any vertical displacement. This means that the frame is not able to sustain the accidental removal of the supporting column and the computation of the DAF is not possible. This can happen if the external loads are too high and/or if the mechanical properties of the structure are too poor. A qualitative example of this case is shown in Figure 5.6:
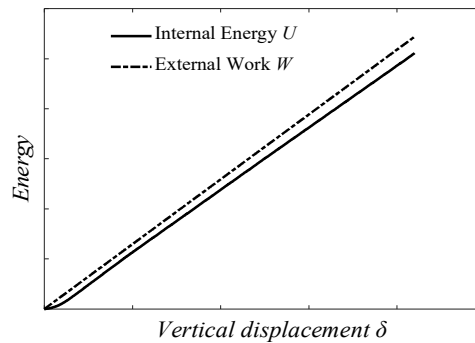
Figure 5.6 Qualitative example of a case where the energetic equivalence is not reached.

- the work done by the external loads equals the internal energy given by the structure in correspondence of the dynamic displacement δ_d as qualitatively shown in Figure 5.7a. In this case, the dynamic load can be found in correspondence of the dynamic displacement in the pushdown curve, as qualitatively shown in Figure 5.7b. Once the dynamic load is computed, by dividing it for the corresponding static load (i.e., Eq. 5.3), the DAF, identified as λ_d, can be computed.
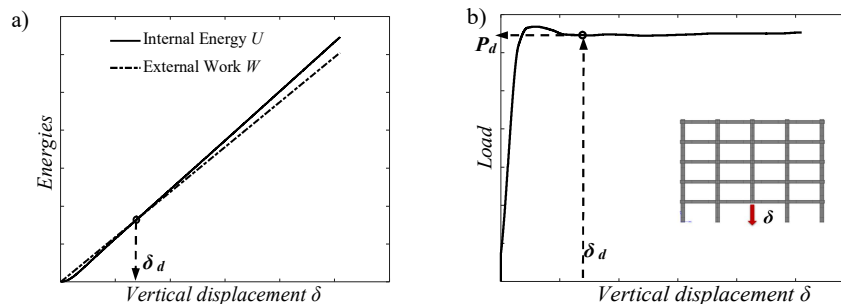
Figure 5.7 Qualitative example of a case where the energetic equivalence is reached: (a) energy curves and calculation of the dynamic displacement; (b) capacity curve and calculation of the dynamic load.

The procedure has been applied for all the three frames and for all the 100 realizations of each frame.

In the following subsections, the probabilistic evaluation of the static gravity load P_o and the corresponding dynamic one P_d is deepened and then the results of the DAFs are shown.

5.4.1 Probabilistic evaluation of the static gravity load P_o

In order to compute the dynamic amplification factor, the static gravity load has to be evaluated for each i-th realization of the three frames. This value is adopted to calculate the work done by the external loads (i.e., W) in order to find the dynamic displacement δ_d in correspondence of the intersection with the internal energy (i.e., U). In addition, by dividing the dynamic for the gravity load, the DAF is computed according to Eq. 5.3.
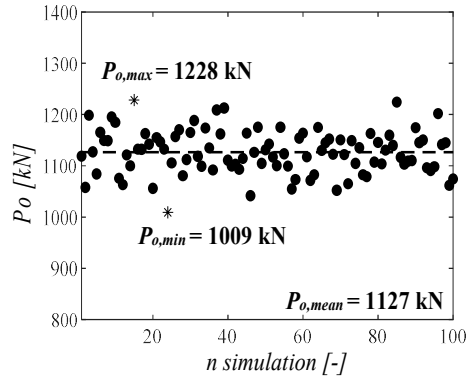
Figure 5.8 Probabilistic evaluation of the static concentrated gravitational load at the top of the removed column. The values are equal for the three frames.

In this framework, the external gravitational load P_o is a probabilistic variable since it derives from the probabilistic sampling, as described in Section 5.3. This value is obtained by multiplying the load per unit meter derived from the sampled distributed gravitational loads for the effective span length, in order to obtain the concentrated load applied in the point of column removal. The sampled distributed gravitational loads are the permanent structural load (i.e., G_1 including the self-weight), the permanent non-structural loads G_2 and the variable loads (i.e., Q_f, Q_r and Q_s). In this work, it is assumed that the external gravitational load is the same for all the three frames since it only depends on the sampled basic variables that do not change. The aleatory values of the static concentrated gravitational load P_o are shown in Figure 5.8 as function of the number of simulations (from 1 to 100), together with the minimum, maximum and mean value.

5.4.2 Probabilistic evaluation of the capacity curves and dynamic gravity load P_d

In this subsection, the probabilistic capacity curves resulting from the displacement-controlled non-linear pushdown analysis are shown. This step coincides with the second one as described in Section 5.2. The capacity curves are needed to compute the internal energy (i.e., U), in order to find the dynamic displacement δ_d in correspondence of the intersection with the external work (i.e., W). In addition, the value of the capacity curve corresponding to the dynamic displacement represents the dynamic load P_d and by dividing its value for the static load, the DAF is computed according to Eq. 5.3.

103
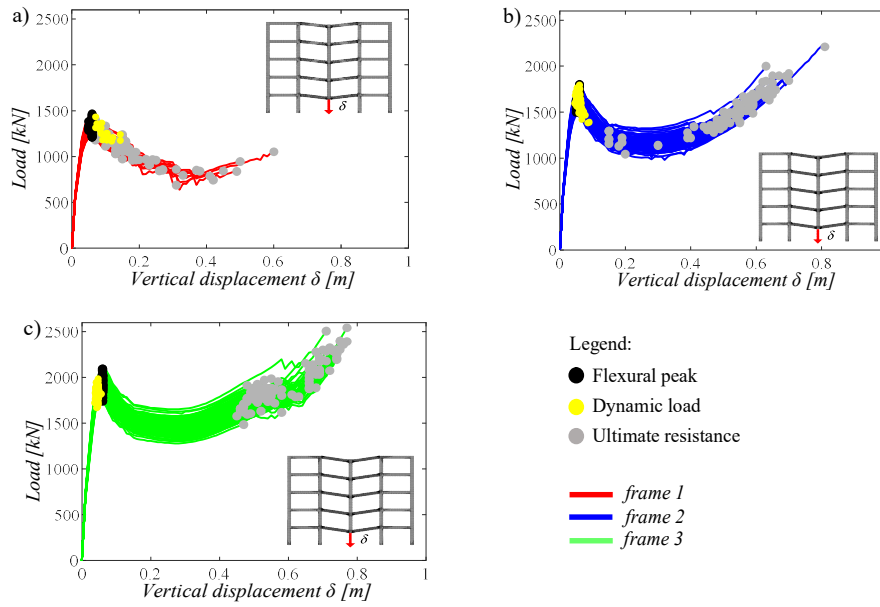
Figure 5.9 Probabilistic capacity curves including the flexural peak (black dots), the dynamic load (yellow dots) and the ultimate resistance (grey dots) for: (a) *frame 1*; (b) *frame 2*; (c) *frame 3*.

To evaluate the capacity curves, three sets of 100 analyses are modeled by varying the mechanical properties of the materials, according to the sampling of Section 5.3. In particular, the frame is modeled without the central supporting column and an increasing vertical displacement is applied in the point of column removal, registering the corresponding reaction. The resulting displacement-reaction curve is the capacity curve. In Figure 5.9, three sets of 100 capacity curves are shown, together with the load in the flexural stage $P_{MAX,FL}$ (black dots), the dynamic load where the energetic equivalence is obtained P_d (yellow dots), and the ultimate resistance P_{ULT} (grey dots).

The following key aspects can be drawn:

- For all the frames and all the realizations, the displacement at which $P_{MAX,FL}$ is obtained is similar. This is mainly due to the quite low dispersion of both the steel yielding strength and steel elastic modulus (i.e., 0.05 and 0.03, respectively).
- The value of the flexural peak (i.e., black dots), varies for the different frames. Notably, $P_{MAX,FL}$ is larger going from *frame 1* to *frame 3* since the amount of longitudinal reinforcement is larger. In addition, this value is varying within the same frame because it is also influenced by the dispersion of the concrete compressive strength (i.e., 0.15) which influences the constitutive law of the equivalent elastic springs and, thus, the contribution of the transversal elements.
- After the flexural peak, the behavior of the three frames is quite different. On the one hand, *frame 1* is mainly characterized by an ultimate resistance that never overcome the flexural one, remaining in the softening stage. On the other hand, both *frame 2* and *frame 3* are characterized by a marked

104

activation of the catenary effect after the flexural stage. This is mainly due to the presence of *side face rebars* as demonstrated in Chapter 4.

- The value at which the ultimate resistance P_{ULT} is reached (i.e., grey dots) is quite variable for *frame 1* with respect to the other two frames since it is mainly governed by a brittle behavior and, thus, by the CoV of the concrete which is quite high (i.e., 0.15). On the other hand, the ultimate resistance P_{ULT} of the other two frames (i.e., *frame 2* and *frame 3*), which is reached during the catenary stage, depends on the aleatory characteristics of the steel ultimate deformation which is influenced by a lower CoV (i.e., 0.09). For those reasons, in general the ultimate response for the three frames is more variable with respect to the peak flexural response.

The yellow dots in Figure 5.9 representing the dynamic load P_d are obtained by applying the energetic equivalence approach for the three sets of 100 aleatory frames, as qualitatively explained in Figure 5.6 and Figure 5.7. It should be noted that for the *frame 1* only about the 25% of cases were characterized by an energetic equivalence, meaning that only for those cases the dynamic displacement and the corresponding dynamic load was found. On the other hand, the energetic equivalence was found in the 100% of cases for both *frame 2* and *frame 3*, confirming the effectiveness of the robustness improvements as explained in Chapter 4.

Figure 5.10 Probabilistic dynamic gravitational load P_d for: (a) *frame 1* (only for the cases with energetic equivalence); (b) *frame 2*; (c) *frame 3*.

In Figure 5.10 the probabilistic value of the dynamic gravitational load is shown for the three frames as function of the number of simulations (from 1 to 100), together with the minimum, maximum and mean value. Those values correspond to the resistances at which the dynamic displacement δ_d is reached within the energetic equivalence approach. It should be noted that for *frame 1* (i.e., Figure

5.10a), only the cases where the energetic equivalence is found are shown. The *frame 3* is characterized by larger values than *frame 2* and this is due to the higher bearing capacity of the structure determined by the larger quantity of longitudinal reinforcement in the beams.

5.4.3 Probabilistic evaluation of the dynamic amplification factor (DAF) λ_d

This section deals with the evaluation of the DAFs for the aleatory frames. This step represents the third one as described in Section 5.2. In particular, by applying the energetic equivalence approach, the value of the i-th λ_d for each frame can be computed by applying the Eq. 5.3.

The results of the dynamic amplification factor are reported in Figure 5.11 as function of the number of simulations (from 1 to 100) together with the minimum, maximum and mean value. It should be underlined that, with reference to the *frame 1*, only for the cases where the energetic equivalence is obtained the DAFs are computed. The larger the bearing capacity of the structure, the larger is its capability to sustain an amplification of the gravitational loads in a dynamic phenomenon. For this reason, *frame 3* shows the largest values of the DAFs if compared to the other frames. In detail, the mean value of the DAFs for the *frame 3* is equal to 1.62 while for the *frame 2* is equal to 1.44. In addition, these results is a confirmation that the value of DAF equal to 2.0 as suggested by GSA (2013) and DoD (2016) for linear static analyses is too conservative. Similar results of DAFs are obtained in different numerical and experimental analyses (e.g., Adam et al., 2020; Zhao et al., 2022).
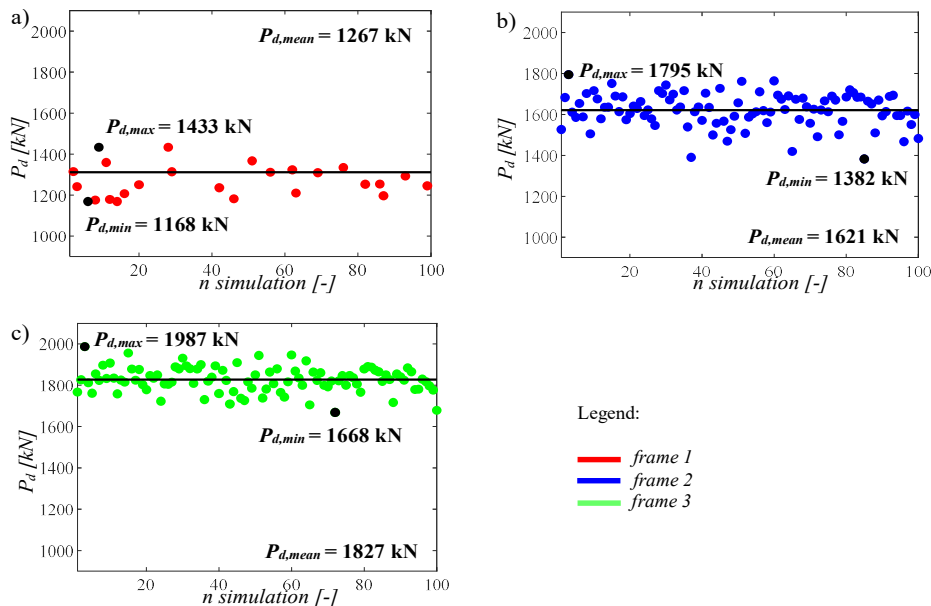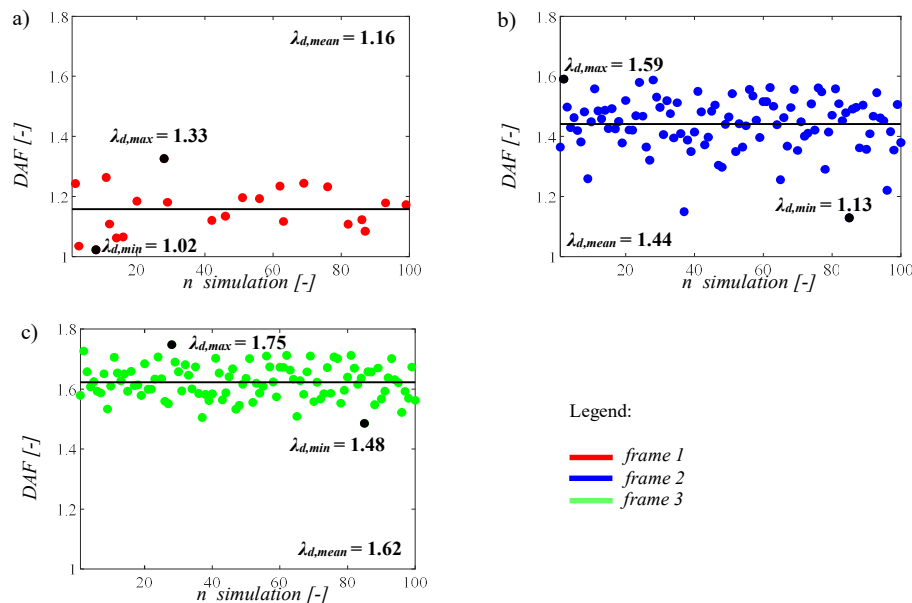

Figure 5.11 Probabilistic dynamic amplification factor λ_d for: (a) *frame 1* (only for the cases with energetic equivalence); (b) *frame 2*; (c) *frame 3*.

5.5 Equivalent static NLFE analysis and reliability assessment – step 4 and 5

This section deals with the reliability evaluation of the robustness of the three frames under study. First, the equivalent static non-linear analyses are described and then the framework to compute the strain-based failure probabilities in specific sections of the frames is deepened.

5.5.1 Equivalent static non-linear analysis

As defined in Section 5.2, the fourth step of the framework consists in applying an equivalent static non-linear analysis. At first, the gravitational loads are applied to the frame modeled with the central supporting column, as shown in Figure 5.12a. The gravity loads are combined through the accidental combination of EN 1990 Standards given in Eq. (1.3). Then, the central supporting column is removed, and the gravity loads are amplified only on the area directly affected by the accidental phenomenon (i.e., central spans) as shown in Figure 5.12b. The other spans are not involved in the amplification of loads since the dynamic effects are damped by the structural elements. This last aspect has been validated by performing a dynamic linear analysis in ADINA (ADINA R&D Inc., 1997) with the mean values of the sampled material and load variables and removing the central supporting column. The results have shown that the DAF computed as the ratio between the dynamic displacement (i.e. the peak value of the displacement after the sudden removal of the column) and the static one (i.e. when the displacement reaches the steady-state response) at different points of the external spans of the structure was not comparable with the same ratio computed in the central spans.
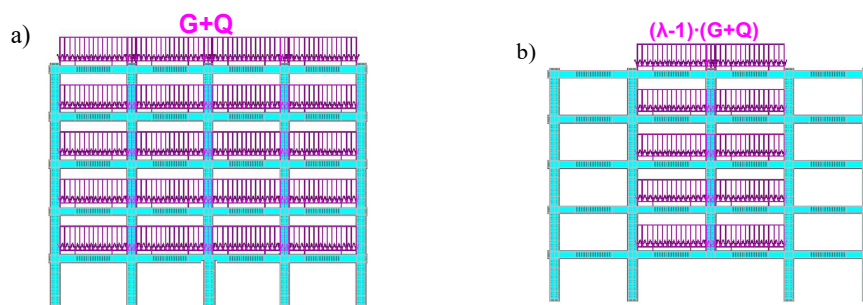
Figure 5.12 Schematic representation of the equivalent static non-linear analysis: (a) application of the gravitational load in the integral frame; (b) removal of the central supporting column and amplification of the gravity loads on the central spans.

Specifically, two sets of 100 static-equivalent NLFE simulations are modeled for the *frame 2* and *frame 3*. By amplifying the loads, collapse was not reached for all the simulations, confirming the prediction of the energetic equivalence approach. Regarding the *frame 1*, similar static-equivalent NLFE simulations are carried out when the DAFs were obtained within the energetic equivalence approach. In the remaining cases, static-equivalent NLFE simulations are run until

to achieve the collapse, by slightly amplifying the loads in the central spans, as predicted by the energetic approach.
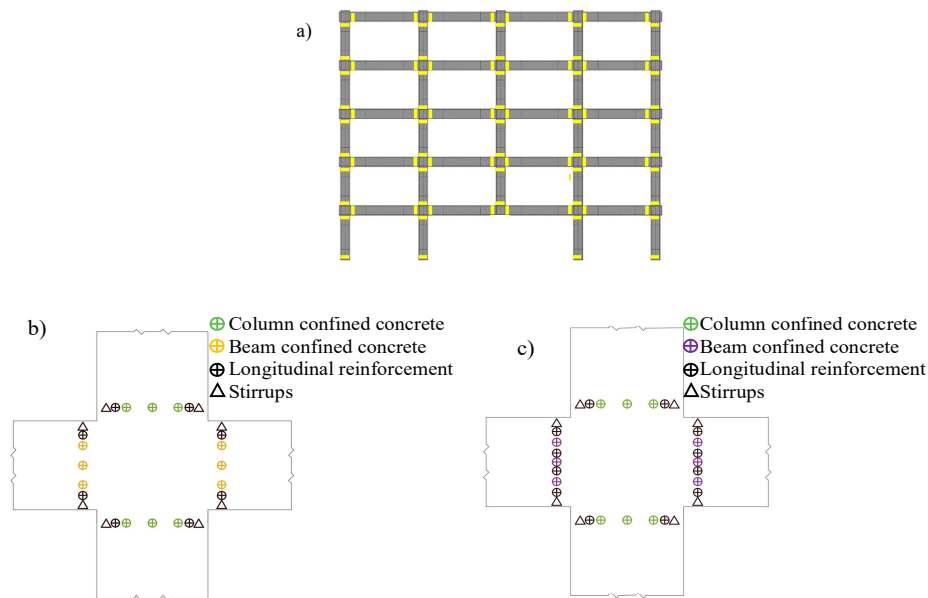
Figure 5.13 (a) cross-sections close to the beam-column nodes; (b) points within the cross-sections where the strain is evaluated for *frame 1* (c) points within the cross-sections where the strain is evaluated for *frame 2* and *frame 3*.

For each set of simulations, the outputs are the principal total strains (ε) at sections near each beam-column node, resulting in four sections for each node (except for corner columns and the last floor, where three or two cross-sections are present, respectively), as shown in Figure 5.13a. Specifically, within each cross-section of both beams and columns, various points are examined, distinguishing between those in the confined concrete core and those associated with reinforcement, including ordinary reinforcement, *side face rebars* (only applicable to *frame 2* and *frame 3*), and stirrups, as shown in Figure 5.13b-c.

5.5.2 Probability of failures and reliability assessment

This section deals with the core of this analysis as described in the fifth and last step of the framework outlined in Section 5.2. In particular, by defining as S the demand (i.e., the monitored aleatory strains at the points as described in Section 5.5.1) and C the capacity (i.e., the aleatory ultimate strain of the materials as sampled in Section 5.3), the failure probability is defined as the probability of the aleatory demand exceeding the aleatory capacity. This computation concerns the Ultimate Limit State (ULS). The probability of failure p_f can be computed by means of a convolution integral between the probability density function (PDF) of the demand and the cumulative density function (CDF) of the capacity as explained in Section 2.5 through Eq. (2.35) and described by the following equation (Haldar and Mahadevan, 2000):

$$p_f = P[C \mid LD] = P(C < S) = \int_0^\infty \left[\int_0^s f_C(c)\,dc \right] f_S(s)\,ds = \int_0^\infty F_C(s) f_S(s)\,ds \quad (5.4)$$

where $F_C(s)$ is the CDF of the capacity C evaluated at specific realizations of the demand (i.e., s), $f_S(s)$ and $f_C(c)$ are the PDFs, respectively, of the demand S and the capacity C.

It is worth noting that the probability of failure computed through Eq. (5.4) represents the probability of collapse given the local damage $P[C|LD]$ at the ultimate limit state as expressed in Eq. (1.2).

This computation has been repeated in each point corresponding to a specific material and in each cross-section close to the beam-column nodes for the three frames. More precisely, for the *frame 1*, the total probability theorem as derived from Eq. (2.11) and expressed in Eq. (5.5), was applied to compute the failure probabilities in the points related to the beams and columns of the central spans, accounting for the failure cases (Jalayer and Cornell, 2009):

$$p_{f,frame1} = \frac{N_{non-collapse}}{N_{total}} \cdot \left[\int_0^\infty F_C(s) f_S(s)\,ds \right]\Bigg|_{non-collapse\ cases} + \frac{N_{collapse}}{N_{total}} \cdot 1 \quad (5.5)$$

where, $N_{collapse}$ represents the number of collapse cases derived from the energy equivalence approach, N_{total} is the total number of samples (i.e., 100) and $N_{non-collapse}$ defines the complementary part of $N_{collapse}$ with respect to N_{total}.
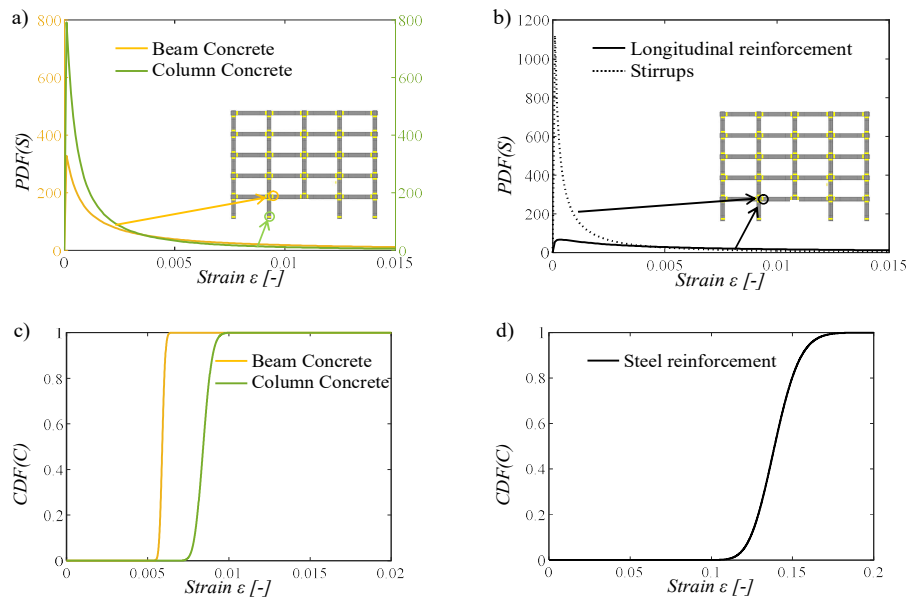
Figure 5.14 Parameters to compute the convolution integral for the *frame 1*: (a)-(b) the PDF of the demand in a specific point of the structure; (c)-(d) CDF of the capacity.

In the remaining parts of the structures, the computation of p_f does not include the failure cases since it is assumed that the dynamic phenomena are damped on the remaining structural elements.

109
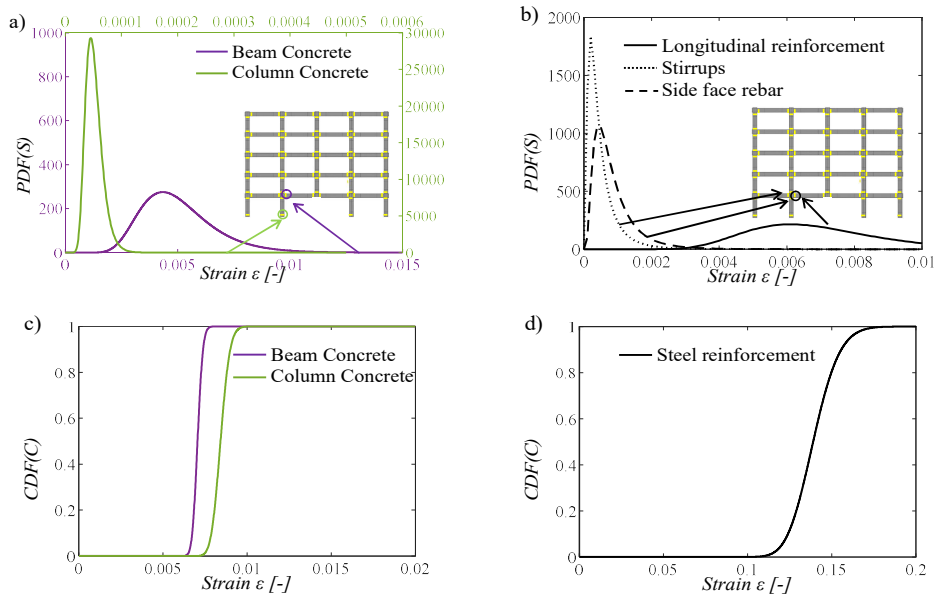
Figure 5.15 Parameters to compute the convolution integral for the *frame 2*: (a)-(b) the PDF of the demand in a specific point of the structure; (c)-(d) CDF of the capacity.
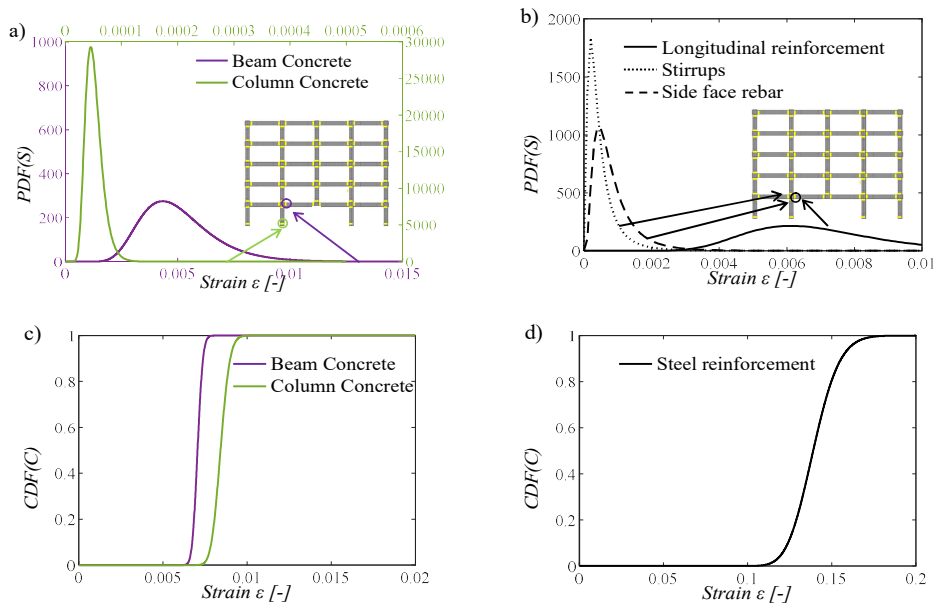
Figure 5.16 Parameters to compute the convolution integral for the *frame 3*: (a)-(b) the PDF of the demand in a specific point of the structure; (c)-(d) CDF of the capacity.

To compute the convolution integral, a probabilistic characterization of both demand and capacity is needed. As for the demand *S*, a statistical inference analysis is carried out with significance level of 5% to investigate the probabilistic distribution for the strains in the different points of the structure and by means of both the Chi-Square and Anderson Darling tests. Also for the demand, the lognormal distribution has been considered as the selected probabilistic distribution since it passes the goodness of fit test with the largest p-values in all the points and for all the three frames. In Figure 5.14a-b, Figure 5.15a-b, Figure 5.16a-b, examples of the PDFs of the demand *S* in the most stressed sections for each material and for

110

the three frames are shown. It is important to notice that a different colour in the graphs refers to a different material, in line with the colours adopted in the constitutive laws of Figure 5.2. As for the capacity C, the ultimate deformation is obtained for each material. In detail, for the steel, the ultimate strain corresponds to the value sampled in Section 5.3, while for concrete, the ultimate strain is evaluated as function of the sampled concrete compressive strength. In particular, it is assumed equal to the value of the strain corresponding to a post-peak strength equal to the 85% of the maximum one. In Figure 5.14c-d, Figure 5.15c-d and Figure 5.16c-d, the CDFs of the capacity C are shown for each material and for the three frames.

Legend:
- 🔴 $1.142 \cdot 10^{-1} < p_f \leq 8.18 \cdot 10^{-1}$ $\beta < 1.072$
- 🟠 $10^{-2} < p_f \leq 1.142 \cdot 10^{-1}$ $1.072 \leq \beta < 2.3$
- 🟣 $10^{-3} < p_f \leq 10^{-2}$ $2.3 \leq \beta < 3.1$
- 🔵 $10^{-7} < p_f \leq 10^{-3}$ $3.1 \leq \beta < 5.2$
- 🟢 $p_f \leq 10^{-7}$ $\beta \geq 5.2$

Figure 5.17 Failure probability for each cross-section of the *frame 1* considering: (a) confined concrete; b) steel longitudinal reinforcement; c) steel transverse reinforcement.

It should be noted that concrete in tension is discarded for the computation of the failure probabilities since it is not considered as a resisting material in the failure modes when large deformation levels are involved.

In Figure 5.17, Figure 5.18 and Figure 5.19 the failure probabilities are shown for, respectively, *frame 1*, *frame 2* and *frame 3*, distinguishing between the confined concrete material in compression, the longitudinal reinforcement (including *side face rebars*), and the transverse reinforcement. The following outcomes can be drawn:

- *frame 1* exhibits the highest failure probabilities across all investigated materials compared to the other cases. Specifically, in concrete (Figure 5.17a), beams adjacent to the removed column on the first floor reach the highest probability (0.818), while beams of upper floor also exceed 10^{-1}. Regarding the lateral spans (i.e., those indirectly influenced by the column loss), probabilities range between 10^{-3} and 10^{-1}. This means that the damage is not only isolated to the central part of the structure, but it is spread outside,

111

violating one of the key concepts for a robust design that is the avoidance of a damage progression. Regarding longitudinal reinforcement (Figure 5.17b), probabilities are lower if compared to the concrete in external spans but significantly large in central spans (much greater than 10^{-1}), indicating insufficient reinforcement for flexural and catenary stages. Stirrup failure probabilities (Figure 5.17c) are comparatively lower due to different stress states with respect to longitudinal reinforcement;

- *frame 2* demonstrates significant improvements, particularly in longitudinal reinforcement (Figure 5.18b) where, a part from beams of the central span on the first floor, all the other sections show very low failure probabilities (below 10^{-7}). This again highlights the importance of *side face rebars* in a robustness-based design. Confined concrete in compression (Figure 5.18a) shows lower failure probabilities compared to the previous case, especially in external spans, indicating reduced mechanical stress due to *side face rebars* and the effectiveness of the robustness improvements;

- similar observations apply to frame 3 (Figure 5.19), with even lower concrete failure probabilities compared to *frame 2*.
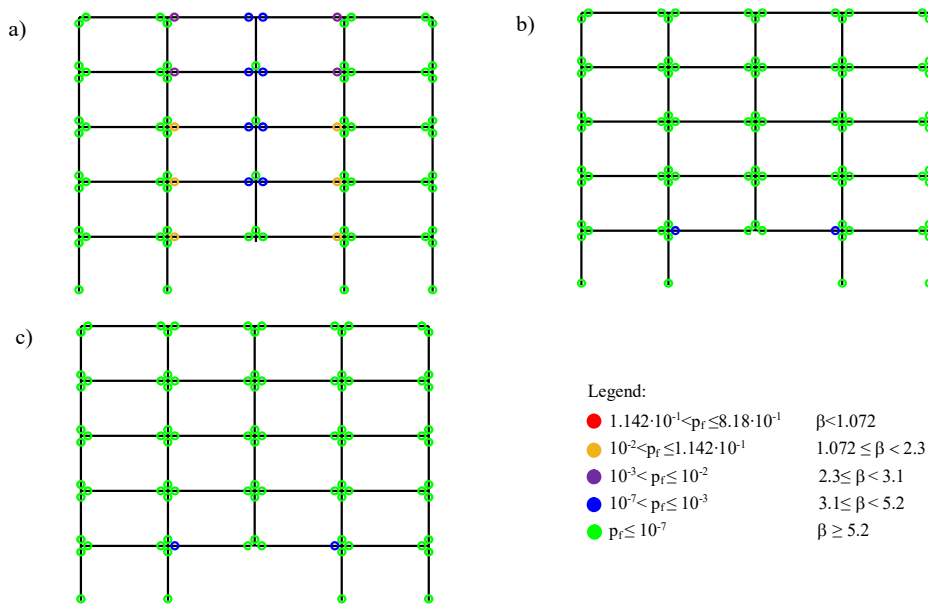
Figure 5.18 Failure probability for each cross-section of the *frame 2* considering: a) confined concrete; b) steel longitudinal reinforcement; c) steel transverse reinforcement.

Regarding the reliability levels for confined concrete (referred to a 50-years reference period), *frame 1* exhibits a β minimum far below 1, while *frame 2* and *frame 3* exceeds 1. Specifically, β minimum is equal to 1.08 for *frame 2* and 1.23 for *frame 3*, aligning with recommended provisions (i.e., CNR, 2018). As for the steel longitudinal reinforcement, β minimum are far below 1 for *frame 1* and reach high safety levels (i.e., 5.11 and 7.45) for *frames 2* and *frame 3*. These values slightly decrease (to around 4) when lower mean ultimate strains are assumed (i.e., equal to 0.075 as suggested in the Italian Codes).

The beneficial effect of *side face rebars* is confirmed by the achieved safety levels, particularly in scenarios involving dynamic phenomena and large displacements, where the steel governs the response.
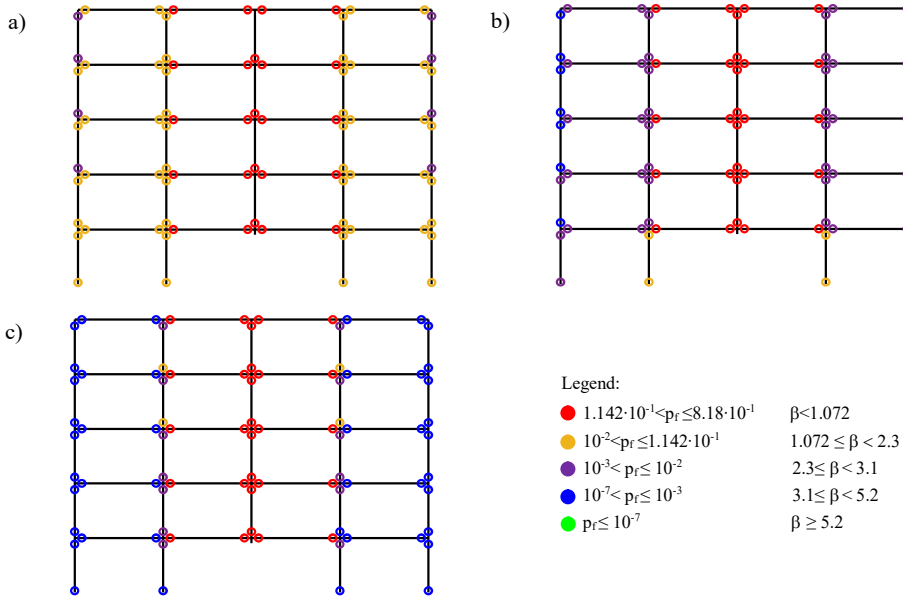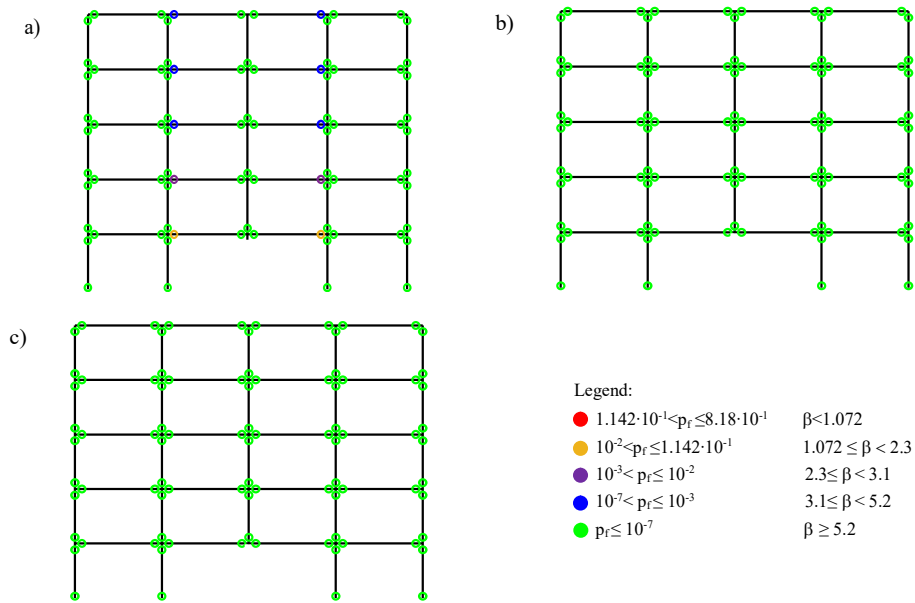

Figure 5.19 Failure probability for each cross-section of the *frame 3* considering: a) confined concrete; b) steel longitudinal reinforcement; c) steel transverse reinforcement.

The maximum failure probabilities obtained in this work (0.82, 0.14, and 0.11 for *frames 1*, *frame 2* and *frame 3* respectively) are comparable to those reported in Zhang et al. (2022), where a force-based reliability computation determines a failure probability of 0.074 for a similar five-story RC frame under a central supporting column loss scenario. The frame studied in Zhang et al. (2022) shares geometric and mechanical characteristics with the frames under investigation, including beam reinforcement continuity and comparable longitudinal reinforcement layouts between lower and upper chords on all floors. However, they adopt a force-based approach instead of a strain-based one, and steel properties are characterized by lower dispersion in the statistical characterization. Furthermore, in the study of Brunesi et al. (2015), failure probabilities around 0.75 are obtained for complete damage limit state in seismically designed 2D RC internal frames, under a lateral column failure scenario. Also in this case, the frames feature continuous and symmetrical longitudinal reinforcement across all floors. Additionally, they use a lower coefficient of variation (0.1) for concrete strength. Another comparison can be done with the results in Droogné et al. (2018), where the failure probability of planar frames of a RC office building is studied by including the membrane actions of one-way slabs. A probability of failure of 0.173 is reached; however, the building has horizontal stiffness provided by the bracings. In addition, no *symmetry* or *floor equality* criteria are adopted, as well as presence of *side face rebars*.

To conclude, for this specific failure scenario and structural typology, the design including *side face rebars* and *continuity* (i.e., *frame 2*) emerges as the optimal solution. It offers comparable safety levels to *frame 3*, which includes

additional design enhancements (*equal* reinforcement among floors and *symmetric* reinforcement in cross-sections), at reduced costs due to decreased reinforcement amount. Thus, the design of *frame 2* represents a favorable balance between robustness principles, sustainability, seismic design, and safety.

It is important to note that the analysis does not include contributions from the orthogonal frame affected by the same column loss. This aspect is dealt in Chapter 6. In addition, infills or membrane effects in the global structural resistance are discarded, leading to a safer assumption. However, the structure is composed by one-way slabs, whose membrane effects are less pronounced than in case of plate slabs.

Chapter 6

Modeling of the 3D effects deriving from orthogonal planar frames

6.1   Introduction

In the previous analyses the effects of the orthogonal framed system in the out-of-plane direction were considered in a simplified way by means of equivalent elastic springs placed in correspondence of the beam-column nodes (a part from the nodes of the columns above the accidentally lost one). However, the effects of the frame in the orthogonal direction, directly involved in the supporting column loss, has not been included. In addition, linear constitutive laws for the equivalent springs are not able to capture the non-linearities involved in a column removal scenario and could overestimate the response.

Three-dimensional effects are crucial in evaluating the response of RC systems to column removal scenarios. The three-dimensionality of structural systems is ensured by the slab (especially for slab plates) and the frames, constituted by beams and columns, in the orthogonal (out-of-plane) direction. For instance, the necessity of incorporating transverse beams in a model of progressive collapse scenario is highlighted through numerical comparisons between 2D and 3D analyses in Fascetti et al. (2015) and Brunesi and Parisi (2017). This finding is corroborated by experimental analyses on the progressive collapse resistance of beam-column subassemblies, considering the effects of transverse beams (Wang et al., 2022). Additionally, the experimental results of Qian et al. (2014) showed that 3D effects of the orthogonal structural system (excluding the slab), could increase the bearing capacity of the frame by more than 100%. Similar conclusions were drawn by Li and El-Tawil (2011), through a numerical comparison between a planar system and 3D models.

While including three-dimensional effects can increase structural robustness, conducting 3D numerical analyses for the design of a new building, especially

dynamically, is not always feasible due to computational and expertise requirements.

This chapter aims to incorporate three-dimensional effects in a simplified manner by modelling non-linear springs in correspondence of each beam-column nodes of the planar frame and summing up the contribution of the frames in the two main directions. The building is the one described in Section 3.2.2 (i.e., second building), where both secondary frames (with wide beams) and seismic resistant frames (with deep beams) are present. In addition, based on the results of Chapter 4 and Chapter 5, the following three structural configurations are considered:

- structural configuration designed according to current *code* rules (i.e., *Code* configuration);
- structural configuration where the criteria of *continuity* of longitudinal reinforcement and the presence of *side face rebars* are included as robustness enhancement suggestions (i.e., *C+rebars* configuration);
- structural configuration where the criteria of *continuity* of longitudinal reinforcement, the presence of *side face rebars, global equal* reinforcement amount in all the floors and *symmetric* in cross-sections are considered as robustness enhancement suggestions (i.e., *CSE+ rebars* configuration).

In addition, four different failure scenarios (FS) are studied, in order to account for the worst possible cases, where the contribution of the infills is not considered. These scenarios are indicated in the in-plan view of the building given in Figure 6.1, together with the indication of the seismic resistant frames (i.e., with deep beams) and secondary frames (i.e., with wide beams). In the following, deep beam is intended as a beam having a height larger than the height of the slab, while wide beams are those having a larger width and the same height of the slab.
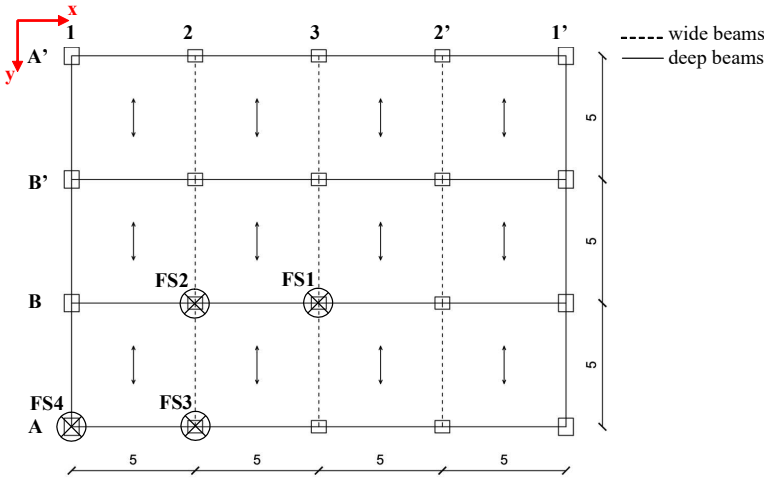

Figure 6.1 In plan view of the building and failure scenarios (FSs). Measurements in m.

The structural detailing of beams, columns and beam-column nodes of the *Code* configuration are given in Table 3.4 of Chapter 3.

Regarding the other two configurations, as for the *C+rebars* design, the presence of additional reinforcement determines a change in the stirrups step of the beams for all the floors from 10 cm to 7.5 cm. The new detailing is described in Table 6.1. This change is necessary in order to respect the capacity design principles. The detailing of the other structural elements (i.e., column and beam-column nodes) remain unchanged.

As for the third configuration (i.e., *CSE+rebars* design), an increasing of the stirrup's diameter in the beam-column nodes of the entire building is needed to respect the capacity design principles. The other structural detailing remains the same of the *C+rebars* configuration. The new configuration in terms of structural detailing is given in Table 6.2.

Table 6.1 Reinforcement detailing of *C+rebars* structural configuration.

Element	Plan location	Floor	Size [mm²]	Longitudinal bars *	Stirrups *
Beams	A1-A1'	1st-3rd	400x500	$4 \phi_u 18 + 3 \phi_l 18 + 4 \phi_f 16$	2-leg $\phi 8$/ 75 (D), 150(ND)
		4th-5th	400x500	$3 \phi_u 18 + 3 \phi_l 18 + 4 \phi_f 16$	2-leg $\phi 8$/ 75 (D), 150(ND)
	B1-B1'	1st-3rd	400x500	$5 \phi_u 18 + 3 \phi_l 18 + 4 \phi_f 16$	2-leg $\phi 8$/ 75 (D), 150(ND)
		4th-5th	400x500	$4 \phi_u 18 + 3 \phi_l 18 + 4 \phi_f 16$	2-leg $\phi 8$/ 75 (D), 150(ND)
	A2-A'2 A3-A'3	1st-5th	230x600	$2 \phi_u 14 + 2 \phi_l 14$	2-leg $\phi 8$/100
Columns	A1, B1	all	600x500	$10 \phi 20$	4-leg $\phi 8$/ 100 (D), 150(ND)
	A2, A3, B2, B3	all	600x700	$16 \phi 20$	4-leg $\phi 8$/ 100 (D), 150(ND)
Nodes	all	all			4-leg $\phi 8$/ 50

*D indicates the dissipative area, ND the non-dissipative area, ϕ_u and ϕ_l are, respectively, the longitudinal reinforcement in the upper and lower chords, ϕ_f are side face rebars. The units of measure are mm.

Table 6.2 Reinforcement detailing of *CSE+rebars* structural configuration.

Element	Plan location	Floor	Size [mm²]	Longitudinal bars *	Stirrups *
Beams	A1-A1'	all	400x500	$4 \phi_u 18 + 3 \phi_l 18 + 4 \phi_f 16$	2-leg $\phi 8$/ 75 (D), 150(ND)
	B1-B1'	all	400x500	$5 \phi_u 18 + 3 \phi_l 18 + 4 \phi_f 16$	2-leg $\phi 8$/ 75 (D), 150(ND)
	A2-A'2 A3-A'3	all	230x600	$2 \phi_u 14 + 2 \phi_l 14$	2-leg $\phi 8$/100
Columns	A1, B1	all	600x500	$10 \phi 20$	4-leg $\phi 8$/ 100 (D), 50(ND)
	A2,A3, B2, B3	all	600x700	$16 \phi 20$	4-leg $\phi 8$/ 100 (D), 150(ND)
Nodes	all	all			4-leg $\phi 10$/ 50

*D indicates the dissipative area, ND the non-dissipative area, ϕ_u and ϕ_l are, respectively, the longitudinal reinforcement in the upper and lower chords, ϕ_f are side face rebars. The units of measure are mm.

The assumptions behind the material modeling are similar to those already explained in Chapter 4, adopting the mean values of the mechanical properties. Especially for the compressive behavior of C25/30 concrete, the confinement effects are included considering the different configurations of the transverse reinforcement. Since different transverse reinforcements are adopted in the

structural elements of the three configurations, the sets of constitutive laws of confined concrete are defined for, respectively, *Code* configuration (i.e., Figure 6.2a-b), *C+rebars* configuration (i.e., Figure 6.2c-d) and *CSE+rebars* configuration (i.e., Figure 6.2e-f), distinguishing between beams, columns and beam-column nodes.
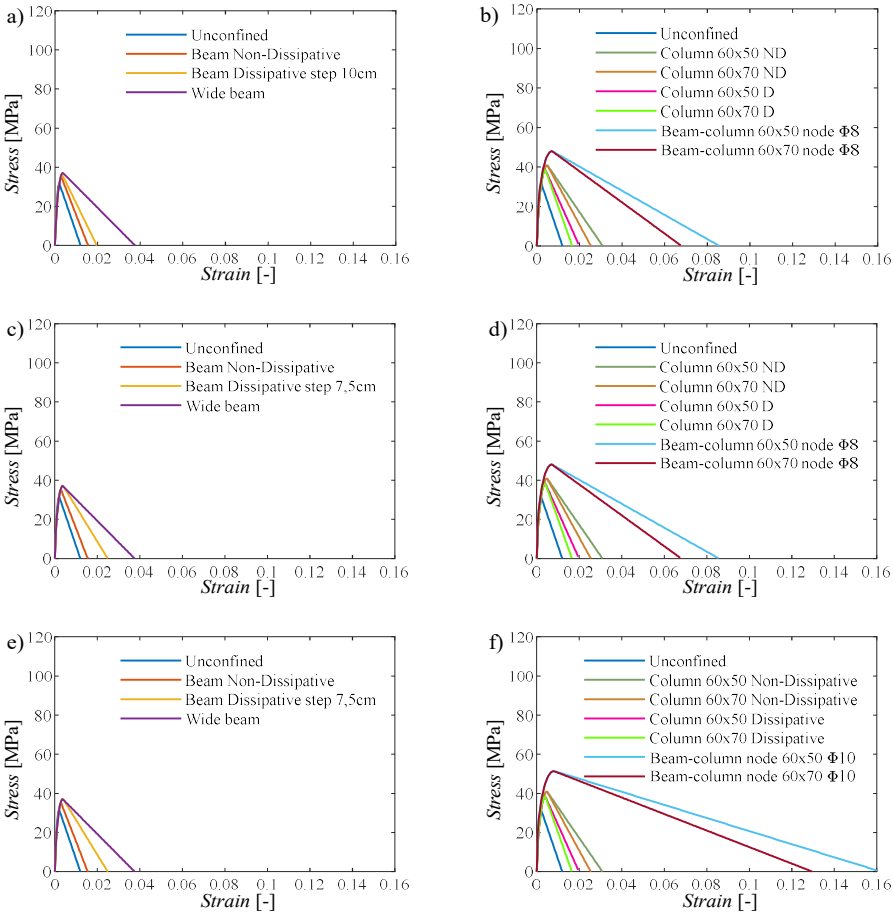
Figure 6.2 Concrete constitutive laws in compression for: (a)-(b) *Code* configuration; (c)-(d) *C+rebars* configuration; (e)-(f) *CSE+rebars* configuration for, respectively, beams and columns.

Regarding the tensile behavior of concrete (Figure 6.3a), it is described by f_{ctm} which is the mean value of the tensile strength (i.e., 2.56 MPa) and E_{cm} representing the mean secant elastic modulus, computed according to CEB-FIP Model Code 90, as function of the strength in compression.

As for the B450C steel property (Figure 6.3b), the elastic modulus is assumed equal to 210 GPa, the yielding strength is equal to 489 MPa, while the ultimate strength is equal to 611 MPa (i.e., by considering an ultimate-to-yielding strength ratio equal to 1.25 as suggested by the Italian Guidelines MIT, 2018). The ultimate strain is equal to 0.18.

The other modeling assumptions for the 2D non-linear finite element analyses are the same explained in the previous chapters.
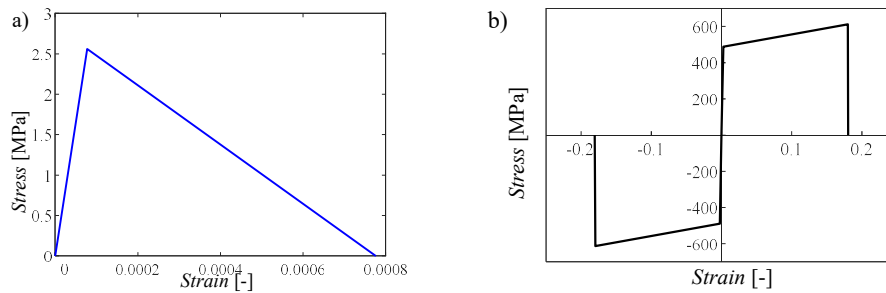
Figure 6.3 Constitutive laws for: (a) concrete in tension; (b) steel reinforcement both in tension and in compression.

In the following, the results of the pushdown analysis for each collapse scenario are given, distinguishing between the three different structural configurations. In addition, the results of the superposition between the capacity curve of the planar frames in the two orthogonal directions are compared with the total capacity curve obtained from a 3D numerical simulation, in order to investigate the possibility of applying the superposition principle when considering 2D FEM analyses.

6.2   First failure scenario (FS1)

This section is about the results in terms of capacity curves for the first failure scenario. In particular, the failure scenario involves the removal of column B3 and affects the frames FS1-x and FS1-y, as shown in Figure 6.4.
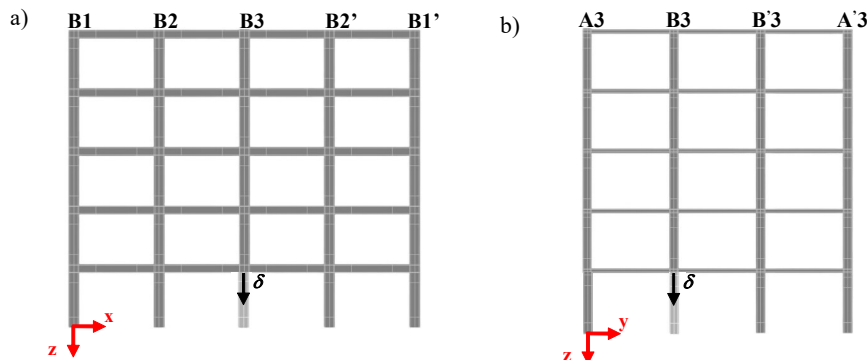
Figure 6.4 Schematic representation of the pushdown analysis for the frames involved in the first failure scenario: (a) FS1-x; (b) FS1-y.

6.2.1 Calibration of non-linear translational springs

To account for the three-dimensional effects of the orthogonal framed system, the procedure already explained in Section 3.4.1 is applied to calibrate the non-linear translational springs.
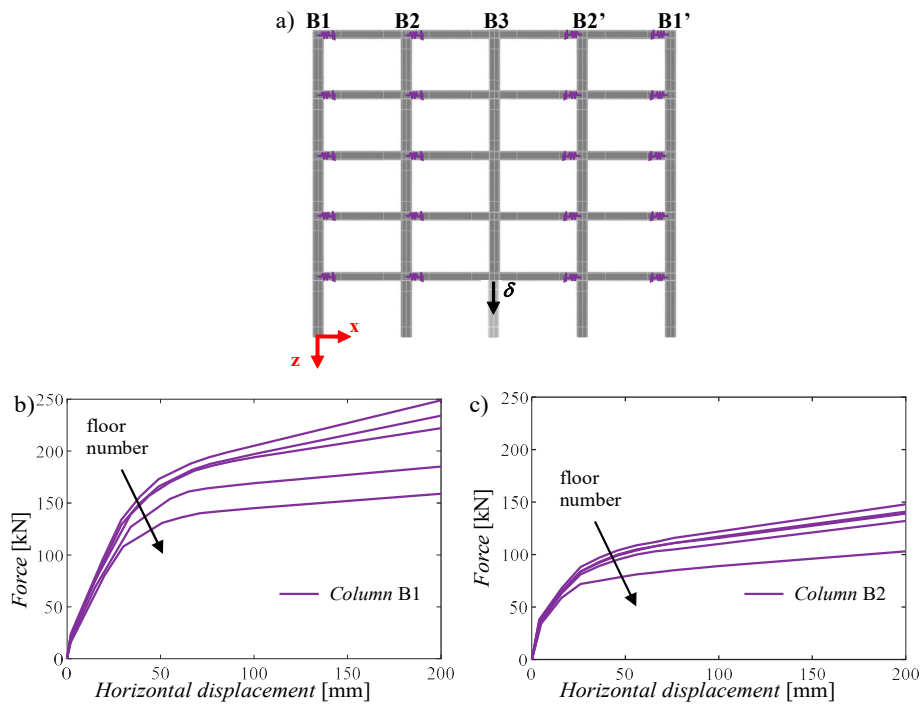
Figure 6.5 Lateral constraint conditions for *Code* configuration: (a) springs positions (in purple) in the frame FS1-x; (b) constitutive laws of the springs for column B1; (c) constitutive laws of the springs for column B2.

The calibration has been repeated for the two frames in x and y directions and for the three structural configurations. An example of constitutive laws calibrated for the *Code* configuration, is reported in Figure 6.5 for the frame FS1-x and in Figure 6.6 for the frame FS1-y.

Regarding the non-linear constitutive laws calibrated for the frames FS1-x (Figure 6.5), the contribution of the framed system in the beam-column nodes of the column B1 (i.e., Figure 6.5b) is more pronounced than the contribution of the column B2 (i.e., Figure 6.5c), since in the former case the orthogonal frame in y-direction is characterized by wide beams, while the orthogonal frame in y-direction for column B2 has deep beams.

As for the non-linear constitutive laws for the frame FS1-y (Figure 6.6), the three sets of constitutive laws do not differ at all since they all depend to frames in the x-direction that are all characterized by deep beams. However, the contribution of the column A3' (i.e., Figure 6.6d) is slightly less pronounced than the other two since the column is farther from the lost one (i.e., column B3).

Another important observation, is that in general the springs are in non-linear regime for a horizontal displacement larger than 2 cm.

Similar results are obtained for the other structural configurations and failure scenarios.

120
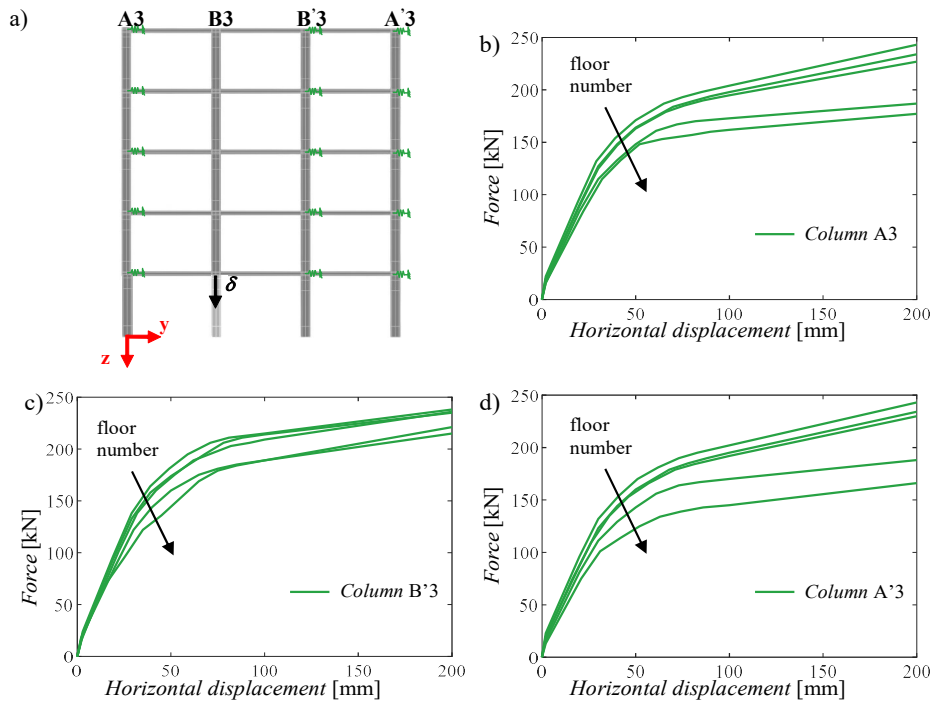
Figure 6.6 Lateral constraint conditions for *Code* configuration: (a) springs positions (in green) in the frame FS1-y; (b) constitutive laws of the springs for column A3; (c) constitutive laws of the springs for column B'3; (d) constitutive laws of the springs for column A'3.

6.2.2 Pushdown analyses for frame FS1-x

This subsection investigates the capacity curves of the three configurations for the frame FS1-x, oriented in the x-direction and subjected to the column removal B3 (i.e., first failure scenario, depicted in Figure 6.1).

The capacity curve related to the *Code* configuration, illustrated in Figure 6.7a, exhibits a maximum resistant load in the flexural phase $P_{MAX,FL}$ of 1129 kN. Subsequently, the capacity curve undergoes an initial softening phase followed by the onset of a catenary effect for a considerable large displacement (approximately 60 cm), as evidenced by the horizontal displacement of beam-column nodes (Figure 6.7b), accompanied by a slight increase in structural resistance. The structure fails when the bars reach their ultimate strain, occurring at a maximum ultimate load P_{ULT} of 1024 kN, with an applied vertical displacement of around 64 cm. This ultimate resistance is lower than the peak in the flexural stage. The vertical displacement of nodes in both columns B1 and B2 (Figure 6.7c) exhibits a decrease followed by an increase: the initial decrease results from the arching behavior of the beams, while the subsequent increase arises due to node rotation during the transition to catenary activation.

The design enhancements in the *C+rebars* configuration, specifically the *continuity* of beam longitudinal reinforcement and the inclusion of *side face rebars*, confer significant advantages, as evidenced by the capacity curve and the horizontal and vertical displacements of nodes in Figure 6.7a,d,e.

Figure 6.7 Results of the pushdown analyses for the FS1-x: (a) capacity curves; (b),(d),(f) horizontal displacement of beam-column nodes; (c),(e),(g) vertical displacements of the beam-column nodes for, respectively, *Code*, *C+rebars* and *CSE+rebars* configurations.

The transition to the catenary phase in the *C+rebars* configuration is notably anticipated (at a vertical displacement below 20 cm). This improvement is evident in both the capacity curve and the horizontal displacements of beam-column nodes, where the change in sign is highlighted. This benefit is ensured by both design enhancements: *continuous* longitudinal reinforcement along the beam length helps in establishing the tying effect at an early vertical imposed displacement, while *side face rebars*, situated in the central part of the cross-sections, experience low strains during the flexural phase, facilitating the early onset of catenary behavior when

122

tensile forces emerge. Furthermore, there is an increase in both the maximum resistant load in the flexural phase and the ultimate resisting load, due to a larger quantity of reinforcement in the beams. Another significant advantage relates to ductility, as the ultimate strain for longitudinal reinforcement (i.e., 18%) is reached at an applied vertical displacement more than 20 cm later compared to the configuration without *side face rebars*.

In comparison to the *C+rebars* configuration, the *CSE+rebars* configuration introduces *equality* in reinforcement arrangements between floors and *symmetry* of cross-sections. This results in increased reinforcement quantities, yielding the following enhancements: higher values for both flexural peak and ultimate resistance, and a slight anticipation of the catenary effect compared to the previous configuration, as evident in Figure 6.7a. The longitudinal reinforcement reaches the ultimate strain (i.e., 18%) at an applied vertical displacement equal to 90 cm.

By observing the horizontal displacements of the beam-column nodes for these last two configurations (Figure 6.7d,f), the springs enter a non-linear regime when the applied vertical displacement exceeds 60 cm (i.e., when the catenary effect is already mobilized). Consequently, non-linear calibration for the orthogonal frame contribution can be crucial, particularly in scenarios involving dynamic phenomena with significant vertical displacements in correspondence of the supporting column.

6.2.3 Pushdown analyses for frame FS1-y

This subsection is about the results of pushdown analyses conducted for frame FS1-y which was subjected to the removal of Column B3.

Figure 6.8 presents the capacity curves and the vertical and horizontal displacements of the beam-column nodes. The results, in terms of capacity curves, exhibit a behavior distinct from that illustrated in Subsection 6.2.2. In fact, for all the three design solutions, the flexural phase has a maximum resistant load $P_{MAX,FL}$ of 159 kN, significantly lower than in the previous scenario. This difference is attributed to the reduced amount of reinforcement in the wide beams (i.e., 2 ϕ14 in the upper chord and 2 ϕ14 in the lower chord of the beams cross-section).

The curves demonstrate a transition to catenary activation occurring between 15 and 20 cm of imposed vertical displacement, substantially anticipating the catenary phase with respect to the previous case. The catenary phase, in turn, is not only anticipated but also significantly more pronounced, with a much larger maximum ultimate load P_{ULT} compared to that recorded at the flexural peak. This can be attributed to two main reasons: i) the longitudinal reinforcement of the wide beams are *continuous* throughout the structural elements, starting from the *Code* configuration, which aids in developing the tying effect; ii) the wide beams exhibit significantly greater ductility than the deep beams, as also demonstrated in Di Trapani et al. (2020).

Observing the horizontal displacements of the beam-column nodes (Figure 6.8 b,d,f), it is noted that the springs enter a non-linear regime when the imposed vertical displacement exceeds 35 cm (i.e., when the catenary effect is already mobilized).
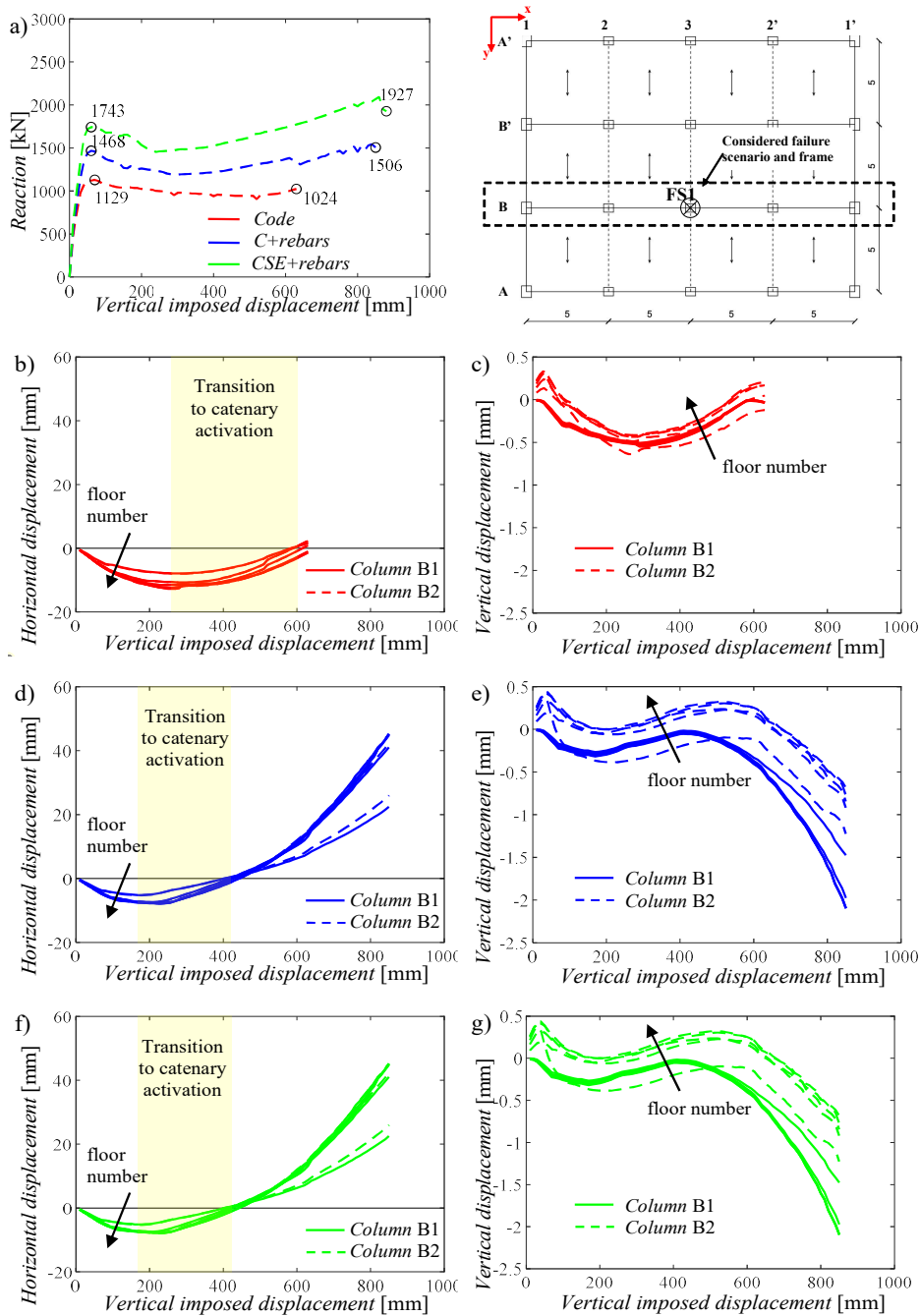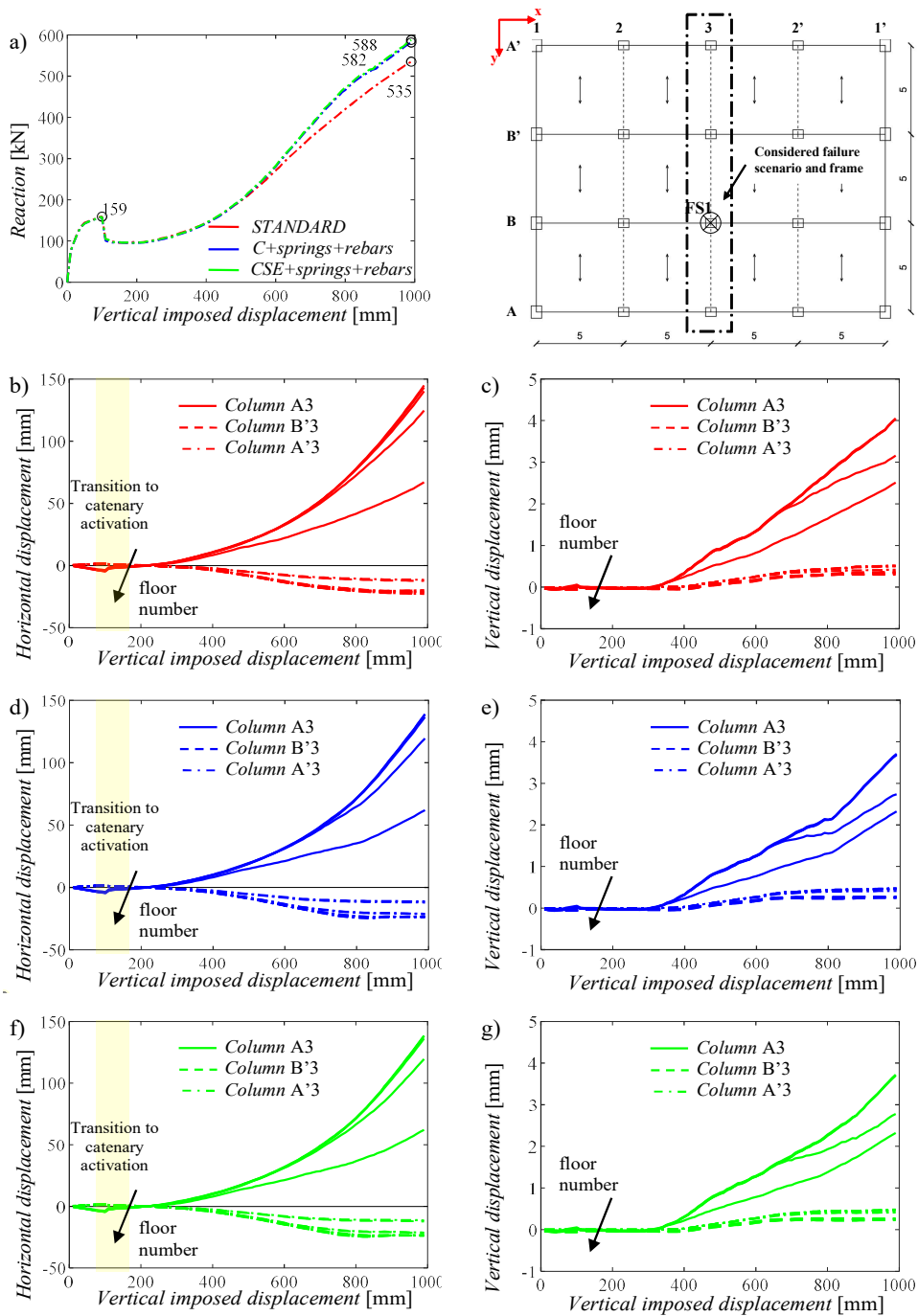
Figure 6.8 Results of the pushdown analyses for the FS1-y: (a) capacity curves; (b),(d),(f) horizontal displacement of beam-column nodes; (c),(e),(g) vertical displacements of the beam-column nodes for, respectively, *Code*, *C+rebars* and *CSE+rebars* configurations.

Consequently, the non-linear field for the translational springs is reached earlier for the frames in the y-direction compared to those in the x-direction. Thus, the non-linear calibration of the springs is essential especially for the case in which wide beams are designed. Additionally, from the capacity curves, it is observed that there is only a slight difference between the *Code*, *C+rebars*, and *CSE+rebars* configurations since the wide beams are not subjected to different design modifications. The minimal differences in the results are attributed to the non-linear

124

translational springs, which were recalibrated considering the design improvements on the other structural elements of the 3D model of the building.

6.2.4 Superposition of the capacity curves and comparison with the 3D model for the FS1

The proposed approach consists in evaluating the global response of a building under a column removal scenario by superimposing the responses obtained from the planar NLFE models. To accomplish this, the capacity curves obtained for the two mutually orthogonal frames subjected to the loss of the same column in the first collapse scenario FS1 (Column B3) are superimposed. This approach has also been validated in an experimental test involving beam-column subassemblies Wang et al. (2022) and Tan et al. (2022).

This process was repeated for the three different configurations to compare the benefits of the design recommendations. From Figure 6.9, it is evident that frame FS1-y (with wide beams) offers minimal contribution in the flexural phase compared to frame FS1-x. However, as imposed displacements increase, its contribution gradually rises due to the greater ductility of frames with wide beams. This behavior is consistent across all the three configurations. Additionally, for all configurations, the transition to catenary activation of the superimposed capacity curve occurs at smaller imposed vertical displacements, with ultimate resistances (governed by the failure of the FS1-x frame) exceeding the flexural peaks. This improvement is particularly pronounced in the *C+rebars* and *CSE+rebars* configurations, ensuring a higher level of safety.

The global capacity curve for the *Code* configuration (Figure 6.9a) exhibits a softening followed by an increase in resistance up to a displacement slightly higher than 60 cm. This trend arises from the exceeding of the ultimate strain in the beam longitudinal reinforcement (18%) in the x-direction frame (seismic-resistant frame), after which only the orthogonal frame in the y-direction contributes. A similar trend is observed for both *C+rebars* (Figure 6.9b) and *CSE+rebars* (Figure 6.9c) configurations, but with larger ultimate vertical displacements (87 cm and 89 cm, respectively).

Comparing the configurations for the first failure scenario, the model with *continuous* beam longitudinal reinforcement and *side face rebars* criteria (*C+rebars* configuration) appears to strike the best balance between enhancing structural robustness and sustainability principles.
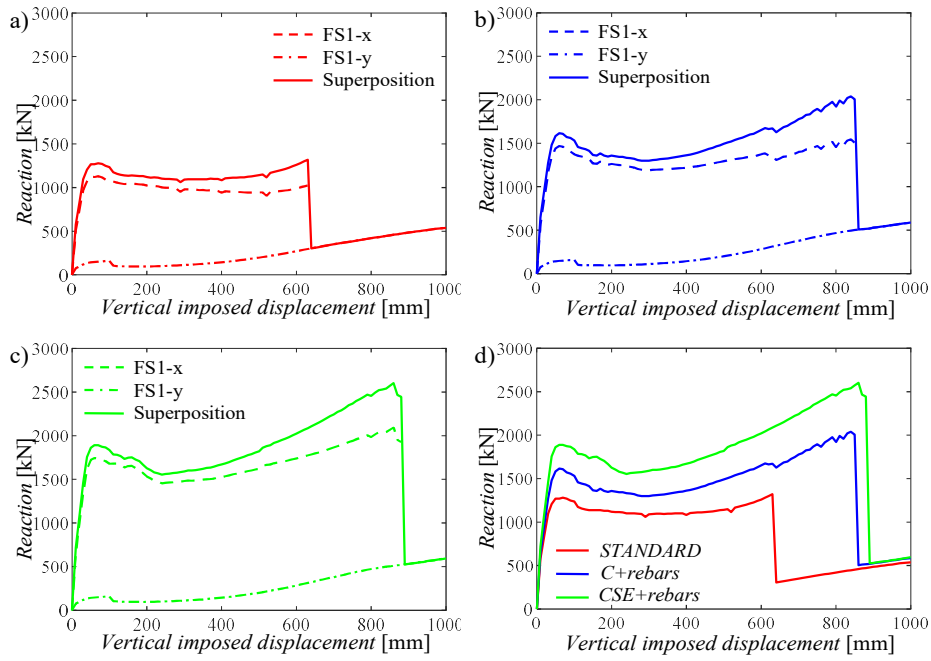
Figure 6.9 Results of the superposition of the FS1: (a) global capacity curve for *Code* configuration; (b) global capacity curve for *C+rebars* configuration; (c) global capacity curve for *CSE+rebars* configuration; (d) comparison between the three global capacity curves.
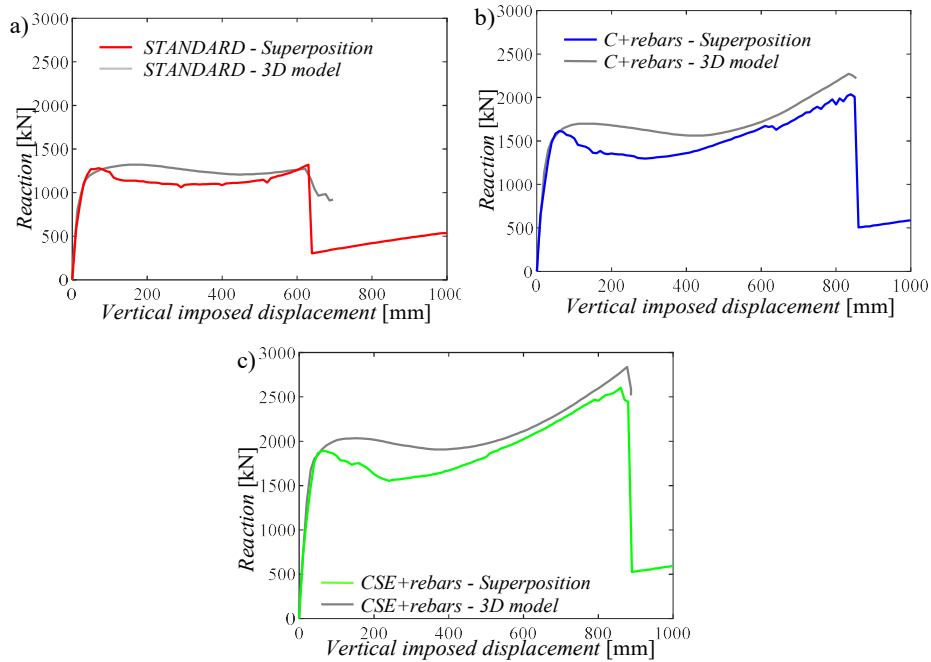
Figure 6.10 Comparison between global capacity curves and 3D capacity curves for the FS1.

To validate the effectiveness of the global capacity curves obtained through the superposition of 2D NLFE analyses on the two orthogonal frames affected by the first failure scenario, a 3D displacement-controlled pushdown non-linear analysis was conducted on the 3D structure modeled in SAP2000. The constitutive laws of both materials used in the 3D model are the same adopted for the NLFEMs. The analysis involves applying increasing vertical displacement, with a step of 1 cm, at

126

the top of the removed supporting column (Column B3), and determining the force exerted by the remaining structure at that specific point. Geometrical non-linearities are also considered in the 3D simulations. The hypotheses behind the fiber modeling are the same adopted for the calibration of the non-linear springs as described in Section 3.4.1.

Figure 6.10 shows a comparison between the capacity curve obtained from the 3D model and the global capacity curve obtained from the superposition of the 2D NLFE analyses. The main difference lies in the softening stage, with a lower reduction in resistance observed in the 3D model. This discrepancy can be attributed to modeling differences between the software codes used. Nonetheless, the results confirm the effectiveness of the superposition of the 2D capacity curves, achieved with reduced computational effort, with differences deriving from the inherent differences of the two modelling software codes (i.e., epistemic uncertainties).

6.3   Second failure scenario (FS2)

This section regards the results related to the second failure scenario, involving the removal of column B2. In this case, the two orthogonal frames directly involved by the FS2 are FS2-x and FS2-y as depicted in Figure 6.11. Notably, FS2-x is a seismic resistant frame constituted by deep beams, while FS2-y is a secondary frame with wide beams.
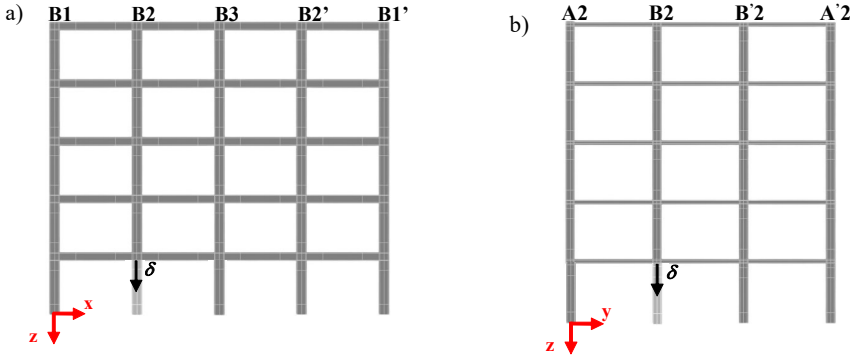
Figure 6.11 Schematic representation of the pushdown analysis for the frames involved in the second failure scenario: (a) FS2-x; (b) FS2-y.

The calibration of the non-linear constitutive laws for the equivalent springs is the same followed for the first failure scenario and involves similar results. In the following, the NLFE results of the pushdown analyses together with the application of the superposition of the capacity curves are reported for the FS2.

6.3.1 Pushdown analyses for frame FS2-x

The pushdown analyses for the frame FS2 in x-direction are shown in Figure 6.12 for the three structural configurations.

The *Code* configuration exhibits a lower flexural peak and ultimate resistance compared to the first collapse scenario, and the catenary effect is absent. This is due to the reduced contribution from the orthogonal frames.
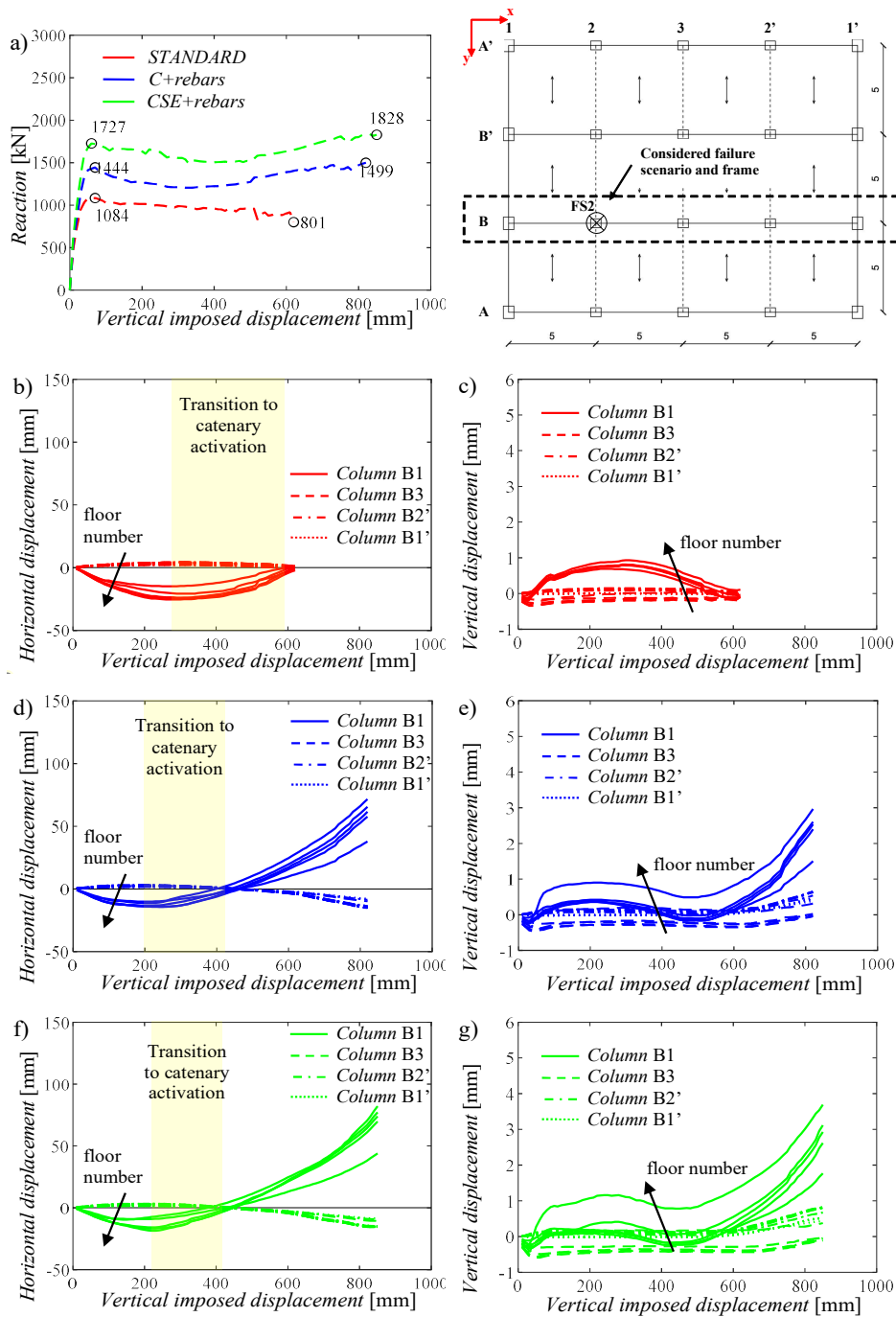
Figure 6.12 Results of the pushdown analyses for the FS2-x: (a) capacity curves; (b),(d),(f) horizontal displacement of beam-column nodes; (c),(e),(g) vertical displacements of the beam-column nodes for, respectively, *Code*, *C+rebars* and *CSE+rebars* configurations.

Conversely, the presence of *side face rebars* in the *C+rebar*s model, as observed in the first failure scenario, leads to an increase of the flexural peak and to the initiation of the catenary effect. Specifically, the transition to catenary effects occurs at a displacement of around 20 cm (Figure 6.12d). Similarly, in the *CSE+rebars* model the criteria of section *symmetry* and *floor equality* further increase the flexural peak and ultimate resistance. The transition to catenary

128

activation occurs at an imposed vertical displacement of 20 cm, only slightly earlier than the *C+rebars* model (i.e., 20 cm).

6.3.2 Pushdown analyses for frame FS2-y

The results for the frame FS2 in y-direction are shown in Figure 6.13.
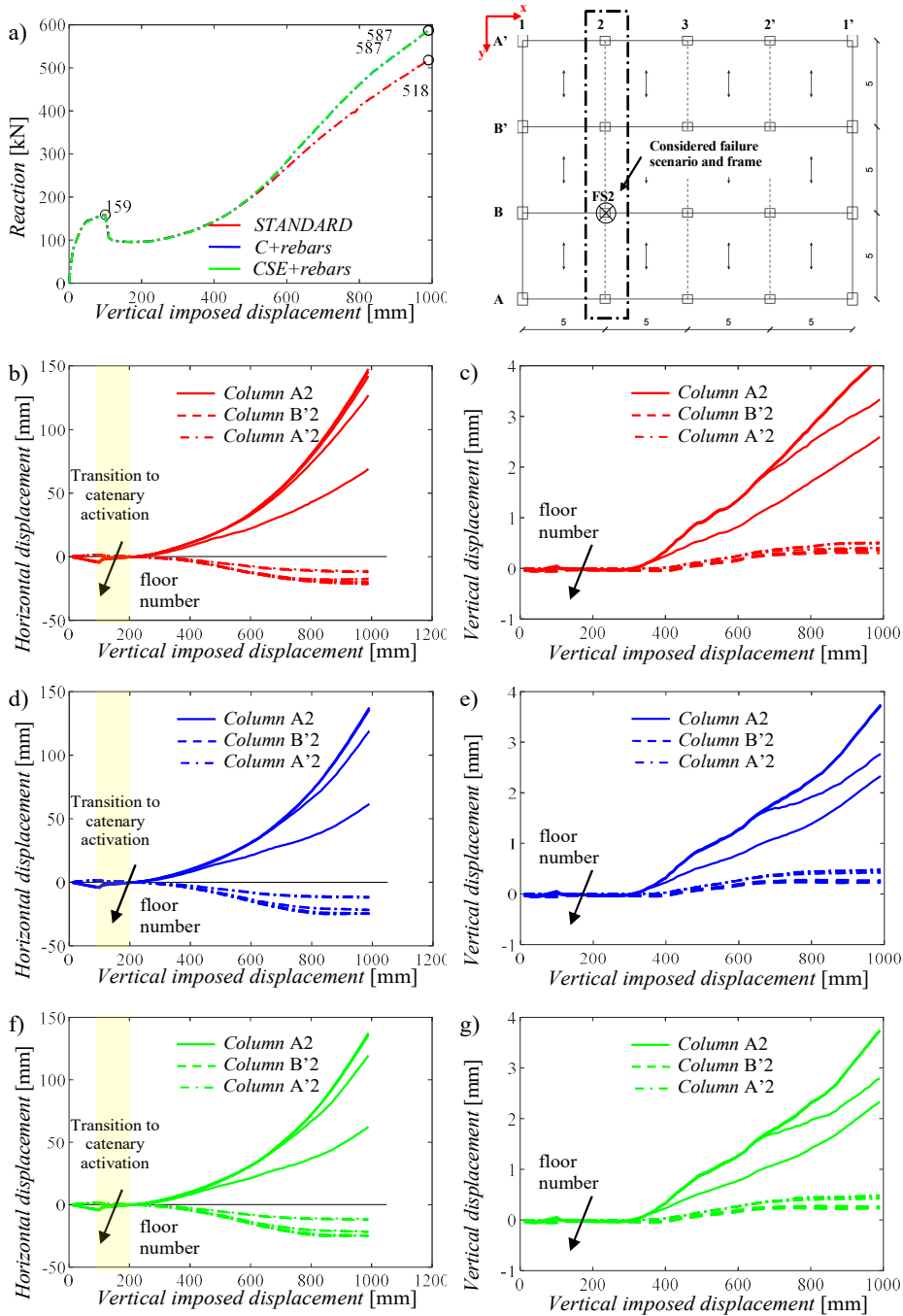
Figure 6.13 Results of the pushdown analyses for the FS2-y: (a) capacity curves; (b),(d),(f) horizontal displacement of beam-column nodes; (c),(e),(g) vertical displacements of the beam-column nodes for, respectively, *Code*, *C+rebars* and *CSE+rebars* configurations.

The results yield to conclusions similar to those reported in the previous collapse scenario: the flexural phase is significantly lower compared to the value reached for the orthogonal collapsed frame, but the transition to the catenary phase is considerably anticipated and more pronounced. The design improvements are not implemented for wide beams, resulting in minimal distinctions among the *Code* model, *C+rebars* model, and *CSE+rebars* model concerning the non-linear translational springs.

6.3.3 Superposition of the capacity curves and comparison with the 3D model for the FS2

In Figure 6.14 and Figure 6.15 the superposition of the capacity curves in the orthogonal directions and the comparison with the 3D model are shown, respectively.
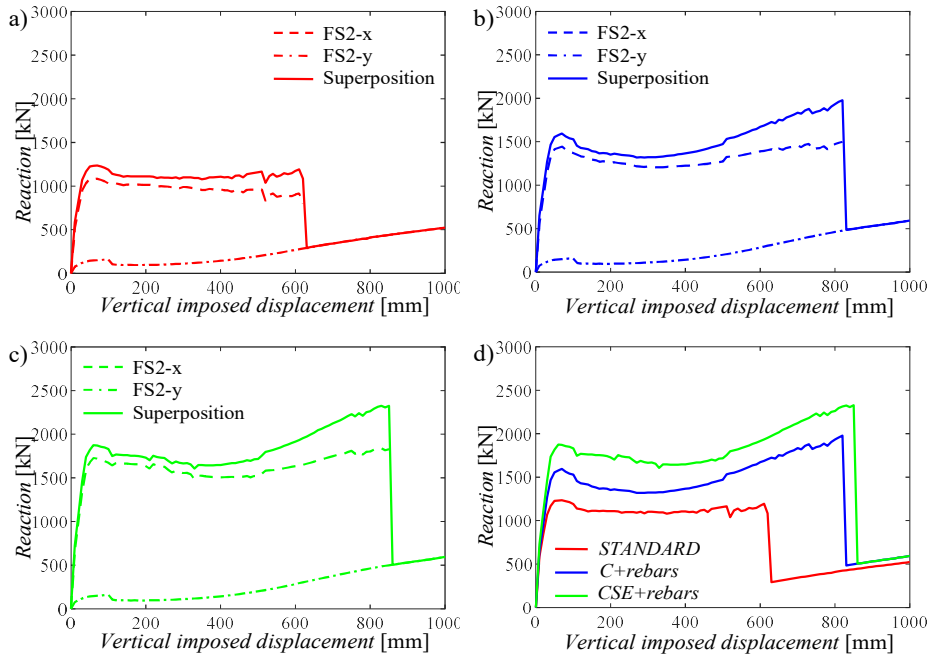
Figure 6.14 Results of the superposition of the FS2: (a) global capacity curve for *Code* configuration; (b) global capacity curve for *C+rebars* configuration; (c) global capacity curve for *CSE+rebars* configuration; (d) comparison between the three global capacity curves.

Comparing the global capacity curves (Figure 6.14d), the *CSE+rebars* configuration shows increased flexural and ultimate resistance compared to the *C+rebars* configuration, along with a higher vertical imposed displacement at collapse is reached. Even in this failure scenario, the *C+rebars* configuration represents the optimal balance between enhancing structural robustness and promoting sustainability.
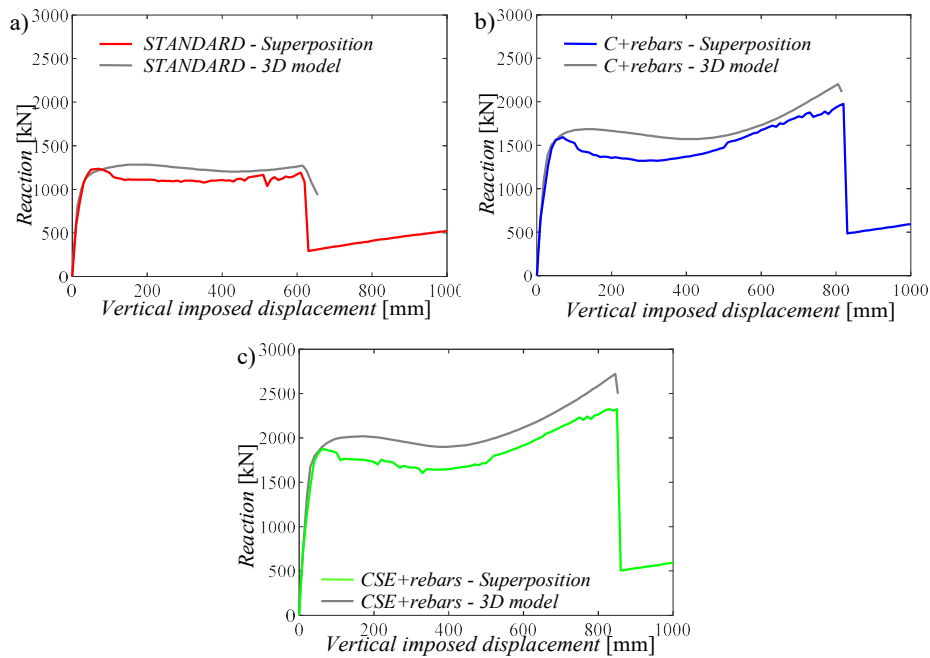
Figure 6.15 Comparison between global capacity curves and 3D capacity curves for the FS2.

By analyzing the comparison between the superposition capacity curve and the one obtained from a 3D model (Figure 6.15), comparable findings with respect to the FS1 can be observed for the FS2: the flexural peaks in the 3D models closely match the values of the global capacity curves, although at slightly higher vertical displacements in the 3D model. The transition through the catenary effect is quite similar, as well as the final drops in resistance occurring at almost identical vertical displacements. In fact, the failure is governed by the ultimate strain of the longitudinal reinforcing bars of the beam. Since the second failure scenario imposes more demanding local stresses, the differences between the two global curves are emphasized, especially in the softening phase due to concrete cracking and crushing, which is not captured by a fiber-based model.

However, these results confirm again the effectiveness of the superposition of the 2D capacity curves for the second failure scenario.

6.4 Third failure scenario (FS3)

This section deals with the results related to the third failure scenario, involving the removal of column A2.

In this case, the two orthogonal frames directly involved by failure are FS3-x and FS3-y as shown in Figure 6.16. This scenario is critical especially for the frame FS3-y, since it involves the loss of a lateral column. In addition, this frame is a secondary one, thus it is characterized by wide beams.

In the following, the NLFE results of the pushdown analyses together with the application of the superposition of the capacity curves is reported for the FS3.
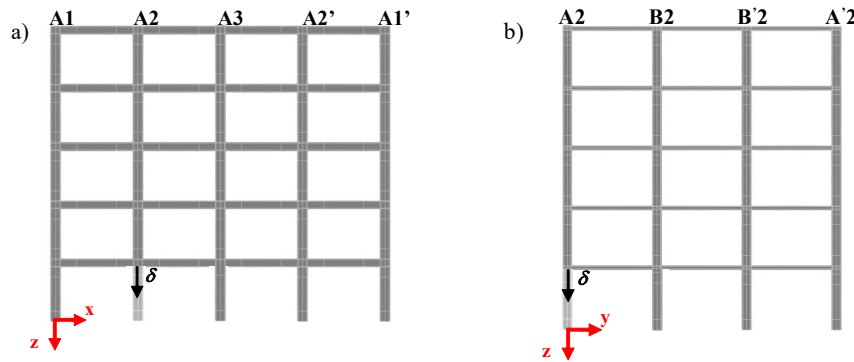
Figure 6.16 Schematic representation of the pushdown analysis for the frames involved in the third failure scenario: (a) FS3-x; (b) FS3-y.

6.4.1 Pushdown analyses for frame FS3-x

The pushdown analyses for the frame FS3 in y-direction are shown in Figure 6.17 for the three structural configurations.

The frame in the x-direction, is a perimeter frame, unlike the previous collapse scenarios: the beams in this frame have a lower quantity of longitudinal reinforcement. The additional presence of bars in *C+rebars* and *CSE+rebars* models leads to an increase in the flexural peaks as well as in the ultimate resistance.

The transition towards the catenary effect is absent in the *Code* model, while it is activated in the *C+rebars* and *CSE+rebars* models. As observed from the horizontal displacements of the beam-column nodes (Figure 6.17d,f), the catenary effect in the last two models occurs between 20 and 40 cm of imposed vertical displacement. The ultimate strain for the longitudinal reinforcement (i.e., 18%) is reached at an imposed vertical displacement of 63 cm in the *Code* model, with a maximum resistant load equal to 877 kN. In the *C+rebars* and *CSE+rebars* models, the ultimate strain is reached at a higher imposed displacement (i.e., at, respectively, 87 cm and 93 cm) with maximum resistant loads of 1356 kN and 1556 kN, respectively.
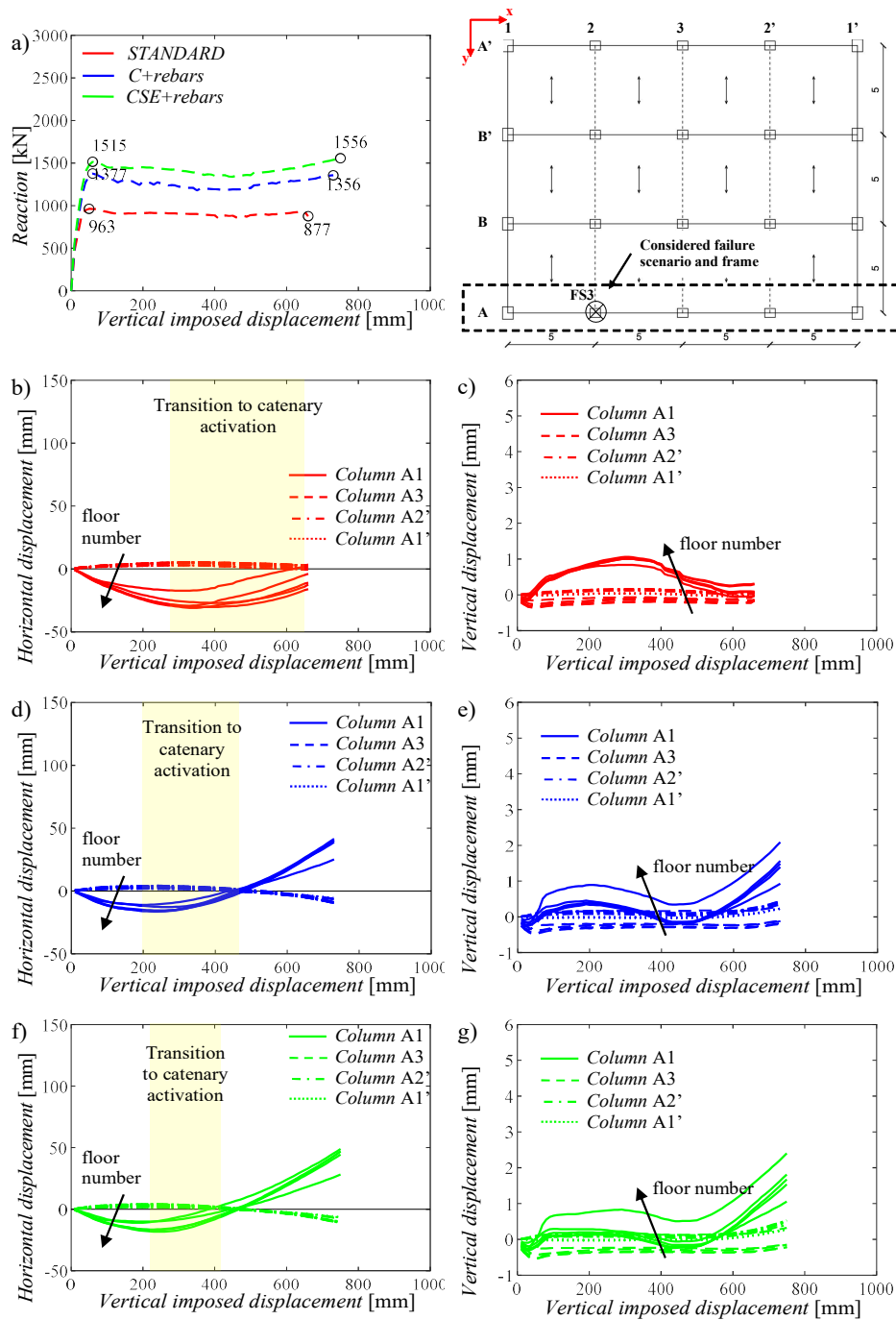
Figure 6.17 Results of the pushdown analyses for the FS3-x: (a) capacity curves; (b),(d),(f) horizontal displacement of beam-column nodes; (c),(e),(g) vertical displacements of the beam-column nodes for, respectively, *Code*, *C+rebars* and *CSE+rebars* configurations.

6.4.2 Pushdown analyses for frame FS3-y

The pushdown analyses for the frame FS3 in y-direction are shown in Figure 6.18 for the three structural configurations.

The response of the three models, as depicted by the capacity curves, shows a very similar pattern due to the reasons previously discussed.

133
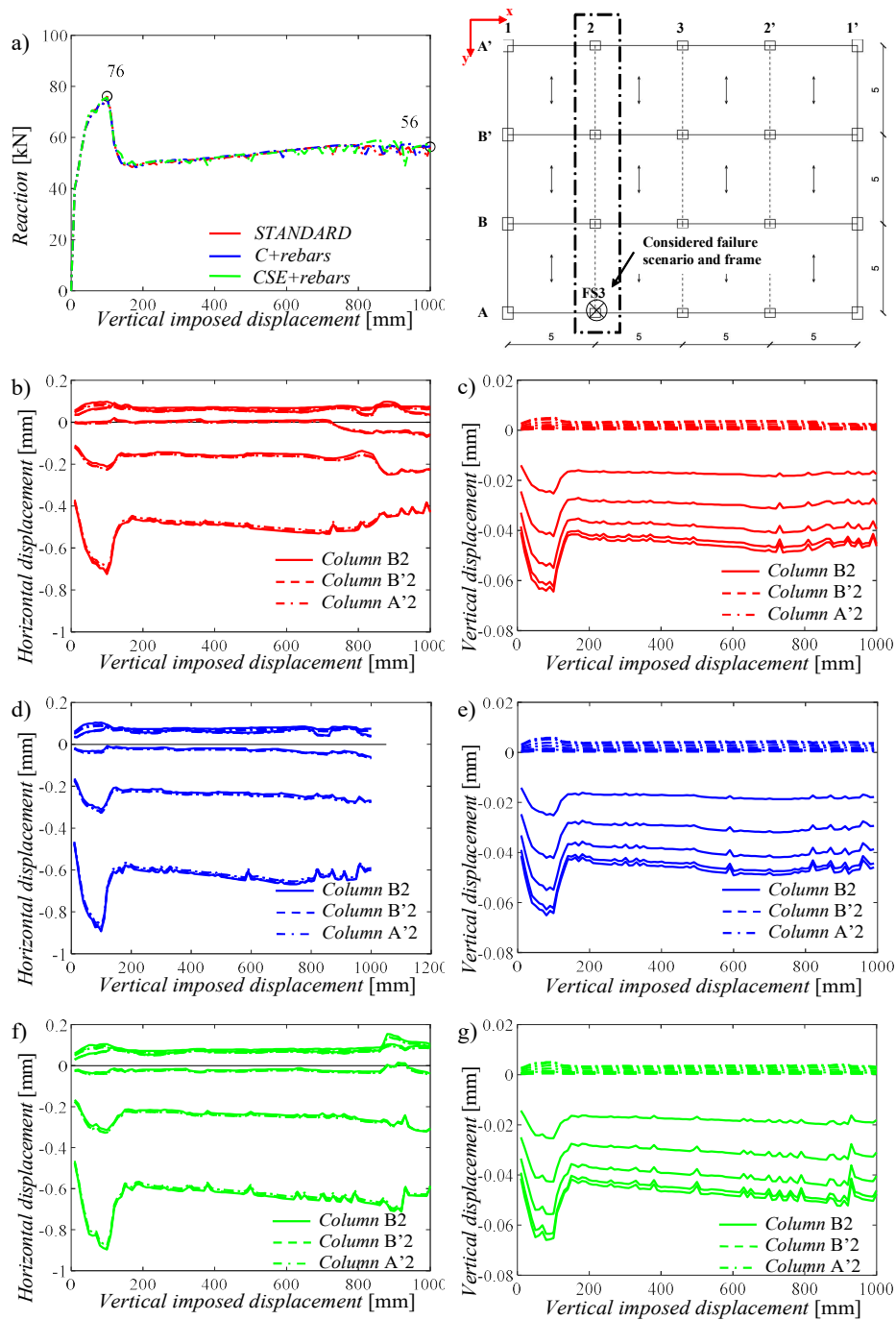
Figure 6.18 Results of the pushdown analyses for the FS3-y: (a) capacity curves; (b),(d),(f) horizontal displacement of beam-column nodes; (c),(e),(g) vertical displacements of the beam-column nodes for, respectively, *Code*, *C+rebars* and *CSE+rebars* configurations.

The capacity curves exhibit a distinct behavior compared to the y-direction frame analyzed in the first and second collapse scenarios, since the frame FS3-y provides a very minimal contribution. Two primary factors contribute to this observation: firstly, the frame under analysis features wide beams with lower resistance compared to other beams in the structure; secondly, column A2 serves as a perimeter column for the analyzed frame, with the resisting mechanism mainly relying on the beams of the outer span.

134

It is crucial to note that the omission of infill walls results in an underestimation of the structural response, especially evident when a perimeter column is removed, as in the analyzed scenario.

6.4.3 Superposition of the capacity curves and comparison with the 3D model for the FS3

In Figure 6.19 and Figure 6.20 the superposition of the capacity curves in the orthogonal directions (i.e., Fs3-x and FS3-y) and the comparison with the 3D model are shown, respectively.
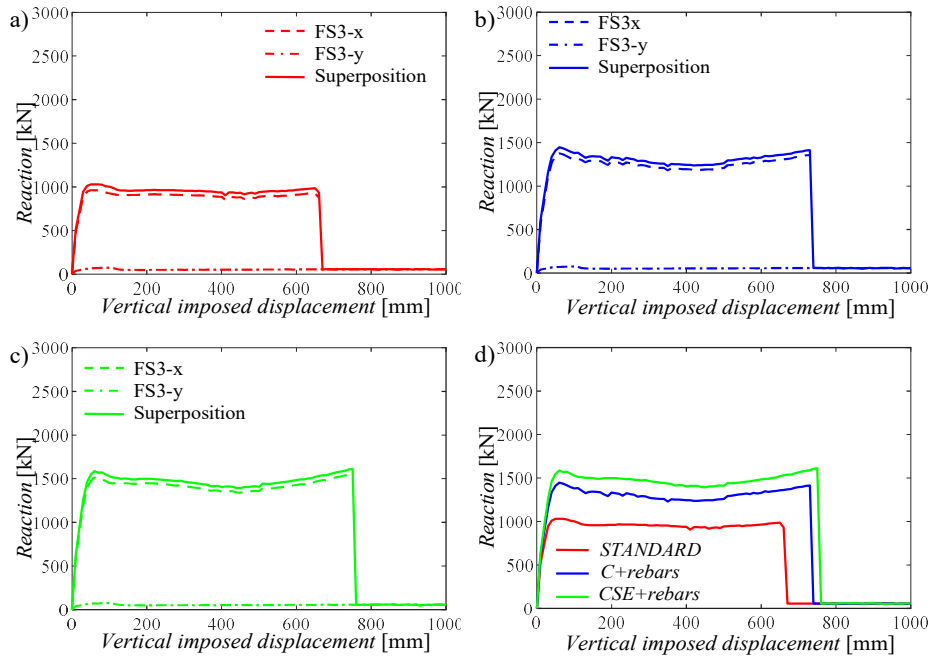
Figure 6.19 Results of the superposition of the FS3: (a) global capacity curve for *Code* configuration; (b) global capacity curve for *C+rebars* configuration; (c) global capacity curve for *CSE+rebars* configuration; (d) comparison between the three global capacity curves.

By observing the superimposed capacity curves (Figure 6.19), the contribution from the frame in the y-direction is minimal compared to the orthogonal frame subjected to collapse, and the enhanced ductility offered by the wide beams remains underutilized, unlike in the previous two failure scenarios.

By comparing the overlapped capacity curve in Figure 6.19d, it becomes evident that even in this failure scenario, the presence of *side face rebars* leads to an increase in the flexural peak as seen in the *C+rebars* model. Moreover, the *CSE+rebars* model, with its larger amount of beam longitudinal reinforcement, shows a further increase in the flexural peak. The *continuity* criterion and the inclusion of *side face rebars* contribute to an anticipated catenary effect; in contrast, in the *Code* model, the transition to the catenary effect begins around 40 cm of imposed vertical displacement, whereas in the *C+rebars* and *CSE+rebars* models, it starts 20 cm earlier. The overlapped capacity curve for the *Code* model displays a vertical drop at 67 cm of vertical displacement due to reaching of the ultimate

strain in the beam longitudinal reinforcement (i.e., 18%) in the frame in the x-direction.

Unlike the previous scenarios where the vertical drop was followed by an increase in resistance, in this case, this recovery in resistance does not occur due to the minimal contribution of the frame in the y-direction. This behaviour is consistent in the other two models as well.

Specifically, the *C+rebars* and *CSE+rebars* models show a drop in resistance at around 75 cm. By comparing the capacity curves obtained from the superposition and from the 3D modelling (Figure 6.20), the flexural peaks are similar, although occur at slightly higher vertical displacements in the 3D curves. The catenary effects are similar and the reductions in resistance occur at the same vertical displacement.
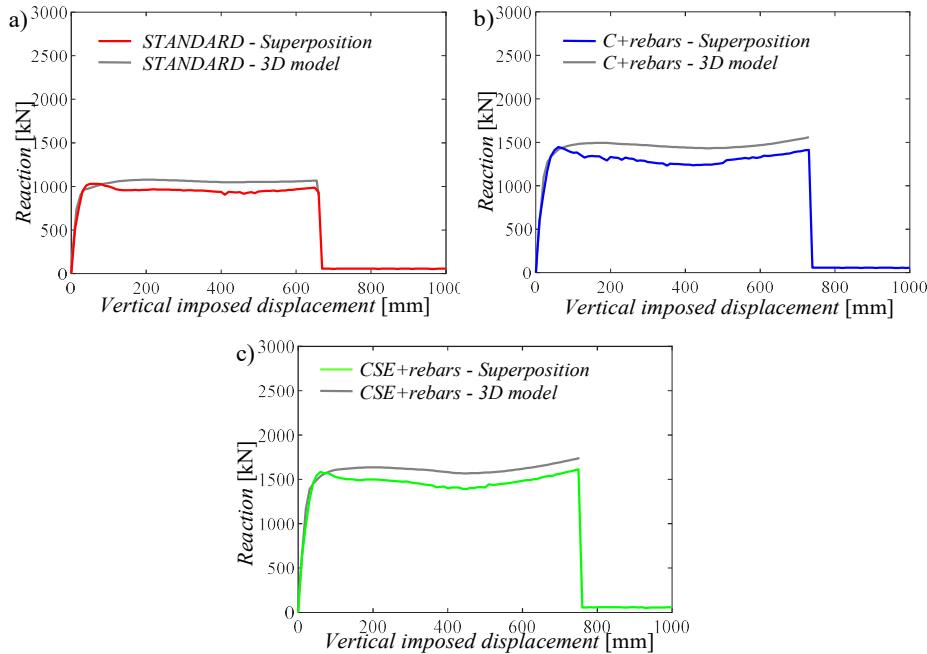
Figure 6.20 Comparison between global capacity curves and 3D capacity curves for the FS3.

6.5   Fourth failure scenario (FS4)

This section is about the fourth and last failure scenario, involving the removal of column A1.
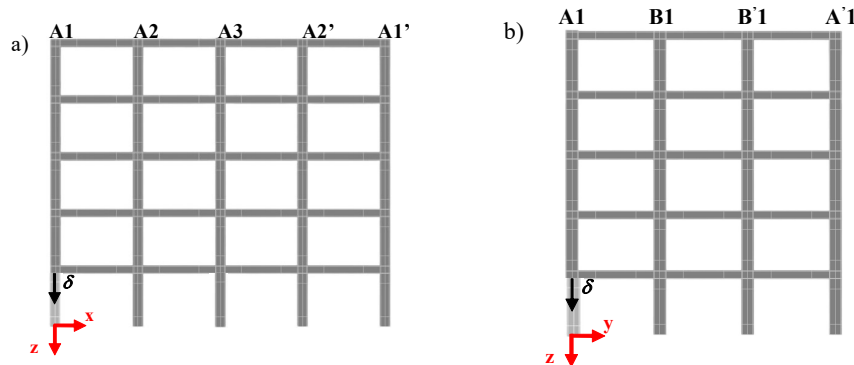
Figure 6.21 Schematic representation of the pushdown analysis for the frames involved in the fourth failure scenario: (a) FS4-x; (b) FS4-y.

The two orthogonal frames directly involved by failure are FS4-x and FS4-y as shown in Figure 6.21. In this case, for the frames in both directions the lost column is the lateral one. However, differently from all the previous cases, both FS4- x and FS4-y are seismic resistant frames, constituted by deep beams. In the following, the NLFE results of the pushdown analyses together with the application of the superposition of the capacity curves is reported for the FS4.

6.5.1   Pushdown analyses for frame FS4-x

The pushdown analyses for the frame FS4 in y-direction are shown in Figure 6.22 for the three structural configurations.

The frame in the analyzed direction serves as a perimeter frame and includes beams with a reduced amount of longitudinal reinforcement. Additionally, the removed column corresponds to a side column. The absence of a catenary effect is notable, and the resistance remains relatively constant until reaching the ultimate strain for the longitudinal reinforcement (i.e., 18%) between 65 cm and 75 cm for the three structural configurations.
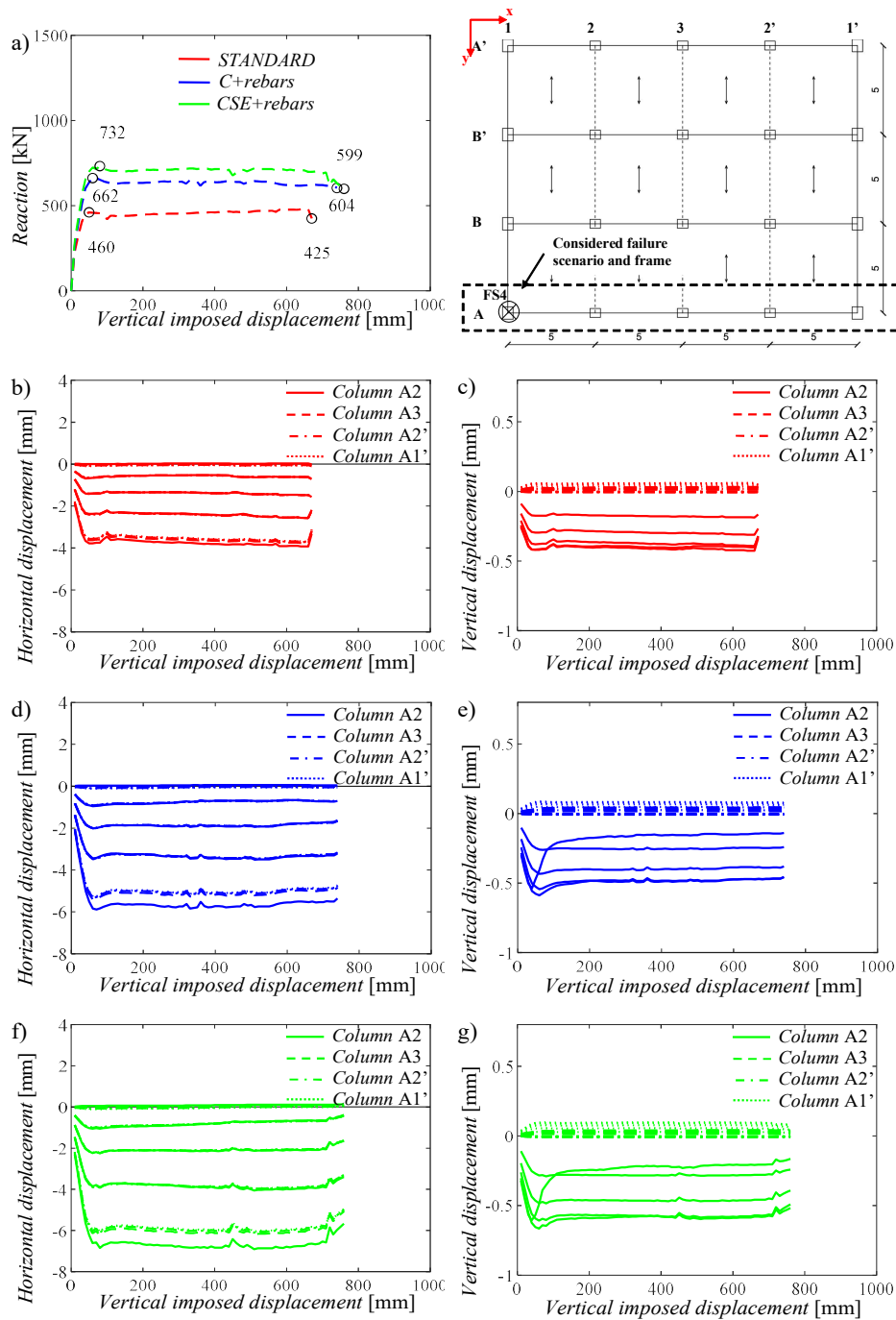
Figure 6.22 Results of the pushdown analyses for the FS4-x: (a) capacity curves; (b),(d),(f) horizontal displacement of beam-column nodes; (c),(e),(g) vertical displacements of the beam-column nodes for, respectively, *Code*, *C+rebars* and *CSE+rebars* configurations.

6.5.2 Pushdown analyses for frame FS4-y

The pushdown analyses for the frame FS4 in y-direction are shown in Figure 6.23 for the three structural configurations. The capacity curves presented here differ from the first three collapse scenarios due to the dimensions of the beams in FS4 y-direction which are deep beams. However, differently from the previous analyses in y-direction, the removed column here is a corner one.
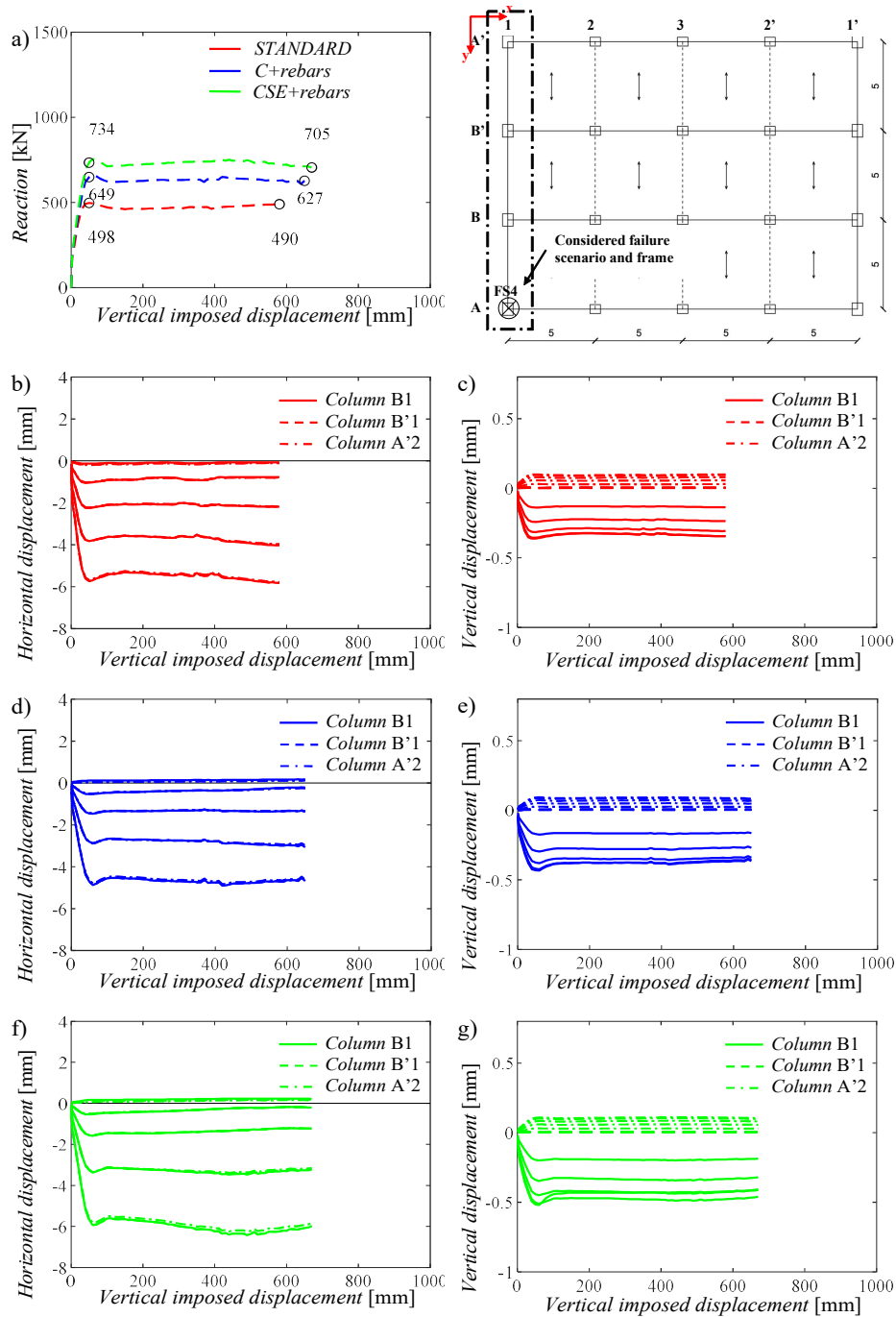
Figure 6.23 Results of the pushdown analyses for the FS4-y: (a) capacity curves; (b),(d),(f) horizontal displacement of beam-column nodes; (c),(e),(g) vertical displacements of the beam-column nodes for, respectively, *Code*, *C+rebars* and *CSE+rebars* configurations.

The capacity curves demonstrate that the *Code* model exhibits a flexural peak of 498 kN, which is very similar to the value recorded in the other direction. The increased total amount of longitudinal reinforcement in the *C+rebars* and *CSE+rebars* models resulting from the design suggestions leads to an increase in the flexural peak. However, the catenary effect is absent in all three models.

6.5.3 Superposition of the capacity curves and comparison with the 3D model for the FS4

In Figure 6.24 and Figure 6.25 the superposition of the capacity curves in the orthogonal directions (i.e., Fs4-x and FS4-y) and the comparison with the 3D model are shown, respectively.

By looking at the superimposed capacity curves (Figure 6.24), the contribution from both frames in each direction is nearly equal, which is the main difference observed for the three structural configurations of FS4 if compared to the previous failure scenarios.

Figure 6.25 provides a comparison between the global capacity curves derived from the superposition and the capacity curves from 3D analyses. Although the ultimate resistance is achieved at a similar value of imposed vertical displacement, slight discrepancies are observed in the ultimate resistance. These differences can be attributed to concrete cracking as well as uncertainties inherent in both modeling approaches.
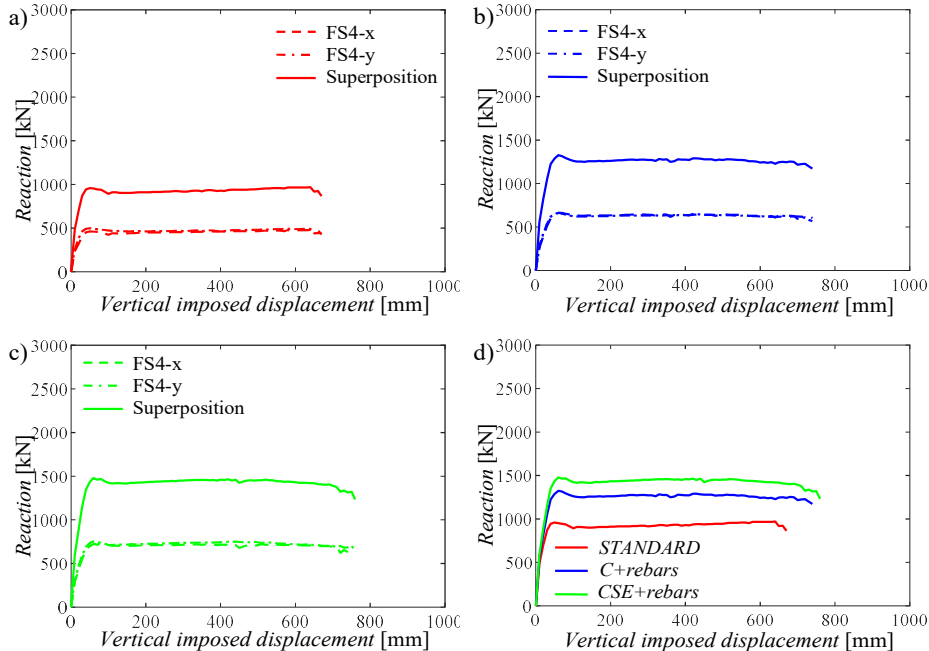
Figure 6.24 Results of the superposition of the FS4: (a) global capacity curve for *Code* configuration; (b) global capacity curve for *C+rebars* configuration; (c) global capacity curve for *CSE+rebars* configuration; (d) comparison between the three global capacity curves.
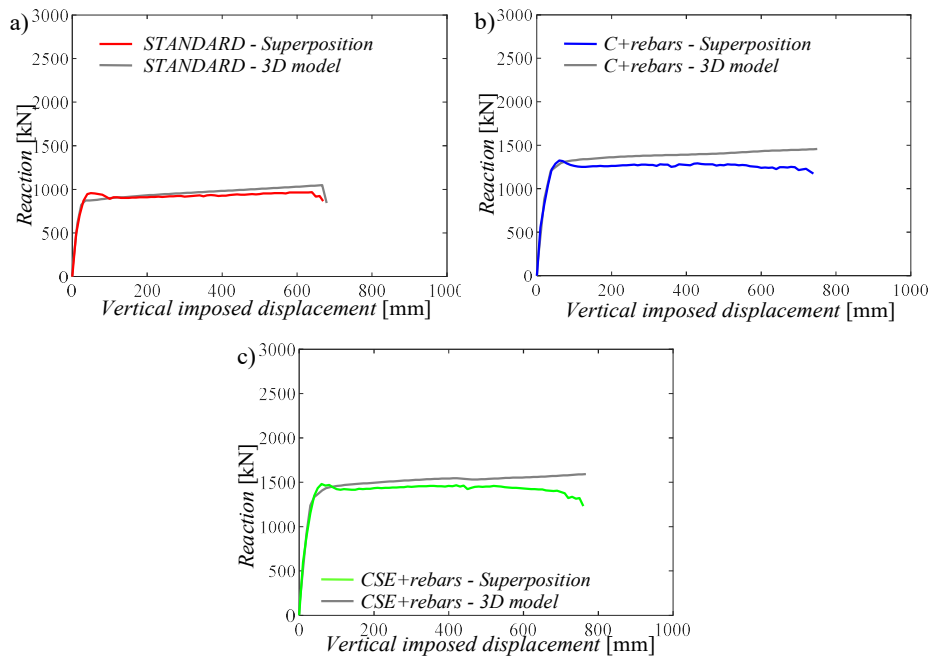
Figure 6.25 Comparison between global capacity curves and 3D capacity curves for the FS4.

6.6 Energetic approach for the four FSs

As already discussed in Section 5.4, the energetic approach by Izzuddin (2008) allows to compute the performance point (i.e., corresponding to a dynamic equilibrium) during an accidental column removal scenario. This point is reached when the external work W, representing the work done by the gravity loads, equals the internal energy U absorbed by the structure.

The work done by the external loads W is herein calculated as the product of gravity loads concentrated at the column removal point and the vertical displacement at that point. On the other hand, the internal energy U is equal to the area under the global capacity curve.

Figure 6.26 compares the internal energy and external work in terms of performance points for the three structural configurations across four different failure scenarios. Notably, for the first (Figure 6.26a) and second (Figure 6.26b) failure scenarios, the performance point is never reached for the *Code* configuration but is reached for vertical displacements between 5 and 10 cm for the other two structural configurations. It is important to mention that in the third (Figure 6.26c) and fourth (Figure 6.26d) failure scenarios, despite the absence of infill walls leading to an underestimation of structural response in terms of internal energy, an energy balance is always achieved. This is because the external work is lower due to the smaller influence area compared to the first two scenarios.
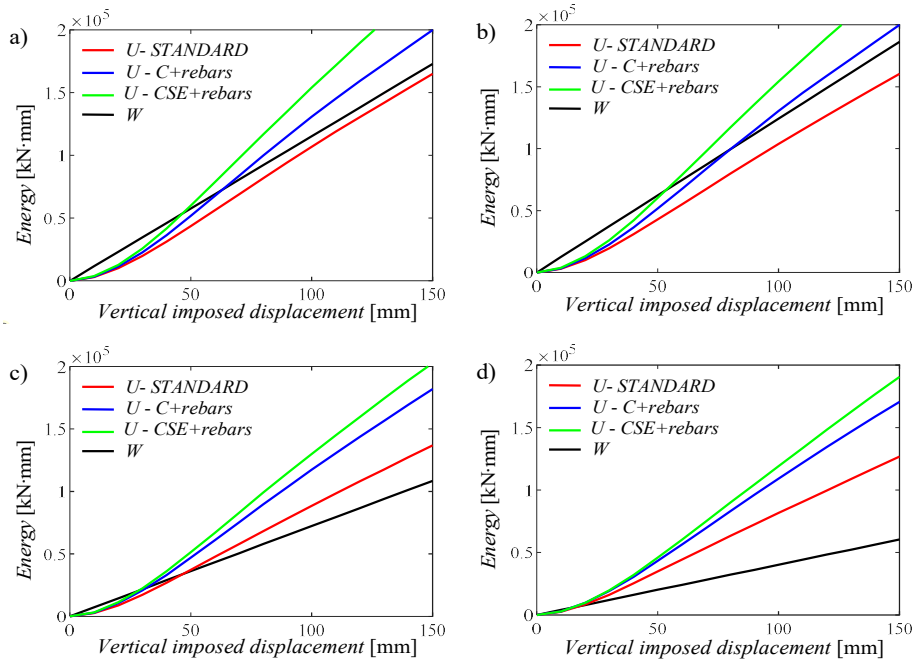
Figure 6.26 Energy equivalence approach for the three structural configurations and considering: (a) first failure scenario FS1; (b) second failure scenario FS2; (d) third failure scenario FS3; (e) fourth failure scenario FS4.

It is crucial to highlight that the calibration of non-linear springs plays an important role in determining the behavior of the 3D structure, especially for capturing non-linear effects such as the softening and catenary stages. This is true for large imposed displacements (i.e., larger than 60 cm) in case of frames having deep beams and medium imposed displacements (i.e., around 35 cm) when deep beams are designed. However, since the performance point (when *side face rebars* are included in the design) is reached at very low vertical displacements, a linear constitutive law may be sufficient in such cases.

Conclusions

This PhD thesis has concerned the evaluation of the structural robustness of ordinary reinforced concrete buildings designed in seismic area, against a supporting column removal scenario. Specifically, the goal was to improve the design of a 3D building by focusing on planar frames by means of robustness enhancements, mainly regarding the arrangement of beam longitudinal reinforcement. More in details, the planar frames were analyzed by including the 3D effects in a simplified way by means of equivalent springs in correspondence of each beam-column node.

The objective of this doctoral thesis has been threefold:

- To perform parametric deterministic analyses to investigate both literature and code rules enhancements as well as new proposals in order to improve the response of planar frames against different column removal scenarios. In particular, the following criteria on the beam longitudinal reinforcement have been considered and properly combined: *support continuity*, *continuity*, *section symmetry*, *global* and *partial floor equality* and *side face rebars*.
- To carry out full probabilistic analyses in order to compare the reliability of three different structural configurations, selected among the ones already studied deterministically. Specifically a 5-step strain-based procedure is proposed. In detail, the frame designed according to actual code rules was compared to other two frames where the previous robustness criteria have been included (i.e., *continuity*, *section symmetry*, *global floor equality* and *side face rebars*). In all the three configurations, the contribution of the orthogonal framed system (i.e., beams and columns composing the frames in the transverse direction with respect to the studied frame) has been included by means of translational equivalent elastic springs properly calibrated in a 3D elastic analysis.
- To obtain the global response of the 3D structure against a supporting column removal scenario by applying the superposition of the capacity curve of the two frames directly involved in the column lost scenario, in the

two main orthogonal directions. In this phase, also the non-linear calibration of the equivalent springs has been performed.

While the first two sets of analyses were performed on a regular building composed by seismic resistant frames in both directions, the third set included both seismic resistant and secondary frames having, respectively, deep and wide beams. The main outcome of this study can be summarized in the following key points:

- The numerical results of the deterministic analysis highlighted that while the seismic criteria and construction details adhering to current code rules may be favorable for robustness, they might not suffice to prevent disproportionate collapse in the event of a supporting column loss. Further considerations aimed to minimize the total amount of reinforcement while ensuring adequate robustness in line with sustainability principles. In fact, the design strategies, such as *continuity*, combined with *side face rebars*, struck a balance between robustness and sustainability, without the need to include other criteria such as *global floor equality* or *section symmetry* that surely enhance a robust behavior but determine a considerable increase in the amount of longitudinal reinforcement. The deterministic analyses emphasized the valuable role of *side face rebars* in increasing flexural peak and anticipating the transition to catenary behavior for lower vertical displacements of the supporting lost column. This led to reduced damage levels in RC frames and stable structural responses even under substantial displacements, crucial for respecting life safety and near-collapse limit states.
- The reliability analyses revealed that the frame designed according to current code rules often failed to withstand the column loss. In fact, by applying the energy equivalence approach proposed by Izzuddin (2008) a balance between internal energy and external work was not reached for the majority of the cases. Conversely, the configurations designed according to the proposed robustness enhancements always found an energy balance, allowing to compute the probabilistic dynamic amplification factors (DAFs). In detail, the two enhanced configurations of the frame demonstrated mean DAFs of 1.44 and 1.62 indicating that a simplified design value of 2.0 is excessively conservative. The failure probabilities were importantly reduced when the *side face rebars* were included in the design, reducing not only the mechanical effort at the concrete level but also the failure probabilities in the longitudinal reinforcement, reaching values lower than 10^{-7}. In addition, the frame designed according to current code rules showed failure probabilities of the order of 10^{-3} to 10^{-1} in the lateral spans, resulting in a spread of the damage from the directly affected spans (i.e., the central ones) to the external spans (i.e., indirectly affected). This was not the case for the two enhanced frames, where the lateral spans were characterized by failure probabilities lower than 10^{-7}, both at concrete and steel level. Additionally, the safety level at the concrete level in terms of β

minimum was far below 1 for the frame designed according to current code while it was equal to 1.08 and 1.23 for the two enhanced frames. Regarding the safety at the longitudinal reinforcement level, the β minimum was far below 1 for the frame designed according to current code and equal to 5.11 and 7.45 for the two enhanced frames.

- The third analyses involved the deterministic investigation of different failure scenarios, considering the removal of central and lateral supporting columns. The study demonstrated the validity of the superposition principle, since similar results were obtained by comparing the capacity curve obtained in a 3D non-linear analysis and the one summing up the contribution of the two orthogonal frames involved in the same column-loss scenario. This is an important outcome since it allows to carry out the design of RC buildings without the need to perform complex 3D analyses. The study underscores the importance of calibrating non-linear constitutive laws for springs, especially for large vertical displacements during the catenary stage and certain failure scenarios, to capture catenary responses. This is crucial especially for wide beams since they show a significant contribution in terms of ductility and the springs enter in a non-linear regime for lower imposed vertical displacement during the softening stage. This is important when large dynamic phenomena are involved because the performance point of equilibrium can be found for large vertical displacements. Additionally, an energetic equivalence approach was applied to global capacity curves to determine performance points for each design configuration and failure scenario. The results emphasize that robustness criteria inclusion, like *side face rebars*, enables reaching performance points at very low vertical displacements, thus enhancing the structural robustness of the system. This stands in contrast to buildings designed solely based on current code rules, which may fail to reach performance points.

It is important to note that the analysis does not include contributions from infills, or membrane effects of the slabs. However, the latter are negligible for one-way joist slabs like those in the building under study. In addition, by neglecting those contributions the reported results are on the side of safety, ensuring conservative estimations of structural behavior. Under these assumptions, the study regarding the reliability evaluation is focused on a specific accidental situation.

Moreover, this dissertation is based on a specific set of frames (i.e., cast-in-situ reinforced concrete frames designed in seismic area). This structural typology has been selected as the most unsafe from a multi-risk point of view. In fact, the presence of shear walls or staircases would have increased the capacity of the system. On the other hand, the basic idea was to explore the advantages of a seismic design approach, combined with the need of modifying the layout of longitudinal reinforcement for the robustness criteria but also respecting, especially, the shear verifications for the capacity design principles.

Future works should provide an analytical solution to have a reliable calibration of the *side face rebars* in order to account for them in a robust-based design. The

important advantage of *side face rebars* is indeed that they are not subjected to large stresses during the initial phase of the collapse scenario (i.e., flexural stage), since they are placed close to the barycenter of the section. However, when catenary effect activates, the role of *side face rebars* is to reduce the mechanical effort of the other longitudinal bars, that have yield during the initial stage. In fact, the ordinary longitudinal bars could fail when large displacements are involved if *side face rebars* are not involved in the tensile response of the beams. Other works should focus on the reliability evaluation of structures against progressive collapses for different configurations or in presence of possible deteriorating phenomena.

References

Adam JM, Buitrago M, Bertolesi E, Sagaseta J, Moragues JJ. "Dynamic Performance of a Real-scale Reinforced Concrete Building Test under a Corner-column Failure Scenario". *Engineering Structures* 210:110414, 2020.

Adam JM, Parisi F, Sagaseta J, Lu X. "Research and practice on progressive collapse and robustness of building structures in the 21st century". *Engineering Structures* 173:122-49, 2018.

ADINA R&D Inc. "ADINA: Theory and Modeling Guide" , *Reports ARD* 97-8, 1997.

Agarwal J, England J. "Recent developments in robustness and relation with risk". *Proceedings of the Institution of Civil Engineers: Structures and Buildings* 161(4):183-188, 2008.

Allen DE, Schriever WR. "Progressive collapse, abnormal loads and building codes". Québec: Division of Building Research Council, 1972.

American Concrete Institute (ACI). "Building Code Requirements for Structural Concrete (ACI 318-02)". Washington, DC, 2002.

American Society of Civil Engineers (ASCE) for the Federal Emergency Management Agency. "Pre-standard and commentary for the seismic rehabilitation of buildings FEMA Report 356". Reston, VA, 2000.

American Society of Civil Engineers (ASCE). "Minimum Design Loads for Buildings and Other Structures (ASCE 7-16)". Reston, VA, 2016.

American Society of Civil Engineers (ASCE). "Minimum design loads and associated criteria for buildings and other structures (ASCE 7-98)". Reston, VA, 1998.

American Society of Civil Engineers (ASCE). "Minimum design loads for buildings and other structures (ASCE/SEI 7-05)". Reston, VA, 2005.

Arshian A, Morgenthal G, Narayanan S. "Influence of modelling strategies on uncertainty propagation in the alternate path mechanism of reinforced concrete framed structures". *Engineering Structures* 110:36-47, 2016.

Avşar Ö, Bayhan B, Yakut A. "Effective Flexural Rigidities for Ordinary Reinforced Concrete Columns and Beams". *The Structural Design of Tall and Special Buildings* 23(6):463-82, 2014.

Ayyub BM, Haldar A. "Decisions in Construction Operation". *Journal of the Construction Engineering and Management Division* 3(4):343-357, 1985.

Baker JW, Schubert M, Faber MH. "On the assessment of robustness". *Structural Safety* 30(3):253–67, 2008.

Baravalle M, Köhler J. "A risk-based approach for calibration of design codes". *Structural Safety* 78:63–75, 2019.

Belletti B, Damoni C, Cervenka V, Hendriks MAN. "Catenary action effects on the structural robustness assessment of RC slab strips subjected to shear and tensile forces". *Magazine of Concrete Research* 71(20):1083-1096, 2019.

Belletti B, Muttoni A, Ravasini S, Vecchi F. "Parametric analysis on punching shear resistance of reinforced concrete continuous slabs". *Magazine of Concrete Research* 71(20):1083-1096, 2018.

Bertagnoli G, Ferrara M, Miceli E, Castaldo P, Giordano L. "Safety assessment of an existing bridge deck subject to different damage scenarios through the global safety format ECOV". *Engineering Structures* 306:117859, 2024.

Bhattacharya B. "A reliability-based measure of structural robustness for coherent systems". *Structural Safety* 89:102050, 2021.

Biondini F, Frangopol DM, Restelli S. "On structural robustness, redundancy and static indeterminacy". *Proceedings of ASCE/SEI 2008 structures congress*, Reston, 2008.

Biondini F, Frangopol DM. "Structural robustness of deteriorating systems". *Proceedings of the handling exceptions in structural engineering*, Rome, 2008.

Bontempi F, Giuliani L, Gkoumas K. "Handling the exceptions: Robustness assessment of a complex structural system". *Proceedings of the 3rd international conference on structural engineering, mechanics and computation (SEMC 2007)*, Rotterdam: Millpress, 1747–52, 2007.

Botte W, Droogné D, Caspeele R. "Reliability-based resistance of RC element subjected to membrane action and their sensitivity to uncertainties". *Engineering Structures* 238:112259, 2021.

Botte W, Gouverneur D, Caspeele R, Taerwe L. "Influence of design parameters on tensile Membrane Action in Reinforced Concrete Slabs". *Structural Engineering International* 25(1):50-60, 2015.

Brett C, Lu Y. "Assessment of robustness of structures: current state of research". *Frontiers of Structural and Civil Engineering* 356–68, 2013.

Brunesi E, Nascimbene R, Parisi F, Augenti N. "Progressive Collapse Fragility of Reinforced Concrete Framed Structures through Incremental Dynamic Analysis". *Engineering Structures* 104:65-79, 2015.

Brunesi E, Parisi F. "Progressive collapse fragility models of European reinforced concrete framed buildings based on pushdown analysis". *Engineering structures* 152:579–596, 2017.

Burnett E. "Abnormal loading and building safety". *ACI Symposium Paper* 48:141-190, 1975.

Cantone R, Belletti B, Manelli L, Muttoni A. "Compressive membrane action effects on punching strength of flat RC slabs". *Key Engineering Materials* 711:698-705, 2016.

Caprili S, Salvatore W. "Mechanical performance of steel reinforcing bars in uncorroded and corroded conditions". *Data in Brief* 18:1677–1695, 2018.

Castaldo P, Amendola G, Giordano L, Miceli E. "Seismic reliability assessment of isolated multi-span continuous deck bridges". *Ingegneria Sismica - International Journal of Earthquake Engineering, Anno XXXIX* (3), 2022.

Castaldo P, De Iuliis M. "Effects of Deep Excavation on Seismic Vulnerability of Existing Reinforced Concrete Framed Structures". *Soil Dynamics and Earthquake Engineering* 64:102-112, 2014.

Castaldo P, Miceli E. "Optimal single concave sliding device properties for isolated multi-span continuous deck bridges depending on the ground motion characteristics". *Soil Dynamics and Earthquake Engineering* 173:108128, 2023.

Cervenka Consulting s.r.o. "ATENA 2D v5". Prague, Czech Republic, 2014.

Cervenka V. "Constitutive model for cracked reinforced concrete". *Journal ACI* 82(6):877–82, 1985.

Chen Y-L, Huang L, Lu Y-Q, Deng L, Tan H-Z. "Assessment of structural robustness under different events according to vulnerability". *Journal of Performance of Constructed Facilities* 2016.

Comité Européen de Normalisation CEN. "EN 1992-1-1:2004: Eurocode 2 – Design of concrete structures - Part 1-1: General rules and rules for buildings". Brussels, Belgium, 2004.

Comité Européen de Normalisation CEN. "Eurocode 1 – Actions on Structures Part 1-7: General actions - Accidental actions". Brussels, Belgium, 2006.

Comité Européen de Normalisation CEN. "Eurocode 8 – Design of Structures for earthquake resistance". Brussels, Belgium, 1998.

Comité Européen de Normalisation. "EN1990:2002: Eurocode 0 - basis of structural design". Brussels, Belgium, 2002.

Comittee Euro-International du Beton (CEB-FIP). Model Code 1990, Bulletin d'information No. 195,196, 1991.

Computers and Structures Inc. (CSI). "SAP2000 Integrated software for structural analysis and Design". Berkley, California.

Consiglio Nazionale delle Ricerche (CNR). "CNR-DT 214 /2018 Istruzioni per la valutazione della robustezza delle costruzioni", 2018.

Cornell, C.A. "A Probability-Based Structural Code". *Journal of the American Concrete Institute* 66(12): 974-985, 1969.

Darwin D, Pecknold DAW. "Inelastic model for cyclic biaxial loading of reinforced concrete". *Civil Engineering Studies*, University of Illinois, 1974.

Department of Communities and Local Government (DoLG). "The building regulations 2010 - structure: approved document A". UK, HM Government, 2010.

Department of Defence (DoD). "Design of buildings to resist progressive collapse (UFC 4-023-03)". Washington, DC: Unified Facilities Criteria, 2013.

Department of Defence (DoD). "Design of buildings to resist progressive collapse (UFC 4-023-03)". Washington, DC: Unified Facilities Criteria, 2009.

Department of Defense (DoD). "Design of buildings to resist progressive collapse (UFC 4-023-03)". Washington, DC: Unified Facilities Criteria, 2016.

Dhakal RP and Maekawa K. "Reinforcement stability and fracture of cover concrete in RC members". *Journal of Structural Engineering* 128:10, 2002.

Di Trapani F, Giordano L, Mancini G. "Progressive Collapse Response of Reinforced Concrete Frame Structures with Masonry Infills". *Journal of Engineering Mechanics* 146(3), 2020.

Ding, Y, Song X, Zhu HT. "Probabilistic Progressive Collapse Analysis of Steel-Concrete Composite Floor Systems". *Journal of Constructional Steel Research* 129:129-140, 2017.

Droogné D, Botte W, Caspeele R. "A multilevel calculation scheme for risk-based robustness quantification of reinforced concrete frames". *Engineering Structures* 160:56–70, 2018.

Dyngeland T. "Behavior of reinforced concrete panels". Trondheim, Norway. BK-Report, 1989:1, 1989.

Ellingwood BR, Leyendecker EV. "Approaches for design against progressive collapse". *Journal of the Structural Division* 104(3):413-423, 1978.

Ellingwood BR. Mitigating risk from abnormal loads and progressive collapse. *Journal of Performance of Constructed Facilities* 20(4):315–23, 2006.

Faber MH, Maes MA, Straub D and Baker JW. "On the Quantification of Robustness of Structures". *Proceedings OMAE2006 25th Offshore Mechanics and Arctic Engineering Conference*, Hamburg, Germany, June 4-9, 2006.

Fallon CT, Quiel SE, Naito CJ. "Uniform pushdown approach for quantifying building-frame robustness and the consequence of disproportionate collapse". *Journal of Performance of Constructed Facilities* 30(6), 2016.

Fascetti A, Kunnath SK, Nisticò N. "Robustness evaluation of RC frame buildings to progressive collapse". *Engineering Structures* 86:242-249, 2015.

Federation International du Beton *fib*. "Model Code for Concrete Structures". 2010.

Federation International du Beton *fib*. "Partial factor methods for existing concrete structures Bulletin no. 80". 2016.

Feng DC, Zhang MX, Brunesi E, Parisi F, Yu J, Zhou Z. "Investigation of 3D effects on dynamic progressive collapse resistance of RC structures considering slabs and infill walls". *Journal of Building Engineering* 54:104421, 2022.

Ferrara M, Gino D, Miceli E, Giordano L, Malavisi M, Bertagnoli G. "Safety assessment of existing prestressed reinforced concrete bridge decks through different approaches". *Structural concrete: journal of the fib*, 2024.

Forquin P, Chen W. "An experimental investigation of the progressive collapse resistance of beam-column RC sub-assemblages". *Construction and Building Materials* 152:1068–84, 2017.

Frangopol DM, Curley JP. "Effects of damage and redundancy on structural reliability". *Journal of Structural Engineering* 113:1533–49, 1987.

Fu G, Frangopol DM. "Balancing weight, system reliability and redundancy in a multi objective optimization framework". *Structural Safety* 7(2):165–75, 1990.

General Services Administration (GSA). "Alternate path analysis and design guidelines for progressive collapse resistance". Washington, DC: Office of Chief Architects, 2016.

General Services Administration (GSA). "Alternative path analysis and design guidelines for progressive collapse resistance". Washington, DC: Office of Chief Architects, 2013.

General Services Administration (GSA). "Progressive collapse analysis and design guidelines". Washington, DC: Office of Chief Architects, 2003.

Gino D, Miceli E, Castaldo P, Recupero A, Mancini G. "Strain-based method for assessment of global resistance safety factors for NLNAs of reinforced concrete structures". *Engineering Structures* 304, 117625, 2024.

Gino D, Miceli E, Giordano L, Marano GC, Castaldo P. "Influence of Masonry Infills on Seismic Performance of an Existing RC Building Retrofitted by Means of FPS Devices". *Applied Science* 13:3509, 2023.

Griffith H, Pugsley A, Saunders O. "Report of the inquiry into the collapse of flats at Ronan Point, Canning Town". Her Majesty's Stationery Office (HMSO), London, 1968.

Haldar A, Mahadevan S. "Probability, Reliability and Statistical Methods in Engineering Design". John Wiley, 77(5), May 2000.

Harbitz, A. "An Efficient Sampling Method for Probability of Failure Calculation". *Structural Safety* 3(2):109-115, 1986.

Hasofer AM and Lind NC. "Exact and Invariant Second Moment Code Format". *Journal of the Engineering Mechanics Division* 100:111-121, 1974.

Hendriks M and Roosen MA. "Guidelines for Nonlinear Finite Element Analysis of Concrete Structures". Rijkswaterstaat Centre for Infrastructure, Report RTD, 1016-1:2019, 2019.

Her Majesty's Stationery Office (HMSO). "Building Regulations". London, 1972.

International Code Council (ICC). "IBC International building code". 2009.

International Standard Organization (ISO). "ISO 2394 General principles on reliability for structures". Swizerland, 2015.

Izzuddin BA, Vlassis AG, Elghazouli AY, Nethercot DA. "Progressive collapse of multi-storey buildings due to sudden column loss - Part I: Simplified assessment framework". *Engineering Structures* 30(5):1308–1318, 2008.

Jalayer F, Cornell CA. "Alternative Non-Linear Demand Estimation Methods for Probability-Based Seismic Assessments". *Earthquake engineering and structural dynamics* 38(8):951–972, 2009.

Jian H, Zheng Y. "Simplified models of progressive collapse response and progressive collapse-resisting capacity curve of RC beam-column substructures". *Journal of Performance of Constructed Facilities* 04014008-1, 2014.

Joint Committee on Structural Safety (JCSS). "Probabilistic Model Code, Part 2 - Load Models". 2001.

Joint Committee on Structural Safety (JCSS). "Probabilistic Model Code, Part 3 - Resistance Models". 2002.

Khandelwal K. "Pushdown resistance as a measure of robustness in progressive collapse". *Engineering Structures*, 33(9):2653–61, 2011.

Kolmar W. "Beschreibung der Kraftuebertragung über Risse in nichtlinearen Finite-Element-Berechnungen von Stahlbetontragwerken". T.H. Darmstadt, 1986.

Leonardo da Vinci Pilot Project CZ/02/B/F/PP-134007. "Implementation of Eurocodes – Handbook 2 – Reliability Backgrounds". Prague, 2005.

Lew HS, Bao Y, Pujol S, Sozen MA. "Experimental study of reinforced concrete assemblies under column removal scenario". *ACI Structural Journal* 11(4):881–92, 2014.

Lew HS, Bao Y, Sadek F, Main JA, Pujol S, Sozen MA. "An experimental and computational study of reinforced concrete assemblies under a column removal scenario". *NIST Technical Note* 1720(106), 2011.

Li H, El-Tawil S. "Three-dimensional effects in progressive collapse modeling". Proceedings of the Structures Congress, 2829–2839, 2011.

Li Y, Lu X, Guan H, Yea L. "An improved tie force method for progressive collapse resistance design of reinforced concrete frame structures". *Engineering Structures* 33:2931-2942, 2011.

Lim NS, Tan KH, Lee CK. "Effects of rotational capacity and horizontal restraint on development of catenary action in 2-D RC frames". *Engineering Structures* 153:613–27, 2017.

Lind NC. "A measure of vulnerability and damage tolerance". *Reliability Engineering & System Safety* 48(1):1–6, 1995.

Lu X, Lin K, Li Y, Guan H, Ren P, Zhou Y. "Experimental Investigation of RC Beam-slab Substructures against Progressive Collapse Subject to an Edge-column-removal Scenario". *Engineering Structures* 149:91-103, 2017.

Maes MA, Fritzsons KE, Glowienka S. "Structural robustness in the light of risk and consequence analysis". *Structural Engineering International* 16(2):101–7, 2006.

Massicotte B, Elwi AE, MacGregor JG. "Tension-stiffening models for planar reinforced concrete members". *Journal of Structural Engineering* 116(11):3039–58, 1990.

Mckey MD, Conover WJ, Beckman RJ. "A comparison of three methods for selecting values of input variables in the analysis from a computer code". *Technometrics* 21:239-45, 1979.

Miceli E, Castaldo P. "Robustness Improvements for 2D Reinforced Concrete Moment Resisting Frames: Parametric Study by Means of NLFE Analyses". *Structural concrete : journal of the fib Structural Concrete* 25(1):9-31, 2024.

Miceli E, Ferrara S, Castaldo P. "Confinement effects within the seismic design of reinforced concrete frames: a reliability assessment and comparison". *Engineering Structures* 118248, 2024b.

Miceli E, Gino D, Castaldo P. "Approaches to estimate global safety factors for reliability assessment of RC structures using non-linear numerical analyses". *Engineering Structures*, 2024a.

Ministry of Housing and Local Government (MHLG). "Flats constructed with precast concrete panels. Appraisal and Appraisal and strengthening of existing high blocks: Design of new blocks". Circular 62/68, 15 November 1968, London.

Ministry of Housing and Local Government (MHLG). "Flats constructed with precast concrete panels. Appraisal and Appraisal and strengthening of existing high blocks: Design of new blocks". Circular 71/68, 20 December 1968, London.

Naji A. "Improving the tie force method for progressive collapse design of RC frames". *International Journal of Structural Integrity*, 9(4):520-531, 2017.

National Institute of Standards and Technology (NISTIR). "NISTIR 7396 Best practices for reducing the potential for progressive collapse in buildings". Gaithersburg, 2007.

Panagiotakos TB, Telemachos B, Fardis MN. "Deformations of Reinforced Concrete Members at Yielding and Ultimate". *Aci Structural Journal* 98:135-148, 2001.

Parisi F, Augenti N. "Influence of seismic design criteria on blast resistance of RC framed buildings: A case Study". *Engineering Structures* 44:78-93, 2012.

Parisi F, Scalvenzi M, Brunesi E. "Performance limit states for progressive collapse analysis of reinforced concrete framed buildings". *Structural Concrete* 20(1):68-84, 2019.

Paté-Cornell ME. "Quantitative safety goals for risk management of industrial facilities". *Structural Safety* 13(3):145-157, 1994.

Paulay T, Priestley MJN. "Seismic design of reinforced concrete and masonry buildings". Wiley, New York, 1992.

Pham AT, Tan KH. "A simplified model of catenary action in reinforced concrete frames under axially restrained conditions". *Magazine of Concrete Research* 1700009, 2017.

Qian K, Li B, Zhang ZW. "Testing and simulation of 3D effects on progressive collapse resisting of RC buildings". *Magazine of Concrete Research*, 66(3–4):163-178, 2014.

Ren P, Li Y, Lu X, Guan H, Zhou Y. "Experimental Investigation of Progressive Collapse Resistance of One-way Reinforced Concrete Beam–slab Substructures under a Middle-column-removal Scenario". *Engineering Structures* 118:28-40, 2016.

Ribeiro LDR., Kroetz HM, Parisi F, Beck AT. "Optimal risk-based design of reinforced concrete beams against progressive collapse". *Engineering Structures* 300:117158, 2024.

Rosenbleuth E, Esteva L. "Reliability Bases for Some Mexican Codes". *ACI Publication* SP-31:1-41, 1972.

Saatcioglu M, Razvi SR. "Strength and ductility of confined concrete". *Journal of Structural Engeenering* 119(10):3109-3110, 1993.

Sadek F, Main JA, Lew HS, Bao Y. "Testing and analysis of steel and concrete beam column assemblies under a column removal scenario". *Journal of Structural Engineering* 137(9):881-892, 2011.

Slobbe A, Rózsás A, Allaix DL, Vliet AB. "On the Value of a Reliability-based Nonlinear Finite Element Analysis Approach in the Assessment of Concrete Structures". *Structural concrete: journal of the fib* 21(1):32–47, 2020.

Sørensen JD. "Framework for robustness assessment of timber structures". *Engineering Structures* 33(11):3087-3092, 2011.

Starossek U, Haberland M. "Approaches to measures of structural robustness". *Structure and Infrastructure Engineering* 7:625-631, 2011.

Starossek U, Haberland M. "Disproportionate collapse: terminology and procedures". *Journal of Performance of Constructed Facilities* 24(6):519-528, 2010.

Starossek U. "Progressive collapse of structures – 2nd Edition". Thomas Telford Limited, 2018.

Starossek U. "Typology of progressive collapse". *Engineering Structures* 29(9):2302-2307, 2007.

Stewart M, Netherton M, Rosowsky D. "Terrorism Risks and Blast Damage to Built Infrastructure". *Natural Hazard Review* 7(3):114-122, 2006.

Tsai MH and Lin BH. "Dynamic amplification factor for progressive collapse resistance analysis of an RC building". *The Structural Design of Tall and Special Buildings* 18(5):539-557, 2009.

Voulpiotis K, Schär S, Frangi A. "Quantifying robustness in tall timber buildings: A case study". *Engineering Structures* 265:114427, 2022

Vrouwenvelder T. "Treatment of risk and reliability in the Eurocodes". *Proceedings of the Institution of Civil Engineers: Structures and Buildings* 161(4):209-214, 2008.

Wang Y, Zhang B, Gu XL, Lin F. "Experimental and numerical investigation on progressive collapse resistance of RC frame structures considering transverse beam and slab effects". *Journal of Building Engineering* 47:103908. 2022.

Xu G, Ellingwood B. "Probabilistic Robustness Assessment of Pre-Northridge Steel Moment Resisting Frames". *Journal of Structural Engineering* 137(9):925-934, 2011.

Xu G, Ellingwood BR. "An energy-based partial pushdown analysis procedure for assessment of disproportionate collapse potential". *Journal of Constructional Steel Research* 67(3):547-555, 2011.

Xuan DP, Tan KH. "Experimental study of beam-slab substructures subjected to a penultimate-internal column loss". *Engineering Structures* 55:2-15, 2013.

Yu J, Rinder T, Stolz A, Tan KH, Riedel W. "Dynamic progressive collapse of an RC assemblage induced by contact detonation". *Journal of Structural Engineering* 140(6):1-13, 2014.

Yu J, Tan KH. "Experimental and numerical investigation on progressive collapse resistance of reinforced concrete beam column sub-assemblages". *Engineering Structure* 55:90-106, 2013.

Yu J, Tan KH. "Special detailing techniques to improve structural resistance against progressive collapse". *Journal of Structural Engineering* 140(3):1–15, 2014.

Yu J, Tan KH. "Structural behaviour of reinforced concrete frames subjected to progressive collapse. *ACI Structural Journal* 114(1):63–74, 2017.

Zhang L, Zhao H, Wang T, Chen Q. "Parametric Analysis on Collapse-resistance Performance of Reinforced-concrete Frame with Specially Shaped Columns Under Loss of a Corner Column". *The Open Construction and Building Technology Journal* 10(1):466-480, 2016.

Zhang Q, Zhao YG, Kolozvari K, Xu L. "Reliability Analysis of Reinforced Concrete Structure Against Progressive Collapse". *Reliability Engineering & System Safety* 228:108831, 2022.

Zhao Z, Liu Y, Li Y, Guan H, Yang Z, Ren P, Xiao Y. "Experimental and Numerical Investigation of Dynamic Progressive Collapse of Reinforced Concrete Beam-Column Assemblies Under a Middle-Column Removal Scenario". *Structures* 38:979–92, 2022.

Zheng T, Zhong W, Bao M., Zheng Y, Duan S. "Effect of various boundary constraints on the collapse behavior of multi-story composite frames". *Journal of Building Engineering* 52:104412, 2022.